The role of reversible ubiquitylation in EGF signalling

Thesis is submitted in accordance with the requirements of the University of Liverpool for the degree of doctor of philosophy

By

Ewan MacDonald

October 2013

List of figures

Chapter 1.

Chapter 2.

Chapter 3.

Chapter 4.

Chapter 5.

Chapter 6.

Supplementary Figures

Abbreviations used in this thesis

EGF- Epidermal Growth Factor (Human).
mEGF- Epidermal Growth Factor (Mouse).
EFGR- Epidermal Growth Factor.
HRS- Hepatocyte Receptor Substrate.
MVB – Multi Vesicular Body.
PDGF- Platelet Derived Growth Factor.
PDGFR- Platelet Derived Growth Factor Receptor.
mAb- Monoclonal Antibody.
SH2- Src Homology domain 2.
FDA- Federal Drug Administration.
ILV- Intra Luminal Vesicle.
MVB- Multi Vesicular Body.
ESCRT- Endosomal Sorting Complex Required for Transport.
USP- Ubiquitin Specific Domain.
JAMM- JAMM/MPN+
OTU- Otubain.
UCH- Ubiquitin Carboxy Hydrolase.
JOS- Josephin.
p….- Phosphorylation.
IP- Immuno Precipitation.
IF- Immuno Fluorescence.
DUB- Deubiquitylase.
UIM- Ubiquitin Interacting Motif.
Ub- Ubiquitin.
Tyr-Tyrosine.
Thr- Threonine.
Ser-Serine.
Y2H- Yeast 2 hybrid.
VPS- Vacuolar Protein Sorting.

Abstract

Deubiquitylases (DUBs) have been implicated in the regulation of cell signaling processes. However, the role of DUBs in the regulation of the Epidermal growth factor receptor (EGFR) signaling is not completely understood. This study has aimed to identify DUBs involved in the regulation of EGFR signaling and downstream cascades. The first part of this study has characterized the role of the DUB USP15 in the regulation of the mitogen activated protein kinase (MAPK) cascade, a pathway downstream of EGFR. An interaction between USP15 and the MAPK negative regulator BRAP had been previously reported. When we tested the USP15 depletion phenotype on MAPK signaling we observed a paradoxical decrease in MAPK activation. Examination of upstream components of the MAPK cascade revealed a decrease in the levels of the CRAF kinase following USP15 depletion. Concordant depletion of CRAF also caused a reduction in MAPK activation, showing that depletion of CRAF phenocopied that of USP15. This work demonstrated that USP15 has a dual role in the regulation of the MAPK through BRAP and CRAF. The dominant signaling effect in the cell lines studied is through maintenance of CRAF levels.

We employed a previously characterized GFP-DUB library to identify DUBs that exhibited EGF dependent distributions. One such DUB, USP46, exhibited MAPK dependent recruitment onto multi-vesicular bodies (MVB). To further characterize USP46 we generated a set of cell lines expressing GFP-USP46 and catalytically inactive GFP-USP46-C44S using the Flp-in system. While the Flp-in cells lines did not exhibit the same EGF dependent recruitment onto the MVB compartment, they did localize to Saponin resistant punctate structures. Furthermore, I observed differential activation of downstream EGFR signaling pathways that USP46 may play an undetermined role in EGF signaling. We combining stable isotope labeling of amino acids in culture (SILAC) with immuno-precipitation (IP) to quantitatively identify interactors of USP46 using mass spectrometry. We identified a

number of candidate interactors and confirmed a novel interaction between USP46 and FBXO11 using western blotting.

Next we aimed to identify DUBs that regulate the retrograde trafficking pathway from the MVB to the trans Golgi network (TGN). We used the localization of the cation independent mannose 6-phosphate receptor (CI-M6PR) as readout of the retrograde trafficking. CI-M6PR constitutively recycles from the TGN to the endo-lysosomal pathway, delivering newly synthesized acid hydrolases, required for degradative action of the lysosome. Depletion of USP8 trapped CI-M6PR in aberrant endosomes and caused a concomitant missorting of the acid hydrolase, Cathepsin D. Cathepsin D is activated through limited proteolysis in the acidic environment of the endo-lysosomal pathway. Depletion of USP8 caused a decrease in the mature cellular form of Cathepsin D. The mislocalization of CI-M6PR could be rescued by re-expression of GFP-USP8. The activated EGFR is degraded via the lysosome and depletion of USP8 has been demonstrated to cause a delay in the degradation of EGFR. The results presented here suggest that the decrease in active acid hydrolases observed in USP8 depleted cells, may contribute to the delay in EGFR degradation.

Acknowledgements

I am indebted to the guidance and support of my supervisors Michael Clague and Sylvie Urbé. Without whom, I certainly would not be scientist I am today. I would like to thank Ian Prior for writing the grant that has supported my PhD studies and also for his advice and encouragement. To Han Liu and Dean Hammond for all their help and providing excellent examples of how to be a quality scientist. I must also specifically thank Sebastian Hayes and Paula Row whose work laid the foundations of my own.

I would also like to thank the remarkable people with whom I have spent the last 3 years. For not only providing a stimulating environment but also a warm and friendly one too. So in no particular order, Jia Lih, Amos Liang, Yvonne Tang, Aitor Martinez-Zarate, Rebecca Eccles, Viktor Malec, Claire Heride, Alice Howarth, Fiona Hood, Maria Hernandez, Ali Beckett, Simon Oliver, Monica Faronato, Monika Chojnowska-Monga, Jenna Kenyani, Andrew Fielding, Sarah Darling, Jenny Martin, Joe Sacco, Judy Coulson, Arnaud Selvais and Emma Rusilowic. I will be lucky if I get to work with such amazing people again. Special thanks must go to Craig Mageean and Liam Cheeseman for being available for a moan and a beer.

I am extremely grateful to the BBSRC for funding my studies, which have enabled me to carry out this work.

I would like to thank my family for all their support and apologies for my absence over the last three years. You are truly inspiring people and I hope that I can replicate your strength and wisdom. To all my friends in particularly MB, JS, JT, PH and AF for helping to remind me there is a world outside the lab. To Lynda Blayney and Leon D'Cruz for inspiring my passion for research. Finally I would like to thank Hanna Sjöberg for taking this journey with me.

Chapter 1 Introduction

1.1.1. The discovery of Epidermal Growth Factor (EGF).

To maintain correct tissue architecture cells need to grow and differentiate in a coordinated manner. The fate of individual cells is tightly controlled by extracellular growth factors. Mutations in the intracellular pathways that respond to growth factors can cause the cell to proliferate independent of these extracellular cues. This causes uncontrolled proliferation and can lead to the development of cancer. Research into understanding the regulation of these pathways and how they become deregulated in cancer has lead to the development of anti-cancer drugs. However, despite many successes there are still gaps in our understanding of how these pathways are regulated. By identifying new regulators there is still potential to open new means to pharmacologically inhibit these pathways.

In 1951 Rita Levi-Montalcini observed that mouse sarcomas implanted in the sympathetic ganglia of chick embryos had growth-stimulating effects[1]. The factor responsible was isolated by Stanley Cohen in 1954, which was duly named Nerve Growth Factor (NGF)[2]. Whilst working on a project isolating NGF from mouse submaxillary glands, Cohen noted that when crude preparations were given to mice it accelerated their development[3]. He concluded that these effects were not attributable to NGF as the purified factor did not have the same effect, so there must be another factor in the crude extract. Using these observations as a readout, he isolated a factor that when given to mice caused the eyelids to open and teeth to erupt earlier in development[4]. By using electron microscopy, it was observed that there was an increase in the keratinization and differentiation of the epidermis in the eye lids of mice treated with the factor compared to control animals[4].

At this point it was unclear how these effects were being generated. Were they generated by the factor itself or did the factor stimulate the release

of another hormone[5]? In 1965 using chick skin organ cultures, it was definitively demonstrated that the factor was stimulating the growth and keratinization of epidermal cells[6]. The factor has since been known as epidermal growth factor (EGF).

This work had another important implication that mouse EGF (mEGF) was able to stimulate avian as well as mammalian tissues. This opened up the possibility that EGF was a conserved factor, which could be important in regulating human tissues. Addition of EGF to cultures of human fibroblast 3T3 cells proved this hypothesis. mEGF could stimulate growth and overcome contact inhibition of human fibroblast cells[7].

The fact that mEGF could stimulate human cells meant that there must be a human equivalent of EGF. This began the search to find human equivalent to mEGF. Human EGF (EGF) was isolated from human urine using affinity column prepared with rabbit antiserum against mEGF[8, 9]. The isolated compound competed for the same receptor[9] and cross-reacted with antibodies against mEGF[8]. Furthermore the isolated compound had similar biological effects on cultured cells as mEGF[9]. However, no sequence was available to confirm that the compounds were the homologous. In the 1970s the development of a two-step method to isolate mEGF from submaxillary glands[10] enabled the biochemical characterization of mEGF.

Greogory et al.[11] (1977) isolated a compound called urogastrone from human urine a molecule known to inhibit gastric acid secretion. When they sequenced urogastrone they found that there was a remarkable similarity to mEGF. With further analysis it was revealed that they had in fact isolated EGF; both compounds elicited the same responses when tested. This work incidentally demonstrated a previously unsuspected role of EGF in regulating gastric acid secretion[11].

1.1.2. The identification of an EGF receptor and the discovery of receptor endocytosis.

Using radio ligand (I^{125}EGF) assays a specific receptor for EGF was demonstrated[12]. I^{125}EGF would bind to the surface of cells at 0˚C and at 37˚C, at 0˚C it takes 4 hours for the receptors to reach saturation compared to at 37˚C, were saturation is achieved after approximately 15mins, furthermore the maximal binding at 37˚C was approximately twice that at 0˚C[12]. After prolonged incubation at 37˚C there was a decrease in the amount of bound EGF, decreasing to 20% of the maximum, whereas at 0˚C no decrease was observed. This effect was not due to destruction of free EGF in the media as the containing media and stimulate another set of cells[12]. Adding fresh EGF to pre-stimulated cells also does not overcome the desensitization[12] and reapplying EGF to stimulated cells failed to illicit a response. These experiments suggested that there was active an cellular process that regulates the abundance of the receptor on the plasma membrane.

Using I^{125}-hEGF bound to the receptor at different temperatures this regulation was teased out. By binding I^{125}-hEGF at 0˚C then maintaining the cells at 0˚C the radio ligand could be washed off from the cells and recovered. Binding the radio ligand and maintaining the cells at 37˚C, there was a reduced amount of label at the cell surface and digestion products of EGF could be detected[12]. By binding at 37˚C and then maintaining the cells at 0˚C, there was a reduced amount radio ligand washed off the cells and now there was no degradation products observed. Additionally adding lysosomal inhibiters to the cells could block the degradation of I^{125}-hEGF at 37˚C[12]. This data was consistent with the hypothesis that the receptor was being internalized following EGF binding and degraded in the endo-lysosomal system.

Using 2 different approaches this hypothesis was confirmed by Cohen and colleagues. The first was to couple EGF to a fluorophore, to test if the EGF molecule was being internalized. Fluorescence microscopy was employed to track EGF, at 0˚C EGF was observed bound to the membrane of

the cells[13]. When the samples were warmed to 37˚C there was internalization of the EGF consistent with the hypothesis that EGF receptor (EGFR) was being trafficked with the ligand into the lysosome. Proof of this hypothesis came when EGF was coupled to ferritin. By electron microscopy the trafficking of the ligand could be traced through the endocytic pathway. After 30mins free pools of ferritin were observed by electron microscopy, as the ligand was released from the degraded receptor[14].

These experiments produced two major findings. First they demonstrated that there was a receptor on the plasma membrane for EGF, the surface levels of which were controlled by EGF binding through the endo-lysomal system. Secondly, because the EGFR was taken into the cell bound to ligand, it suggests that this was one mechanism by which EGFR can reach intracellular targets. Indeed this point still has not been resolved today with numerous groups reporting conflicting information on the importance of EGFR signaling from the endosome, see section 1.2.4 for further discussion.

1.1.3. EGFR is a tyrosine kinase.

By 1978 application of EGF had been demonstrated to increase cell growth and induce changes in DNA synthesis[15, 16]. However, it still remained elusive how the EGFR was able to induce these changes. At the time there was mounting evidence that phosphorylation was an important regulator of metabolic processes and that kinases existed on the plasma membrane, leading to the hypothesis that EGFR may function as a kinase[17, 18]. In a landmark paper from Carpenter et al. (1978)[19], the authors demonstrated that EGFR was amenable to phosphorylation. They took membrane preparations of A-431 cells, which were known to express large quantities of EGFR and using P^{32}-ATP they demonstrated a substantial incorporation of P^{32} into the membrane fraction of A-431 cells after EGF application. When these membrane samples were run on SDS gels, multiple phosphorylated bands were observed by autoradiography, two prominent bands at 150 and 170kDa stood out[19]. Subsequent work identified the prominent bands as the receptor itself. One possibility from these experiments was that the EGF receptor was

both a kinase and the substrate. In support of this hypothesis, phosphorylation of the receptor could still be observed in affinity-purified preparations of EGFR[20, 21].

The next question was, what type of phosphorylation was this? In 1980 Tony Hunter and colleges demonstrated that $pp60^{SRC}$ was a tyrosine kinase[22] and in doing so demonstrated for the first time the existence of tyrosine phosphorylation. At the same time there was mounting evidence of the relatedness of $pp60^{SRC}$ to EGFR, as antibodies against $pp60^{SRC}$ specifically cross-reacted with EGFR, suggesting that they shared a similar structure[23] It had been originally reported that EGF receptor preferentially phosphorylated threonine residues[24], however this was artifact of the system used as threonine and tyrosine migrated at the same levels. After Tony Hunter and colleagues established a method to analysis pTryosine it became clear that EGF receptor was in fact a Tyrosine kinase[25].

1.1.4. The structure of EGFR

In 1984 Ullrich et al.[26] cloned the cDNA sequence of EGFR revealing it's primary structure. Partial sequences had been previously cloned by Downward et al. (1984)[27] indicating that there was a close similarity between the v-erb-B transforming protein and EGFR. The cloning of EGFR revealed a single pass transmembrane protein that was indeed highly homologous to v-erb-B. This was a major breakthrough for two reasons because it linked EGFR to a known oncoprotein encoded by a transforming virus, demonstrating a clear link between EGFR and cancer.

From the sequence of EGFR two distinct domains were identified, an extracellular EGF binding domain and an intracellular kinase domain, which is homologous to the *SRC* family of kinases. What's more, by cloning EGFR from pancreas cDNA and from A431 cells Ullrich et al. (1984)[26] identified that part of the EGF recognizing domain of EGFR was deleted (in A431 cells)[26], suggesting a mechanism by which the receptor activity is disconnected from the control of extracellular EGF. Also demonstrating for the first time a structural change in EGFR that was linked to development of cancer.

The identification of EGFR as a single pass trans-membrane protein raised a problem. How does EGF binding to the extracellular domain influence kinase activity of the intracellular domain? There was mounting evidence to suggest that EGFR could oligomerize and induce trans-phosphorylation. Yarden et al. (1987)[28] provided several lines of evidence for an allosteric activation of EGFR. By crosslinking EGFR derived from solubilized membrane extracts of A431 cells with monoclonal antibody (mAb), there was an increase in the phosphorylation of EGFR and in the affinity for EGF. Conversely immobilizing EGFR on solid matrices prevented EGF from inducing phosphorylation of EGFR. This demonstrated that trans- phosphorylation was required for activation of the receptor.

EGFR is part of a larger family of RTK called the ErbB family named because of their homology to the erythroblastoma viral gene[29]. There are four family members, ErbB1-4, that form a basic functional unit of a dimer[29]. The different monomers have differing signaling properties and ligands between different heterodimers, which increase signal diversity. ErbB1/EGFR recruits a number of scaffolds (Grb2 and SHC)[30], which recruit and activate downstream RAS and the MAPK cascades (discussed later in this chapter). Activated ErbB1 also recruits Cbl, an E3 ligase which ubiquitylates and triggers the internalization of the receptor[31]. ErbB1 receptor however, does not contain any sites, which directly activate AKT, but is activated via RAS. ErbB2 is the preferred partner for heterodimers and can be considered as a non-autonomous amplifier of the network as it is unable to directly bind EGF like ligands[32]. ErbB2 receptors also under go a slower rate of endocytosis and recycle back to the cell surface more frequently[33]. ErbB3 is kinase deficient but is however strongly tyrosine phosphorylated by hetro-dimerization. It lacks binding sites for Grb2 but can strongly activate PI3K signaling and is able to evade ligand-induced degradation[34]. ErbB4 shares many of the features of ErbB1, it is unclear whether it can recruit Cbl and it exhibits a slower rate of degrtion than ErbB1[33].

The question remained how was the oligomerisation of the receptor being driven. Was it through bivalent EGF bringing two receptors together or did EGF binding confer structural changes that increased the affinity of the receptors to dimerize? A clue for this mechanism is provided by the fact that hetrodimers of the ErbB family can be formed with ErbB2, which is not activated by any known EGF ligand.

It is now recognized that dimerization is a common feature of RTK activation[35]. There are some notable exceptions to this rule for example Inuslin receptor that forms a stable dimer. Growth factor induced dimerization through a bivalent ligand occurs in the RTK family members for example the VEGF receptor, in the case with EGFR ligand binding induces conformational changes which are more important[35]. The extracellular domain is split into 4 domains, crystallography studies have reveled that ligand binding unmasks a binding arm in domain 2, which is buried in an intermolecular interaction in domain 4 in unstimulated conditions, which is unique to EGFR within the family of RTKs. In an inactive confirmation the arm in buried by intramolecular interactions in a “tethered” confirmation, which is broken with ligand binding. When exposed the arm allows an EGFR molecule to bind to other ligand bound receptors (Figure 1.1)[36].

Structures of EGFR activation show that EGFR forms an asymmetric dimer where one receptor acts as an “activator” and the other as a “receiver”[37]. Contacts between the two receptors induce conformational changes in the N-lobe of the “receiver” receptor that disrupts auto-inhibitory interactions that are present in the monomer. These structural changes cause the “receiver” receptor kinase domain to adopt an active confirmation[37]. Providing supporting evidence for these structural studies, mutations in the auto-inhibitory interaction interfaces are found in non-small cell lung cancer patients (NSCLC)[38] and cause constitutive activation of the receptor without ligand binding[37].

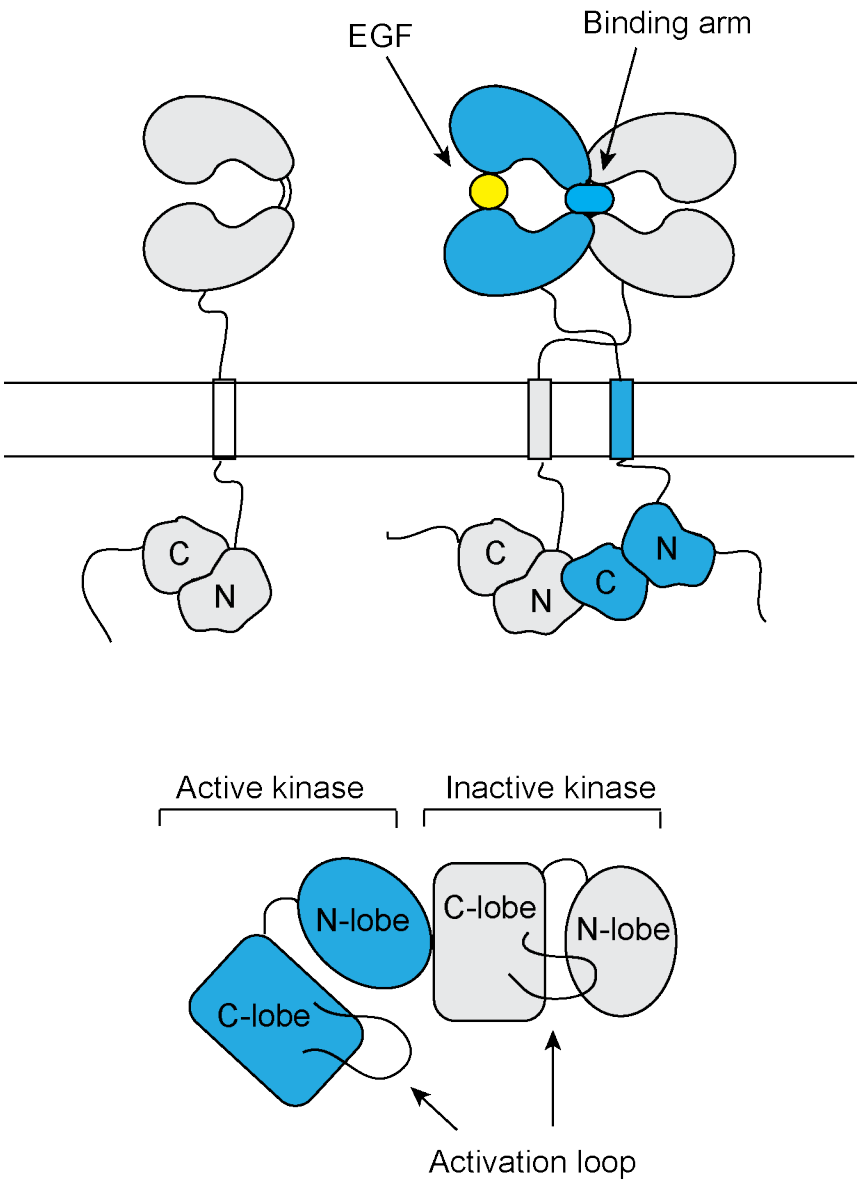

Figure 1.1. EGFR activation.

Ligand binding induces changes in the structure of EGFR that activates the intracellular kinase domain. Ligand binding exposes a binding arm unique to EGFR, which drives dimerization. The intracellular domain forms an asymmetric dimer; one molecule acts as an activator while the other acts as a receiver, contacts between the two receptors disrupt auto-inhibitory interactions that are present in the monomer and lead to the exposure of the activation loop.

Structural studies on the EGFR molecule in the 1990s and 2000s provide a mechanistic understanding of the EGFR. By studying EGFR in different disease states they helped establish EGFR as an oncogene and provided valuable insights for the development of therapeutics against EGFR. In many ways the development of inhibitors against EGFR has been a success story in the treatment of cancer, especially from the perspective of basic research, which played a key role in drug discovery. EGFR inhibitors are currently being used in the clinic but as I will discuss later in this chapter, there are still challenges and opportunities to exploit EGFR and downstream targets therapeutically.

1.1.5 The emergence of EGFR as a drug target

In the 80s and 90s there began to be compelling evidence to suggest that EGFR would be a good cancer drug target. EGFR had been linked with cell proliferation and demonstrated to be overexpressed in tumor cell lines[39]. The localization of the EGFR further increased interest, as a plasma membrane protein it was seen as particularly accessible to inhibitory mAb and small molecule inhibitors[39].

Work from Mendelson and Sato lab's was instrumental in establishing EGFR as a target to treat cancer. Gill et al. (1984)[40] developed a panel of mAb that inhibited the binding of EGF to the receptor by at least 95%. When applied to membrane extracts of A431 cells they inhibited EGF phosphorylation and when applied to human foreskin fibroblasts inhibited proliferation. In 1984 Masui et al.[41] raised another mAb against EGFR. Using a xenograft of A431 and T222 cells in athymic mice, they demonstrated that administration of the mAb prevented tumor formation. This had two important conclusions, first the amount of receptor on the membrane was not a determining factor of mAb inhibitory effects, as A431 cells had approximately 100 fold more receptors then T222, therefore EGFR inhibition was not limited to cases of overexpression. The second was the demonstration *in vivo* that mAb had anti-proliferative activity providing proof of principle for immunotherapeutic agents against EGFR. In 1989 Phase 1 trials were

initiated for mAb against EGFR[39]. The aims of the studies were to define toxicity and pharmokinetics of antibodies. Using radiolabelled antibodies the trials were able to confirm that antibodies reached sites of presumed metastasis. Importantly, patients treated with the anti-mAb displaced no toxicity over 3x 1-hour infusions, at levels that would be expected to saturate the receptors. Patients did however produce an anti-mouse immune response[39].

These studies laid the groundwork for development of humanized mAb therapy to treat EGFR driven cancers. Cetuximab (partially humanized EGFR mAb) was approved by the FDA for the treatment of colorectal cancer[42] and has since been approved for treatment of Head and neck cancer in 2006[43]. In 2006 FDA granted approval for a second immunotherapeutic therapeutic agent, Panitumumab (a fully humanized mAb) for the treatment of colorectal cancer[44].

1.1.6 EGF signaling: A layered network.

By the end of the 80s, research into the EGFR had reached a bottleneck. EGFR had been demonstrated to be a receptor tyrosine kinase but it was unclear how EGFR activation lead to increases in proliferation and differentiation. One possible explanation was through the observation that EGF caused changes in DNA synthesis[16] but how EGFR activation could affect process in cellular compartments distinct from its own was unclear. Work from Cohen's lab had documented that EGFR could enter the cell through the endo-lysosomal system[24], which was proposed to be one mechanism how EGFR could reach intracellular targets. But to causes changes in DNA synthesis it was clear that the must be processing steps, to stimulate changes in the nucleus.

During the 80s there was a rapid expansion in the capabilities of molecular biology techniques. From this there was recognition that the genes encoded in many transforming virus had cellular equivalents (such as CRAF and PLC-Y)[45]. These genes in turn became known as proto-oncogenes;

genes that had potential to become oncogenic factors. It is also frequently observed that when many of these the cellular equivalents where aberrantly expressed in cells, they caused similar effects as the transforming virus. These results lead to the hypothesis that proto-oncogenes that similar effects to vERB led to the hypothesis that they may all function as part of a larger network.

The first breakthroughs for this hypothesis came in 1989. A raft of papers identified that phospholipase-C-Ɣ (PLC-Ɣ) was tyrosine phosphorylated in response to PDGF or EGF stimulation[46]. Subsequent papers found an association between PLC-Ɣ and EGFR through its SH2 domain that was dependent on the activation of the receptor[47]. A second oncogene CRAF (also known as Raf-1) was also found to associate with PDGF receptor (PDGFR) in a ligand dependent manner. Importantly the interaction between CRAF and PDGFR could be reconstituted in a cell free system, were pre-treatment of the PDGFR with phosphatase prevented the interaction[48]. These and other papers introduced the concept that there was second messenger signaling downstream of RTKs.

Also during the 80s, there were major breakthroughs in the biochemistry of the RAS proto-oncogenes, which are signaling hubs tying together many signaling pathways. RAS are a family of small GTPases which are cyclically bound GTP and GDP, when in the GTP bound form an effector binding domain is exposed which is masked in its GDP bound form, this domain enables it assemble signaling complexes and act as a molecular switch. RAS families of proteins have intrinsic GTPase activity, which allows them to hydrolyze bound GTP with the help of GTPase activating protein (GAP). Satoh et al. (1990)[49] found the first direct link between EGFR and RAS; they were able to demonstrate that when cells were stimulated with EGF, RAS was found in a GTP bound (active) form. Furthermore they found that RAS mutated at G12V was insensitive to EGF and constitutively bound to GTP[49] as the mutation prevents GTP hydrolysis trapping RAS in it's active GTP bound form[50, 51].

In the following decades two canonical signaling pathways have emerged (although this is by no means the only signaling pathways that are downstream of EGFR). The PI3K-AKT (AKT) and RAS-RAF-MEK-ERK (MAPK) signaling pathways have been associated with many of the oncogenic effects of EGF signaling. Each pathway is comprised of a tier of kinases that are activated through phosphorylation and in turn phosphorylate downstream kinases (Figure 1.1). Both of these pathways, each converge on two master kinases AKT and ERK, which influence the regulation of apoptosis and gene transcription respectively. Each kinase is able to target transcription factors, which alter gene expression that drive cellular events[52].

During the late 1980s there were still questions about how protein networks were recruited through tyrosine phosphorylation. Work from Tony Pawson's laboratory identified a non-catalytic SRC homology domain in the v-Fps kinase (SH2)[53, 54]. SH2 domains were identified in distinct proteins whose common feature was that they were signaling proteins, which interact with tyrosine-phosphorylated proteins[55, 56]. SH2 domains emerged as a mechanism to explain how signaling proteins interact with tyrosine-phosphorylated proteins. Anderson et al.[56] demonstrated that SH2 domains of PLC-Y and SRC were critical for their interaction with EGFR[56]. This helped provide a framework for how networks of signaling proteins can be brought together through interactions with phosphorylated proteins.

The identification of downstream signaling greatly advanced our understanding how RTK exert their effects on the cell. It described how signaling networks could be mediated by tyrosine phosphorylation. In the next section I will discuss how one downstream signaling cascade, the MAPK pathway (Figure 1.1), has emerged as a driver of cancer and how detailed understanding of the pathway has lead to pharmaceuticals to treat cancer.

1.1.7. Negative regulation of EGF signaling

EGF signaling is a dynamic process and as such there are multiple levels of negative feedback[57]. Discussed here are 3 ways in which EGF signaling can be negatively regulated, through phosphatases, through transcriptional responses and scaffold proteins that hold kinases in inactive confirmations.

The kinase action of EGFR can be apposed by phosphatases, several phosphatases have been identified that directly dephosphorylate and inactivate signaling components downstream of EGF. Examples would be PHLLP[58] and PP2a[59] phosphatases that dephosphorylate AKT at position S473 a site, phosphorylated by mTOR and required for AKT to adopt an active confirmation and T308, opposing the activating action of PLCγ respectively. In the MAPK pathway PP1 and PP2A can directly dephosphorylate MEK kinase and dual specificity phosphatases (DUSPs) such as MKP3 can inactivate by apposing the activating action of ERK phosphylation as well as other MAPKs, JNK and p38[60]. Many of the DUSPs are immediate early genes (IEG), which are transcribed rapidly after MAPK action. In this way, action of ERK can establish negative feedback loops which attenuate MAPK signaling[61]. Unbiased approaches to identify phosphatases involved in oncogenic RAS signaling identified several additional phosphatases that contribute to MAPK and AKT signaling, such as PTPN2 and PTPRJ, however, the mechanism of action are yet to be established[62].

Phosphatases can be recruited directly to EGFR itself via SH2 domains which interact with pTry on the activated receptor such as, PTPN6 and PTPN11[35]. Phosphatases can also regulate EGFR activity by regulating internalization into MVBs, PTP1B is a tyrosine phosphatase located on the cytoplasmic face of the ER. It's localization means that endocytosis is required for an interaction with EGFR to be possible; therefore it allows its phosphatases action is restricted to a pool of EGFR that is undergoing ESCRT mediated sorting. Functional studies have confirmed this

demonstrating that PTP1B activity is required for sorting of EGFR into MVBs[63].

In addition to kinase and phosphatase there are a several other inhibitors of EGF signaling which regulate signaling complexes. The RAF kinase inhibitor protein (RKIP) is an example of a scaffolding protein that inhibits interactions between RAF kinase and downstream MEK kinases[64]. Sproty (SPRY) is another example of a negative regulator that can regulate signaling by interfering with formation of Grb2-SOS complex downstream of EGFR (figure 1.1)[57, 65-67].

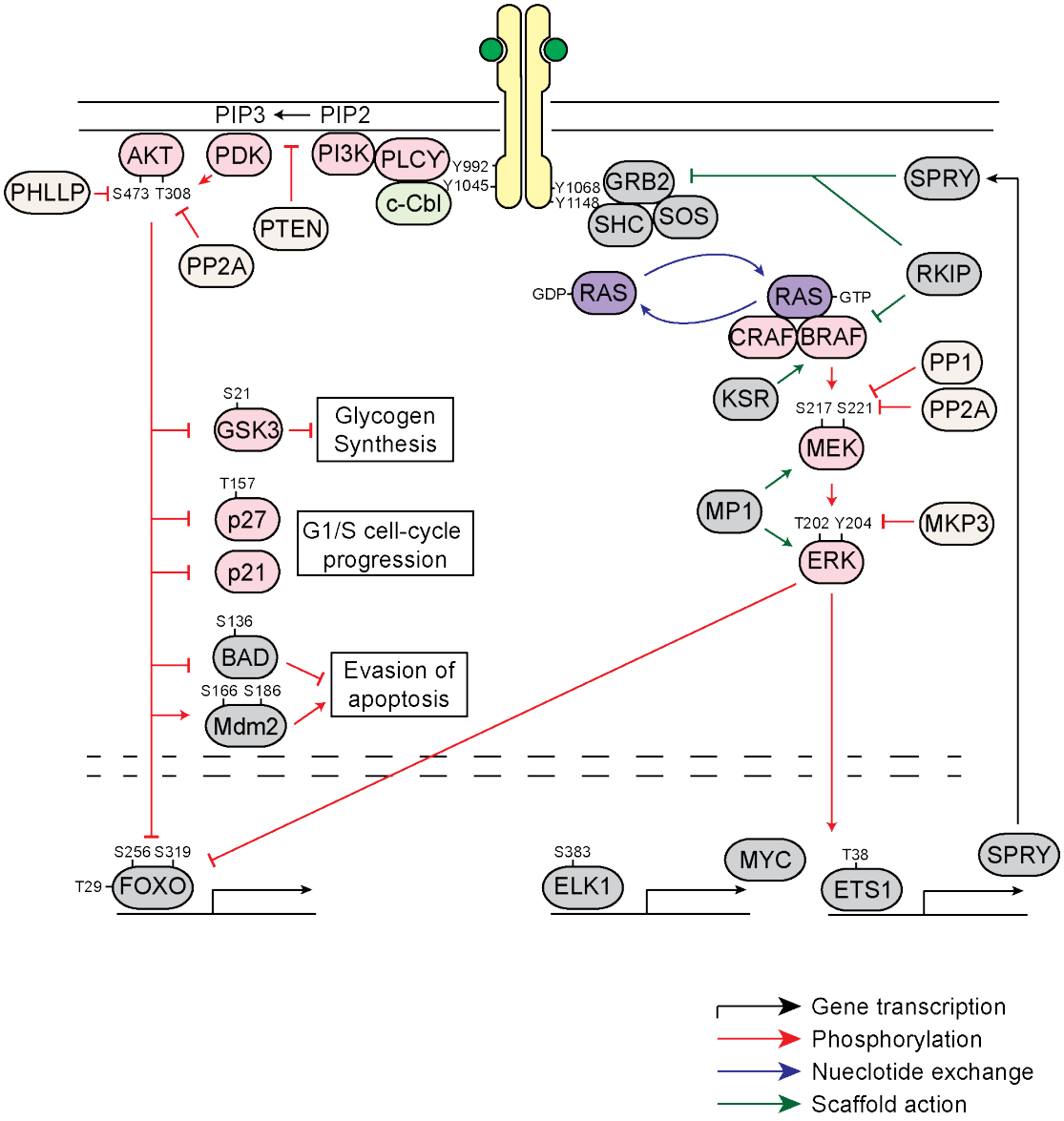

Figure 1.2. The EGF signaling cascade.

EGF binding to its receptor at the plasma membrane initiates an activating auto-phosphylation event, which then initiates downstream signaling cascades. Activating phosphylation events can be apposed by phosphatases. Numerous scaffolds have been identified which can play both positive and negative regulating cell signaling. The two canonical pathways downstream of EGFR are annotated here, the RAS-RAF-MEK-ERK pathway which drives changes in cell proliferation through changes in gene transcription and the PLC-γ-PI3K- AKT pathway that drives changes in survival.

1.1.8. The MAPK pathway: A driver of cancer.

There has been a rapid increase in our understanding of how downstream signaling from the EGFR contributes to cancer in the last decade. The MAPK cascade has become a good example of where a molecular understanding has enabled the development of personalized medicine to treat cancer. As with the EGFR pharmacological intervention of the MAPK pathway has provided both opportunities and challenges.

In 1999 Hoshino et al.[68] demonstrated using phospo-specific antibodies against activated ERK 1/2, that hyper activation of the MAPK pathway occurs in approximately 35% of tumor cell lines tested. Interestingly a tissue specific pattern emerged from the study; hyperactivation was frequently observed in pancreas, colon, lung, ovary and kidney but infrequently observed in brain, stomach, liver and cells derived from hematopoietic origin also had a lower frequency. Hyperactivation of ERK 1/2 was correlated with activation of CRAF and MEK, even in cases with no RAS mutation[68]. This indicated hyperactivation was not necessary due to mutation of the MAPK or RAS but rather due to deregulation RAF/MEK kinases (Figure 1.1).

It has been long known that components of the EGF signaling pathway could transform cells from work on transforming viruses (v-RAF, v-SRC, vERB)[45]. However there remained questions as to whether these exogenous forms of EGF signaling proteins were endogenously misregulated in cancer. Activating mutations in the EGFR signaling pathway were known since the cloning of EGFR from A-431 cells and since then approximately 15% of tumors have been demonstrated to carry activating RAS mutations[26]. In 2002 Davies et al.[69] demonstrated that BRAF was mutated in approximately 66% of melanomas and at lower frequency in other cancer types. Other cancer types with significant levels of BRAF mutation are papillary thyroid cancer (36%-53%) and colorectal cancer (5%-22%)[69]. In melanoma mutations all fell in the kinase domain of BRAF, the most common mutation being $BRAF^{V600E}$ [70]. $BRAF^{V600E}$ mutants are 500 times more activate in vitro[71] and in NIH3T3 cells

stimulated proliferation and transformation through constitutive activation of ERK[72]. This highlighted tissue specific EGF signaling mutation.

In vivo $BRAF^{V600E}$ mutations are commonly found in benign skin lesions known as naevi and in premalignant polyps in the colon[73]. Using a knock-in $BRAF^{V600E}$ mouse, which was expressed from one of the endogenous allele, the Marais lab demonstrated that conditional expression $BRAF^{V600E}$ induced the formation of naevi and induced melanocyte senescence[73]. This study established BRAF mutation as a founder event in the development of melanoma. Mice expressing $BRAF^{V600E}$ developed melanoma more quickly than mice expressing H-RAS^{G12V} after 6 months. 3% of H-RAS^{G12V} expressing mice versus 11% of $BRAF^{V600E}$ expressing mice, developed melanoma by 6 months. After 14months 64% of mice expressing $BRAF^{V600E}$ had developed melanoma [73]. The study suggested a model were $BRAF^{V600E}$ could induce the formation of naevi and melanocyte senescence, however another gene mutation would then be needed to overcome the senescence.

BRAF emerged as an oncogene in melanoma with had pharmacological potential. Work studying the molecular biology and structure of BRAF in the last decade has led to the development of BRAF kinase inhibitors to treat melanoma that are proving successful in the clinic, for a disease which there has been little pharmacological success[74]. This work also provides a paradigm for how studying the molecular biology of EGF signaling cascade, has unveiled drug targets in tissue specific cancers.

1.1.9. The development of tyrosine kinase inhibitors: New opportunities and challenges.

During the late 80s and 90s there was overwhelming evidence for the importance of kinases in the regulation of cancer-associated pathways. However there was resistance from many to the notion of kinase inhibitors largely because a perceived notion that it would be difficult to achieve sufficient specificity[75]. Secondly because the intracellular concentration of ATP was very high (mM range) raising questions over whether drugs could by

developed with sufficient affinity to overcome this. Although are still very real challenges, however both of these problems have been overcome through exploiting additional hydrophobic pockets that exist around the ATP binding pocket[75].

In 1988 Yaish et al.[76] synthesized the first tyrosine kinase inhibitors. They were able to develop a number of compounds showing specificity towards EGFR with three orders of magnitude compared to the insulin receptor. Importantly a number of the compounds effectively retarded EGF dependent cell proliferation in A431 cells. This study provided a proof of principle, that small molecule inhibitors of tyrosine kinases could be an effective way of inhibiting EGF dependent proliferation.

Exploiting the known structure of EGFR, Ward et al. (1994)[77] developed new classes of tyrosine kinase inhibitor. It had been found that EGFR formed a ternary complex with ATP and the substrate proteins. EGFR interacts with the protein substrate at Arg^{817} through a carboxylate group which deprotonates the tyrosine hydroxyl of the substrate, activating it as a nucleophile. The activated tyrosine group is then able to attack the Ɣ-phosphorus of ATP. Ward et al. (1994)[77] devised a strategy to search compound libraries for structures that would mimic ATP Ɣ-phosphate, tyrosyl hydroxyl and tyrosyl aromatic ring, which all interact tightly with the enzyme during catalysis. Using this strategy 4-(3-chloroanilino) quinazoline (CAQ) was identified as a competitive inhibitor of ATP binding to EGFR. This strategy of targeting the ATP binding pocket of kinases has since become a favored strategy by many pharmaceutical companies when designing kinase inhibitors[75].

Imatinib was the first tyrosine kinase demonstrated to be clinically effective. Imatinib was designed as a treatment chronic myeloid leukaemia (CML) a disease characterised by a translocation between the long arms of chromosomes 9 and 22. This results in a fusion protein of BCR-ABL a constitutively active tyrosine kinase receptor that is able to drive CML and is dependent on the tyrosine kinase activity of the BCR-ABL. The first phase 1

trial for Imatinib in patients with CML reported potent antileukemic effects. Kinase inhibitors have now been produced against several target kinases and have been improved for the treatment of various cancers.

Gefitinib another tyrosine kinase inhibitor that targets EGFR, has been developed and approved for the treatment of non-small cell lung cancer and colon cancer. Vemurafenib another competitive ATP antagonist has been developed and was approved by the FDA in 2011 for treatment of unresectable or metastatic melanoma were the patient is harbouring a $BRAF^{V600E}$ mutation. The development of these inhibitors has demonstrated that rational design and application of tyrosine kinases could be used to treat cancer. However a trait seen with many kinase inhibitors is the emergence of resistance after prolonged treatment and intrinsic resistance in caused by different genetic backgrounds. These challenges represent some of the biggest hurdles today in developing effective drugs to treat cancer.

1.1.10. Overcoming resistance

There are multiple mechanisms underpinning resistance to inhibitors. They can be split into intrinsic mechanisms, where different genetic backgrounds produce unanticipated effects and acquired mechanisms. An acquired mechanism is were cells gain new mutations to develop resistance. A common mutation seen in kinases is the mutation of the gatekeeper threonine residue, which has been exploited by many kinase inhibitors for specific binding in the ATP binding pocket[78]. One of the disappointing features of BRAF and MEK kinase inhibitors has been the rapid onset of resistance[79]. Detailed molecular studies have addressed why some patients and cancers types with activating BRAF mutations, do not respond well to BRAF inhibitor.

BRAF activating mutations are also common in colon cancer but patients are largely unresponsive to BRAF inhibitors. Using a siRNA screen to identify secondary targets that could sensitize colon cancer cells lines to BRAF inhibitors Prahallad et al. (2012)[80] identified EGFR as target. With further investigation the authors found that BRAF inhibition was causing a

feedback loop by driving the suppression of CDC25C, a phosphatase that negatively regulates EGFR. This in turn caused an increase in the activity of EGFR and downstream signaling through the AKT signaling pathway. This mechanism of resistance is not seen with melanoma cells due to the differences in expression levels of EGFR, colon cells express EGFR at high levels while melanocytes express EGFR at relatively low levels[80]. This study provides another example of the benefits of dual therapy in overcoming resistance to kinase inhibitors.

Probably the best-characterized example of resistance to BRAF inhibitors is the so-called BRAF inhibitor paradox. The underlying principle to this resistance is attributed to the mechanism of activation of the RAF kinases. RAF kinases are activated through dimerization; this can be through heterodimers that are combinations of ARAF, BRAF, CRAF and the RAF like pseudo-kinase KSR[81]. Activation is not driven through trans-phosphorylation but rather dimerization cause RAF kinases to adopt an active confirmation that is then stabilized by phosphorylation[81]. This effect is highlighted by the oncogenic $BRAF^{E558K}$ mutation that falls outside the kinase domain. Instead functioning by promoting dimerization with, and activation of CRAF.

In Melanoma cell lines that harbor mutations in NRAS (20%) or KRAS (2%) inhibition of BRAF results in a paradoxical activation of MAPK signaling. A raft of papers in 2010 detailed the molecular mechanism that underlies this paradoxically activation[82-84]. In the presence of oncogenic RAS, BRAF is maintained in an inactive confirmation in the cytosol through an auto-phosphorylation event. When the kinase activity of BRAF is inhibited, oncogenic RAS now promotes its recruitment to the plasma membrane where it can form heterodimers with CRAF and act as a scaffold promoting MAPK signaling through CRAF[84].

Dysregulation of the EGF signaling pathway is major factor in the pathogenesis of many cancers. Pharmaceuticals have been developed to modulate the EGF signaling pathway, which are now having success in the clinic. However, as with many anti-cancer therapies, drugs resistance is a

major issue, the strategy of dual therapy is one potential avenue to overcome resistance. Future therapeutic strategies will rely on understanding the mechanisms of modulators of pathways and cross-talk between pathways.

1.2. Control of EGFR endocytic trafficking and signaling by reversible ubiquitylation.

1.2.1 Ubiquitin

Ubiquitin is a 76 amino acid polypeptide that is attached to a substrate through the sequential action of E1, E2, E3 cascade. Ubiquitin moieties are covalently attached to a substrate via an isopepide bond, between a lysine molecule of the substrate and the COOH terminus of ubiquitin[85]. Ubiquitin is conjugated to a substrate in a three step process, first ubiquitin in adenylated and conjugated to an E1 enzyme via a thioester bond to the catalytic cysteine residue. The ubiquitin is then transferred onto an E2 enzyme that binds the ubiquitin via a second thioester bond. The ubiquitin molecule can then be either directly transferred onto a substrate with the aid of a RING E3 ligase[86] or transfer the ubiquitin onto a HECT E3ligase, which then transfers the ubiquitin onto the substrate (figure 1.2)[87]. E3 ligases are the more numerous than the E1 or E2 components and form the substrate-recognizing component of the system.

A single ubiquitin molecule can be extended to a chains of ubiquitin built from any of the 7 internal lysines of ubiquitin. This allows chains with different topologies to be built. The nature of these chains means that they adopt different steric distributions producing additional levels of complexity[88]. Building chains of ubiquitin has two major advantages over mono-ubiquitylation; it increases the avidity between the ubiquitylated protein and the ubiquitin interacting protein. Secondly, it adds an additional layer of specificity, as each chain linkage can encode different signals, the complexity of ubiquitin chains can be further complicated by the existence of mixed and branched chains[89]. For this reason ubiquitylation can be thought of as a more

complex signal than phosphorylation. Quantitative mass spectrometry studies in Hek293t cells have demonstrated that Lys48 (52%) and Lys63 (38%) are the most abundant chains in the cells. While Lys29 (8%), Lys11 (2%) account for significant populations, Lys6, Lys27, Lys33 and linear ubiquitin represent 0.5% or less of the total population of chains[90]. However, it should be noted that abundance of chains is not necessarily linked to importance, for example linear chains play an important role in regulating the NfKB pathway[91, 92].

1.2.2. The Function of proteasomal DUBs

The proteasome is a major site for degradation of proteins in the cell[93]. It primarily recognizes substrates via ubiquitin chain linkages and has a preference to bind mutli-ubiquitinylated proteins[94]. It is a large multimeric complex composed of a regulator 19s particle and a core 20s particle formed from a stack of ATPase ring complexes in a barrel shape. Substrate proteins are captured by the regulatory protein and translocated into the central pore of the regulatory core where they are hydrolysed[94]. In order for substrate proteins to be transferred into the 20s core particle proteins need to be unfolded to enable them to pass through tight pores between the stacks of ATPases. Unfolding is generally performed within the 20s particle and translocation and unfolding are generally considered coupled events[94].

In eukaryotes there are 3 DUBs that are associated with proteasome, UCHL5, RPN11 and USP14. The DUBs perform 2 major functions to regulate the substrate-proteasome interaction and to maintain the cellular levels of ubiquitin[94]. In *S. Cerevisiae* deletion of Ubp6 the ortholog of USP14 causes pleiotorpically stress-sensitive as a consequence of ubiquitin depletion[95]. The proteasomal DUBs each belong to separate families (UCH, JAMM and USP respectively) and have distinct evolutionary origins. The deubiquitylating activity of RPN11 promotes degradation of substrates[96], ubiquitin is a very stable proteins and retains its structure even with large fluctuations in pH and heat, therefore ubiquitin chains need to be removed before the substrate can pass through the central pore and be hydrolyzed[97]. In contrast to RPN11, siRNA mediated depletion of UCHL5 and USP14 increases the rate

degradation of substrates[98, 99]. The activity of RPN11 is thought to occur once a substrate has been committed to degradation while the activity of USP14 and UCHL5 is thought to occur once the substrate is docked onto the 19s regulatory particle[94]. The second distinction is that RPN11 differs for the other two in that it is able to cleave at the base of ubiquitin chain where UCHL5 and USP14 trim from the distal end of the chain. Increased chain length increase the affinity between the chain, it has been proposed that by trimming the length of the chain from the distal end, UCHL5 and USP14 can fine tune the life-time of the proteasome-substrate interaction[100]. USP14 and UCHL5 also have non-catalytic activities at the proteasome. Binding of ubiquitin to USP14 and UCHl5 can open the gate of the 20s particle[101] and can stimulates the activity of ATPase activity of the proteasome[102].

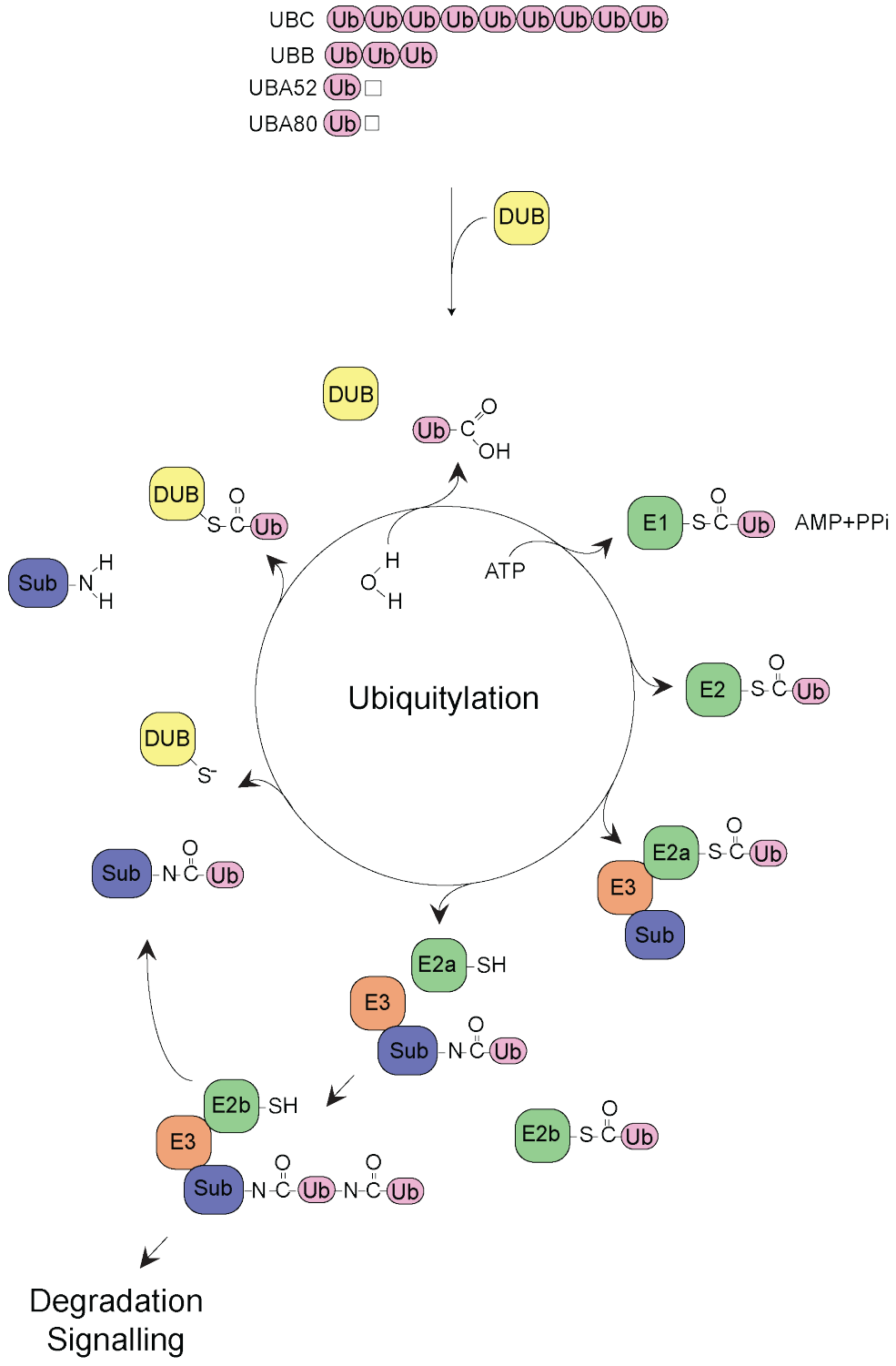

Figure 1.3. The ubiquitylation cycle.

Ubiquitin is encoded by 4 separate genes ubiquitin is transcribed as a fusion protein and needs to be processed by deubiquitylases (DUBs) to produce free ubiquitin. Ubiquitin is conjugated to a substrate by the sequential action of E1, E2, E3 cascade. This is apposed by the action of DUBs.

1.2.3 Endocytosis of EGFR

The surface expression of many plasma membrane proteins such as EGFR is regulated through the endo-lysosomal pathway. It has been known since the 1970s that activated EGFR is internalized and degraded via the lysosome[12]. This couples the control of plasma membrane levels of EGFR to the extracellular concentration of EGF and prevents excessive signaling. Reversible ubiquitylation is an important mediator of EGFR trafficking. Ubiquitylation is a reversible post-translational modification that can regulate the degradation of proteins at all the major sites degradation in the cell[93].

Activated EGFR is ubiquitylated and internalized either via clathrin-coated vesicles or through clathrin independent mechanism[103]. The route of internalization appears to be dependent on the concentration of the EGF the cells are exposed to[103]. Upon receptor activation c-Cbl an E3 ligase is recruited and ubiquitylates EGFR. The receptor is then internalized and delivered to the sorting endosome via direct fusion of the transporting vesicles. Where mono-ubiquitylation can mediate the internalization of the receptor, Lys63 linked chains are required for the sorting of cargo at the endosome[104]. Once EGFR reaches the sorting endosome, there are two fates that are possible, either the receptor is trafficked back to the plasma membrane via the recycling endosomes or it is internalized in the intra-luminal vesicles (ILV) in the multi-vesicular body (MVB). Internalization into ILV is mediated through the ESCRT complex[105]. ESCRT0 component recognize ubiquitylated proteins via ubiquitin interacting motifs and through sequential action of the ESCRT machinery, trans-membrane proteins are internalized into ILV. Internalization of cargo into ILV is often seen as the point of no return. MVBs are then able to fuse with lysosome releasing their contents into the lumen of the lysosome (figure 1.2)[105].

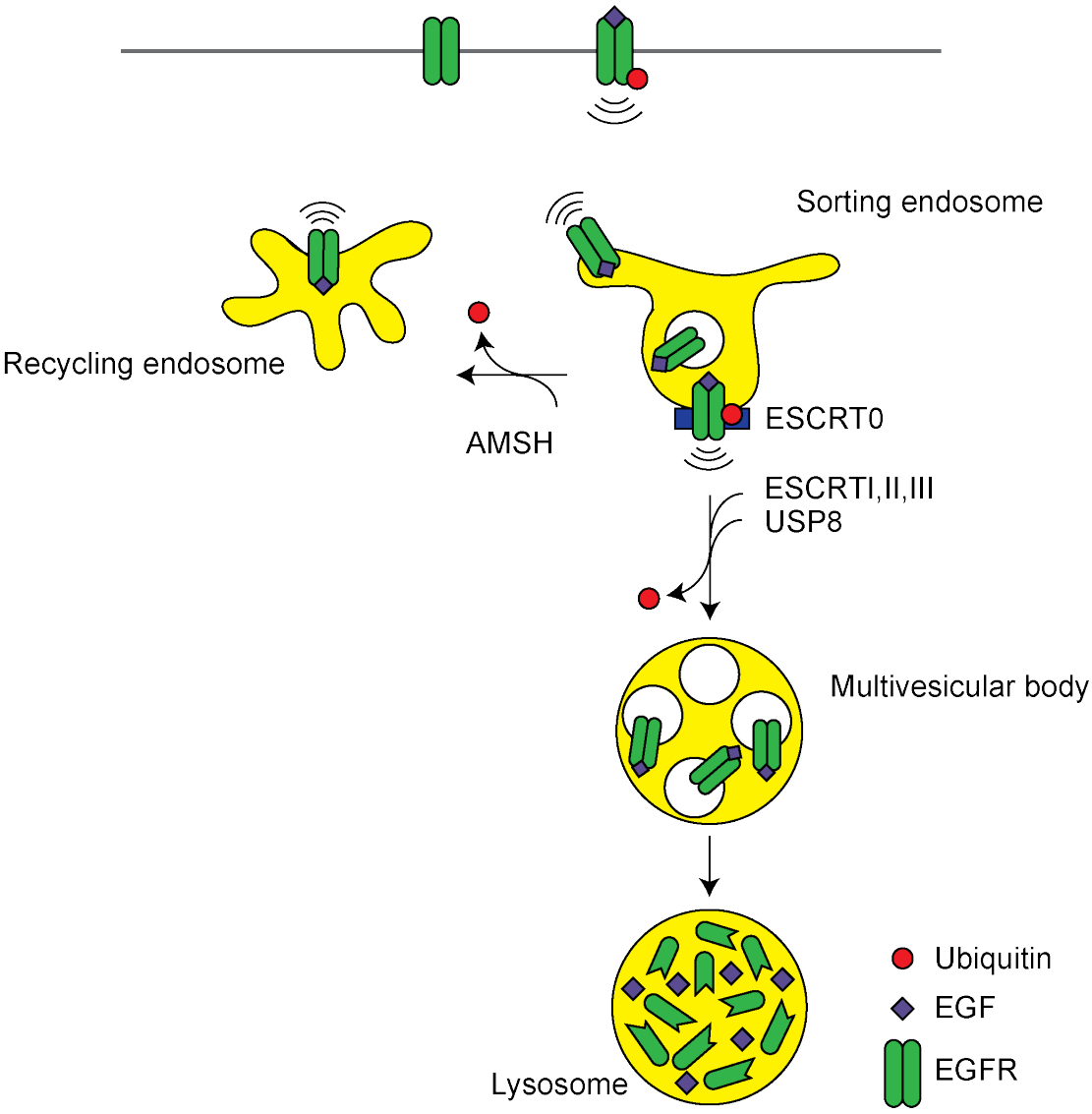

Figure 1.4. The endocytic pathway.

Activated EGFR is internalized into the endocytic compartment. Once EGFR reaches the sorting endosome there are two outcomes, either the receptor is recycled back to the plasma membrane or the receptor is recognized by the ESCRT complex and internalized into intra luminal vesicles of the multi-vesicular body (MVB). The MVB can then fuse with the lysosome transferring its contents. The receptor is degraded in the lysosome by lysosomal proteases. The DUB ASHM removes Lys63 ubiquitin chain from EGFR rescuing it from lysosomal degradation. The ESCRT machinery recognizes and internalizes ubiquitylated EGFR in ILVs, this process is aided by USP8.

Conjugation of a single molecule of ubiquitin to a membrane protein is sufficient to induce internalization and targeting to the MVB. However, Lys63 linked chains can more efficiently sort proteins[89]. Mass spectrometry studies have implicated all chain configurations to some extent in targeting proteins for degradation by the proteasome, except for Lys63 chains, which are generally thought to implicated in non-proteasomal functions of ubiquitin and Lys63 are not accumulated after proteasomal inhibition[90]. Comparisons of Lys63 versus mono ubiquitylation on the trafficking of GAP1 permase reveled that mono-ubiquitylation is sufficient to trigger internalization but Lys63 ubiquitylation was required for sorting at the MVB[106]. Furthermore, Huang et al. (2013)[104] generated chimeras of EGFR and AMSH (Lys63 specific deubiquitinases) which had depletion in the levels of conjugated Lys63 chains and a modest increase in mono-ubiquitylation and Lys48 chains compared to the wild type EGFR. The chimera could still undergo internalization but there was delay in receptor degradation and an increase in MAPK signaling, providing direct evidence for the importance of Lys63 chains in endosomal trafficking of EGFR[104].

1.2.4 ESCRT pathway

The formation of MVBs is a key step in the sorting of cargo into lysosomes. George Palade and Keith Porter first reported the existence of MVB, describing them as “two large vesicles with smaller vesicles inside”[107, 108]. Later work, described previously in this chapter by Stanley Choen and colleagues described how stimulated EGFR receptor was internalized into MVBs but it wasn’t until 2001 that the Endosomal Sorting Complex Required for Transport (ESCRT) were determined[109]. First ESCRT complex to be identified was ESCRT-I[109] and a year later two papers were published describing ESCRT-II and ESCRT-III[110, 111].

In total there are there are 5 ESCRTs, which have two major functions first to recognize and sort cargo into the ILVs and secondly to form ILVs through the deformation of lipid membranes. The ESCRT complexes can be

broadly split into three steps[112]. ESCRT-0 is the cargo recognition component, ESCRT-II brings ESCRT-III is involved in the maturation of the ILV and recruitment of DUBs to deubiquitylate cargo and finally VPS4 disassembles the complex from the membrane[112].

Ubiquitin is an important signal for the sorting of cargo into MVB and to this end multiple components of the ESCRT machinery (ESCRT0, I and II but not ESCRT III) contains distinct ubiquitin interacting motifs[113]. The Ubiquitin interacting motifs are low affinity ranging from 100μM-500μM, ESCRT0 posses multiple ubiquitin interacting motifs which facilitates it's function as a cargo recognition complex[113]. ESCRT0 is composed of two subunits in eukaryotes, HRS and STAM1/2, HRS contains UIM domain composed of a single alpha-helix that can interact with two molecules of ubiquitin. ESCRT-I binds Ubiquitin through an ubiquitin E2 variant (UEV) domain which has a similar structure to E2-ubiquitin conjugating enzyme[114, 115]. Most ubiquitin binding domains recognize the Lle44 hydrophobic patch of ubiquitin, UEV domain however can recognize an additional hydrophilic patch based around Gln62 of ubiquitin[115]. ESCRT-II is able to recognize ubiquitin via a GLUE domain that binds ubiquitin along the edge of beta sandwich motif. ESCRT proteins also contain domains that allow them to bind with clathrin which aids in cargo recognition[116].

1.2.5. Ubiquitin interacting domains

The ubiquitin conjugating system can be thought of as the writer. The reader in which decodes ubiquitin signals are ubiquitin interacting motifs (UIM). Most UIM-ubiquitin interactions are mediated through the hydrophobic patch on ubiquitin Leu8, Ile44 and Val70 in the beta sheet of ubiquitin. As most UIM target the same surface of ubiquitin the specificity is defined by the chain topology[117]. In solution different ubiquitin chains topologies can adopt different states with and chains can fluctuate between different states. The equilibrium between different states can be driven in a specific different direction by UIM motifs, which trap ubiquitin chains in different states[118]. For example linear and Lys63 linked chains adopt an open confirmation while

Lys48 chains adopt a closed confirmation. This provides a rational for understanding how different chain topologies can generate different signalling outcomes.

Hrs (Hepatocyte receptor substrate) is a member of the ESCRT 0 complex. Hrs recognizes ubiquitylated cargo entering the sorting endosome through an UIM. Hrs concentrates ubiquitylated material on the limiting membrane of the sorting endosome via its UIM and engages ubiquitylated cargo with the ESCRT machinery. Deletion of the UIM in HRS and depletion of HRS prevents the internalization of EGFR and into the lumen of MVBs[119].

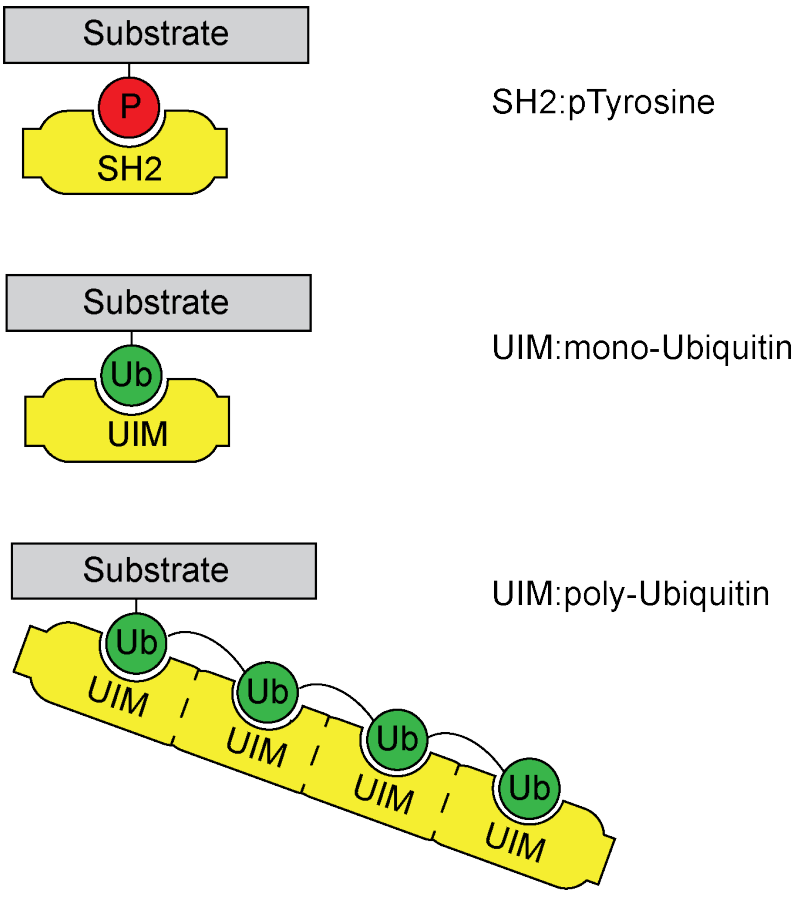

Figure 1.5. SH2 and UIM interacting domains

SRC homology 2 (SH2) domains mediate interactions between tyrosine-phosphorylated proteins and their interactors. Ubiquitin interacting motifs (UIM) mediate interactions with ubiquitylated proteins and their interactors; avidity of the ubiquitin:interactor binding can be increased by additional UIM domains that can bind to chains of Ubiquitin.

1.2.6. The importance of endocytosis for EGFR signaling.

The signaling function of EGFR internalization has been the subject of intense debate since its discovery in the 1970s. The topology of the receptor means that the kinase domain will face the cytosol during the internalization and can bind downstream signaling molecules until it is internalized into intra-luminal vesicles of MVBs and the kinase domain is finally sequestered away from the cytosol. Experiments to elucidate the relationship between endocytosis and signaling have been complicated by the fact that receptor activation effects endocytosis and that many signaling proteins also have endocytic functions. This makes it difficult to design experiments that perturb one system and not the other[120].

Endocytosis can attenuate EGFR signaling in a number of ways. By regulating the abundance of EGFR at the plasma membrane, endo-lysosomal pathway can directly influence the strength and duration of EGFR signaling. Receptor down regulation may not determine the maximal signaling but can shift the dose response curves so that a higher concentration of ligand is required to reach achieve a maximal response. Endocytosis can also remove the EGFR away from its downstream effectors[120]. PI3K signaling is increased through disruption of endocytosis because the components of the PI3K are localized to the plasma membrane; internalization of EGFR physically removes EGFR and decrease EGFR signaling[121]. Counter this MAPK scaffolds are recruited on the endosomes and can maintain signaling from this compartment[122, 123].

The consequence of endosomal signaling is not fully understood. Studies analyzing gene transcription downstream of EGFR, found little difference on the transcription profile in cells depleted of Hrs to retain EGFR on the limiting membrane of MVBs. Conversely depletion clathrin heavy chain and dynamin 2 to prevent internalization of the receptor internalization caused an increase in the transcriptional out put of EGF pathway[124]. Using phospho proteomics Omerovic et al. (2013)[125] found that 40% of EGF responsive phospho site were sensitive to inhibition of endocytosis, however, this means

that the majority of sites were unaffected by inhibition of endocytosis[126]. After decades of research on this question the true significance of EGFR signaling from the endocytic compartment is still not fully understood due to limitations in technology.

1.2.7. DUBs in EGFR trafficking.

Ubiquitylation is apposed by the action of group of enzymes known as deubiquitylase (DUB) that catalyze the removal of ubiquitin from a substrate. Deubiquitylase perform 3 major functions in the cell, the first is to process ubiquitin that is transcribed as linear fusion protein with multiple copies of ubiquitin or fused to a ribosomal protein. The second is to maintain cellular pools of ubiquitin by removing ubiquitin from proteins committed to lysosomal or proteasomal degradation. Finally, DUBs function to rescue proteins from degradation by removing ubiquitin before a commitment to degradation (figure 1.3)[127].

There are approximately 90 DUBs encoded in the genome that are split across 5 families, Ubiquitin specific proteases (USP), ovarian tumour proteases (OTUs), Ubiquitin carboxy hydrolases (UCH), Josephins (JOS), and the JAB1/MPN/MOV34 family (JAMM). The first four are cysteine proteases while the JAMM family are metalloproteases and they differ in there mechanism of action, see Clague et al. 2013[128] for a review addressing this. A number of DUBs have been implicated in the trafficking of plasma membrane proteins, traversing the endo-lysosomal pathway. The two best characterised endosomal DUBs are AMSH and USP8[105].

AMSH is a Lys63 specific DUB belonging to the JAMM family. A proportion of AMSH is localised on the endosome, with pools in the cytosol and nucleus[129]. However, only endosomal functions of AMSH have been reported to date. Depletion of AMSH via siRNA leads to an increase in the rate of degradation of EGFR[129]. AMSH has been proposed as a mechanism for rescuing incoming ubiquitylated proteins into the sorting endosome and owing to its specificity, it is unlikely that AMSH plays a role rescuing proteins

from proteasomal degradation. AMSH knockout mice die after 3 weeks, and display a loss of hippocampal neurons and atrophy in the cerebral cortex reminiscent of EGFR knockout mice[130]. A homolog to AMSH, AMSH-lp, also has an endosomal localisation and like AMSH has specificity for K63 chains. Endosomal functions of AMSH-lp are relatively unexplored with early studies suggesting that AMSH and AMSH-lp will have separate roles on the endosome[131].

USP8 belongs to the USP family of DUBs and shows no preference for any chain linkage. USP8 has an endosomal localisation that shows a dependency on the activation of EGFR; under serum starvation conditions USP8 is largely cytosolic and is recruited onto endosomes with EGF stimulation[132]. Depletion of USP8 causes an accumulation of cellular levels of ubiquitin and predominantly on endosomes as judged by immunofluorescence[133]. However, there is conflicting evidence on the phenotype of depletion of USP8 on the rate of degradation of EGFR is dependent on the degree of and time of depletion. Some researchers reporting an increase in EGFR degradation with USP8 depletion[134], while other researchers, including work from our laboratory[132, 135, 136], have shown a delay in EGFR degradation with USP8 depletion. This delay in degradation is coupled with a loss of the ESCRT0 complex and ultrastructural studies have indicated there is a delay in the sorting of EGFR into ILV with USP8 knock down. This effect appears to be a delay in sorting and after a longer time most EGFR is trafficked to the lysosome[137]. USP8 has been identified as a drug target to overcome Gefitinib resistance in lung cancer[138]. But there still remain questions about how USP8 affects EGFR trafficking and this can how best this can be exploited pharmacologically.

USP2a is another DUB that has been localised to the early endosomal compartment using immunofluorescence and cell fractionation. Overexpression studies of USP2a indicate that USP2a prevents the recycling of EGFR in Rab11 positive endosomes[139]. Other DUBs that have not been reported as endosomal can also influence EGFR trafficking. In a family wide siRNA screen to identify DUBs that increase the rate of EGFR degradation.

Cezanne was identified; Cezanne specifically regulates the degradation of EGFR and not another RTK c-MET and depletion of Cezanne leads to a decrease in the ubiquitylated species of EGFR[140]. However, the localisation of this interaction is unclear, as Cezanne has been reported to have a non-restricted localisation. USP12 and USP46 are two highly related DUBs that have both been implicated in the trafficking of plasma membrane proteins, Notch receptor[141] and GluR1 respectively[142], through the endo- lysosomal pathway. What is not clear is if USP12 and USP46 specifically regulate notch and GluR1 trafficking respectively or if they play more general roles in endocytic trafficking.

Ubiquitylation is an important mediator of endocytic trafficking of EGFR. While endo-lysosomal trafficking of EGFR is crucial to regulate the plasma membrane levels of EGFR, it is still not clear what is the signalling significance of EGFR trafficking. Several DUBs have now been identified as regulator of plasma membrane trafficking. However, there are still questions over the specificity and mechanisms of action.

1.3. Retrograde trafficking.

Internalisation in the ILV of the MVB is often viewed as the point of no return before degradation in the lysosome[89]. Recycling of proteins via retrograde transport from the MVB to the TGN, provides one mechanism to prevent lysosomal degradation[143]. Retrograde transport has been implicated in various pathologies and the pathway is utilised by pathogens such as HIV and toxins such as Shiga, cholera and ricin[144]. Components of the pathway are mutated in a subset of Parkinson's disease and diabetes patients[145 146]. One of the best-characterised physiological roles for retrograde transport is the delivery of newly synthesised acid hydrolases from the TGN to endo-lysosomal pathway. Acid hydrolases are actively sorted at the TGN by the mannose 6-phosphate receptors (M6PR) and delivered to the endosomes via clathrin-coated vesicles. The receptor is then trafficked back the TGN through the retrograde pathway allowing it to pick up more cargo, if the retrograde trafficking pathway is disrupted then there is no longer active sorting at the

TGN and the acid hydrolases are secreted into the extracellular environment via bulk flow[147].

The components that are required for the different aspects of retrograde trafficking are beginning to be identified. For retrograde transport to occur there needs to be several steps, cargo recognition, tubulation of the membrane, scission of the membrane and endosomal budding (figure 1.4.)[148]. The cargo recognition components of the retrograde pathway were identified through genetic screens in *Saccharomyces cerevisae,* characterising vaculor protein sorting mutants (VPS). Through these studies VPS10 was identified as a receptor delivering newly synthesised vacuolar hydrolases from the TGN to the vacuole, VPS10 mutants were characterised by secretion of vaculor hydrolase in to the extracellular environment. Although there is little sequence similarity, VPS10 functions as the *Saccharomyces cerevisae* equivalent to the mammalian M6PR. Genetic studies revealed that VPS35, VPS29 and VPS26 exhibited the same defect in vacuolar hydrolases sorting, and subsequent work has shown that they form the cargo recognition complex of the retromer[149]. Through crosslinking experiments VPS5 and VPS17 were identified as part of the complex[150]. They are SNX-Bar proteins also called SNX1 and SNX2, which function to sense membrane curvature and help deform membranes of the endosome[151, 152].

The WASH complex is necessary for the tubulation of membranes from the MVB[153]. WASH is a member of the Wiskott-Aldrich syndrome protein (WASP) family. WASP proteins bind actin and Arp2/3 complex to stimulate the nucleation of actin[153]. WASH is recruited on to endosomes in a complex with at least 5 other co-factors, CCDC53, FAM21, SWIP and Stumpellin, collectively called the WASH regulatory complex (SHRC)[153-155]. Though the WASH complex, F-actin is nucleated on the endosome providing the force required for the formation of tubules. WASH activation can be promoted by several signalling molecules among them is SRC kinase[156], although WASH is thought to be dispensable for EGFR trafficking[153]. In 2013 Hao et al.[157] established the MAGE-L2-TRIM27 E3 ligase complex, localises to endosomes and stimulates retrograde transport through the Lys63

ubiquitylation of WASH. Disruption of WASH ubiquitylation inhibited retrograde transport but as of yet no DUB has been identified to regulate retrograde transport.

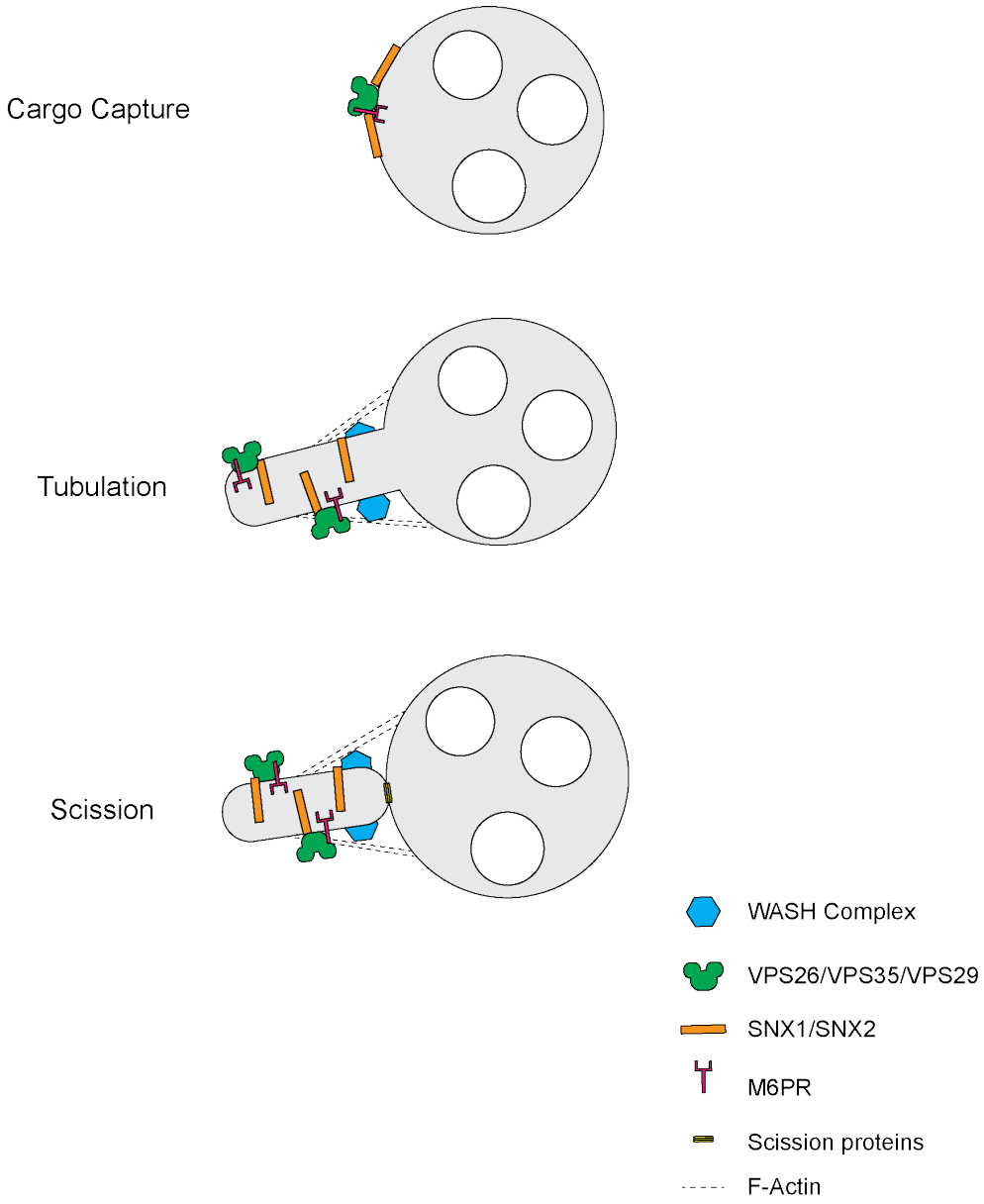

Figure 1.6. Endosomal budding.

Retrograde transport from the MVB is achieved through the sequential processing steps. First there is a cargo recognition phase with VPS26/VPS35/VPS29 complex binding to cargo and recruiting SNX1/SNX2. Next is membrane remodelling achieved through the action of SNX1/SNX2 and the WASH complex that nucleates F-Actin and providing force to remodel the membrane. Finally there is a scission step and endosomal budding.

1.4. Aims of this project

Previous work in the lab has established USP15 as a regulator of the E3 ligase BRAP. BRAP can in turn regulate the action of the MAPK scaffold KSR. One aim of this project is to understand if and how USP15 is regulating the MAPK signaling pathway.

In order to identify novel DUBs as effectors of the EGFR we will perform a screen using GFP-DUB to assess DUB that exhibit EGF localizations.

The final part of this project will be to establish if any of the known endocytic DUBs play a role in the regulation of retrograde transport.

Chapter 2 Materials and methods

2.1. Molecular biology.

2.1.1. Reagents.

The following items were sourced from Invitrogen (Paisley, UK). SOC media (#15544-034), TOP10 competent cells (#C4040-30), DH5α subcloning efficiency competent cells (#18265-017), electrophoresis grade agarose (#15510-019), pEF-FRT-V5 TOPO cloning kit (#45-0226). Nuclease free water was obtained from Sigma (#W4502). Luria Bertani (LB) agar and broth (LAB-168 and LAB-191 respectively) was purchased from LAB M limited (Bury, UK). The following items were sourced from Agilent Technologies (Santa Clara, USA), XL-1 Blue ultra competent cells (#200314), Pfu Hot start Ultra (#600390) Deoxynucleotide mix (100mM, #200415).

50x TAE buffer (#B9-0030) was purchased from National Diagnostics (Hull, UK). Gel extraction kit (#28706), Miniprep Kit (#27106), HiSpeed Maxiprep kit (#12663) from QiaGEN (Crawley, UK). All restriction endonucleases, 1kb Hyper-ladder (#NO468), 100bp Hyper-ladder (#NO467), were sourced from New England Biolabs (Herts, UK). Pfu Hot start Ultra (Stratagene, #600390), Taq polymerase (Bioline, #BIO-21040). All other chemicals were obtained from Sigma Aldrich (Poole, UK) unless otherwise stated.

2.1.2. Agarose gel electrophoresis

Agarose gels (between 0.8-1%) were prepared from electrophoresis grade agarose dissolved in 1x TAE buffer (40mM Tris Acetate, 1mM Na_2EDTA) by heating the mixture in a microwave. Once the mixture had cooled, ethidium bromide was added to agarose solution to a final concentration of 0.5µg/ml and allowed to set in a gel mold. DNA samples were loaded in 1x sample buffer (5%w/v glycerol, 0.1mM EDTA, 0.005%

bromophenol blue) at volumes typically between 10-15µl and DNA standard ladder was loaded as a comparison (NEB, Hyper-ladder 1kb). Bands were resolved in TAE buffer in a horizontal midi electrophoresis tank (Fisher Scientific) at 90V for 1hour. Bands were visualized using a UV gel dock (Uvi-dock).

2.1.3. Bacterial transformation

TOP10 (Invitrogen), DH5α (Invitrogen) and XL-Blue (Agilent) cells were transformed according to the manufactures' instructions. Typically 50µl of competent cells were incubated with less than 100ng of DNA on ice for 20mins. The bacteria were then heat shocked at 42˚C for 42secs, followed by 2mins rest period on ice. 200µl of SOC media was added to the cells and the mixture was incubated at 37˚C (rotating shaker at 225rpm) for 1 hour. Bacterial cells were streaked on to antibiotic supplemented LB agar plates and incubated at 37˚C overnight.

2.1.4. Polymerase Chain reaction (PCR)

To sub-clone GFP-USP46* and GFP-USP46*-C44S into the pEF-FRT vector, PCR products were generated to produce a blunt end DNA product with an introduced 5'-CACC and a blunt 3' end required for directional TOPO cloning. Pfu Hot start Ultra (Stratagene) was used in all the reactions, and the PCR reactions were prepared in 0.65ml Thermowell (Corning) at 4˚C. Recipes for PCR reactions and thermal cycle program are detailed in Table 2.1 and 2.2. Primers and template were pre diluted to 125ng/µl and 10ng/µl respectively. Primers used in this study are detailed in table 2.3; all primers were custom made from Eurofins MWG operon.

Stage	N° Cycles	Temp (˚C)	Duration (min:sec)
1	1	95	2:00
2	25	95	0:30
		55	0:30
		72	2:42
3	1	72	30:00

Table 2.1 Thermocycler settings to amplify GFP-USP46

	Positive PCR	Negative PCR
H_2O	40.5µl	41.5µl
10x Pfu-Buffer	5µl	5µl
dNTPs (25mM each)	0.5µl	0.5µl
Primer-F (125ng)	1µl	1µl
Primer-R (125ng)	1µl	1µl
10ng Template	1µl	-
Pfu Hot Start Ultra (2.5U/µl)	1µl	1µl
Total	50µl	50µl

Table 2.2. Typical PCR recipes.

Primer name	Sequence	TM(˚C)
GFP_general_forward	5'-CACCATGGTGAGCAAGGCG	61.5
USP46_rev	5'-GTTGGGTATTATCTTGACTGATAGAATA	59.3

Table 2.3. Primers used in this study.

2.1.5. Gel Extraction.

Bands of interest were extracted from the agarose gel using a scalpel. DNA was extracted using QiaGEN gel extraction kit to the manufacturers instructions.

2.1.6. TOPO subcloning into pEF-FRT-V5 plasmid.

8ng of purified PCR product was subcloned into TOPO- pEF-FRT vector. Reagents were mixed in a thermowell tube (Table 2.4) and incubated at 22˚C for 30mins. 2µl and 4µl of the reaction mixture was transformed into TOP10 competent cells (Invitrogen) according to the manufacturers protocol.

	Volume (µl)
PCR product (8ng/µl)	1µl
Salt Sol^{n}	1µl
H_2O	3µl
TOPO Vector	1µl
Total	6µl

Table 2.4 Recipe for TOPO cloning into pEF-FRT vector.

2.1.7. Site directed Mutagenesis.

Mutagenesis was performed on USP46 and USP15 to render them resistant to siRNA, and to mutate the active cysteine residue to a serine in USP46 only. Mutagenesis was performed using the Quick-change mutagenesis kit (Agilent Technologies) and Pfu Hot start Ultra (Stratagene). pDONR223-USP46 and pDONR223-USP15 were used as templates; primers were designed to be complementary to the sequence surrounding the desired base changes (primers are shown in table 2.5, changes are highlighted in yellow). A comparison to the original sequence and mutated sequence are detailed in Table 2.6. Primers were typically designed to introduce silent mutations that modified restriction endonuclease sites so that the mutant peptide could be identified by restriction endonuclease digest.

PCR reactions were prepared in 0.65ml Thermowell (Corning) tubes; recipes and cycle times are documented in table 2.7 and 2.8 respectively. Following the PCR reaction, DPN1 was added to the reaction mixture to digest methylated DNA from bacterial origin, leaving the unmethylated mutated DNA. 1-2µl of mutated plasmid was then transformed in to XL-Blue ultra competent cells to the manufacturers instructions.

Target	Primer name	Primer Sequence
USP15	USP15*_F	GCATACATGAAGAAGGGAGCCCAAGTGAAATGG
	USP15*_R	CCATTTCACTTGGGCTCCCTTCTTCATFTATGC
USP46	USP46*_F	GTCCGAAACATAGCCAGCATTTGTAATATGGGAA CCAATGCCTC
	USP46*_R	GAGGCATTGGTTCCCATATTACAAATGCTGGCTAT GTTTCGGAC
USP46	USP46_C44S_F	GGAAACACATCCTACTGTAACTCCGTGCTTCA
	USP46_C44S_F	TGAAGCACGGAGTTACAGTAGGATGTGTTTCC

Table 2.5. Primers used for mutagenesis in this study.

	Base change	AA change	Construct name
WT	ggC TCA	-	pDONR223-USP15siRES1
Mutant	ggG AGC		
WT	atc gcc tcc atc tgt aat atg ggc	-	pDONR223-USP46siRES8
Mutant	atA gcc AGC atT tgt aat atg ggA		
WT	tGc	C44S	pDONR223-USP46-C44S
Mutant	tCc		

Table 2.6. Base and amino acid changes introduced in this study.

	Positive PCR	**Negative PCR**
H_2O	40.5µl	41.5µl
10x Pfu-Buffer	5µl	5µl
dNTPs (25mM each)	0.5µl	0.5µl
Primer-F (125ng)	1µl	1µl
Primer-R (125ng)	1µl	1µl
10ng Template	1µl	-
Pfu Hot Start Ultra (2.5U/µl)	1µl	1µl
Total	50µl	50µl

Table 2.7. Typical PCR reaction recipes for site directed mutagenesis.

Stage	N° Cycles	Temp (˚C)	Duration (min:sec)
1	1	95	2:00
2	18	95	0:30
		68	0:30
		72	4:00
3	1	72	10:00

Table 2.8. Typical thermo cycle setting for site directed mutagenesis.

2.1.8. LR Gateway cloning in expression vector.

LR cloning was used to shuttle constructs from the destination plasmid into a mammalian expression plasmid. This was performed using the LR-Clonase ii (Invitrogen) mix to the manufactures' instructions.

2.1.9. Bacterial Colony PCR.

Bacterial colony PCR was used to screen for colonies that had been successfully transformed with the pEF-FRT-GFP-USP46* and pEF-FRT-GFP-USP46*-C44S. A master mix was prepared using the recipe described in table 2.10. Bacterial colonies were picked with a sterile pipette tip and dipped in to the 1x master mix. The same colony was then used to seed 5ml of LB culture supplemented with Ampicillin, grown for 16 hours at 37˚C (on rotating shaker at 225rpm), for DNA amplification and extraction. T7 and BGH primer (Invitrogen) (Table 2.11) sequence flanked the gene of interest and were used to screen for positive colonies by the size of the PCR product. Typical program for the thermocycler is shown in table 2.9.

Stage	N° Cycles	Temp (˚C)	Duration (min:sec)
1	1	95	5:00
2	35	95	1:00
		55	1:00
		72	3:00
3	1	72	5:00

Table 2.9. Typical thermo cycle setting for bacterial colony PCR.

	1x
H_2O	6.9µl
10x Pfu-Buffer	1µl
$MgCl_2$	0.4µl
DNTPs (25mM each)	0.25µl
Primer-F (125ng)	0.7µl
Primer-R (125ng)	0.7µl
Bioline Taq	1µl
Total	10µl

Table 2.10. Typical recipe setting for bacterial colony PCR.

Primer name	Sequence	TM(˚C)
T7_F	5'-TAATACGACTCACTATAGGG	48.0
BGH_R	5'-TAGAAGGCACAGTCGAGG	54.8

Table 2.11. Primers used for bacterial colony PCR in this study.

2.1.10. Restriction endonuclease analysis.

Restriction endonuclease testing was routinely carried out to test the identity of constructs. Depending on the optimal conditions for the enzyme, typically 500ng of DNA would be subjected to restriction digestion for 1 hour at 37˚C. Table 2.12 details a typical recipe for restriction digest.

	Vol^{m} (µl)
500ng of DNA	1µl
Restriction endonuclease	0.8µl (x2 0.4µl for double digestion)
Reaction Buffer	1µl
10x BSA	1µl
H_2O	6.2µl
Total Vol^{m}	10µl

Table 2.12. Typical recipe for restriction endonuclease digestion.

2.1.11. Glycerol stock.

Glycerol stocks were produced from 5ml of overnight culture inoculated from a single colony. The culture was spun down at 1000g for 10mins, the pellet was resuspended in a solution of 40% Glycerol and 60% LB medium. Glycerol stocks were frozen at -80˚C.

2.1.12. Plasmid sequencing.

Plasmid sequencing was performed by Dundee Sequencing services.

2.2. Protein Biochemistry.

2.2.1. Reagents.

Tween-20 (#EC-407), 20% SDS solution (#EC-894), Resolving buffer (#EC-893), Stacking Buffer (#EC-870), Protogel (#EC-890) was obtained from National Diagnostics (Hull, UK). NuPage gels, NuPage MOPs running buffer (#NP-001-02), NuPage Antioxidant (#NP0005) were purchased from Invitrogen (Paisley, UK). Protran nitrocellulose membrane (#B3-0059) was bought from Geneflow (Litchfield ,UK). Pierce BCA assay kit (#23225) was sourced from Thermo scientific (Rockford, Il). All other chemicals were sourced from Sigma Aldrich (Poole, UK) unless otherwise stated.

2.2.2. Cell lysis.

A confluent mono-layer of cells were washed twice in ice cold PBS and lysed in either NP40 buffer (0.5% NP40, 25mM Tris pH 7.5, 100mM NaCl) or RIPA (10mM Tris-HCl pH 7.5. 150mM NaCl, 1% Triton X-100, 0.1% SDS, 1% Sodium deoxycholate) buffer supplemented with mammalian protease inhibitors (1:250) and where appropriate Phos-Stop tablets (1 tablet in 10ml, Roche) on ice for 10mins with rocking. Lysates were then spun at 16,200g for 10mins (4˚C) to remove the insoluble faction.

2.2.3. BCA protein assay.

Protein concentrations of cell lysates were determined using BCA protein assay kit (#23225, Pierce) to the manufacturers instructions.

2.2.4. SDS polyacrylamide gel electrophoresis.

SDS polyacrylamide gel electrophoresis was performed using either custom made using the BioRAD system or the Invitrogen precast NuPage gel system. The recipes detailed in Table 2.13. and 2.14. were used according to need to make BioRAD gels.

	8%	**10%**
Protogel	5.34ml	6.66ml
Protogel Resolving Buffer	5.2ml	5.2ml
Water	9.24ml	7.92ml
APS	0.2ml	0.2ml
TEMED	20µl	20µl

Table 2.13. Recipe for 2x resolving mini-gel.

	Stacking Gel
Protogel	0.65ml
Protogel Stacking Buffer	1.25ml
Water	3.05ml
APS	25µl
TEMED	5µl

Table 2.14. Recipe for 1x 4% stacking gel.

2.2.5. Western Blotting.

Western blotting was performed to transfer proteins resolved by SDS page onto 0.45μm nitrocellulose membrane for immuno detection of proteins. Protein transfer was performed using a genie blotter full submersion apparatus (Idea scientific) at 0.9A for an hour. Nitrocellulose was then stained with Ponceau-S stain to visualize bands and removed by washing in PBS. The membrane was blocked using either 5% Milk in TBS-T (20mM Tris, 137mM NaCl, pH 7.5, 0.1% Tween20) or 5% BSA/ TBS-T for 1 hour. Primary antibodies were incubated according to the conditions required. After incubation in the primary antibody the membrane was then washed in TBS-T 0.1% for 3x 5min. Fluorescent secondary antibodies raised against the primary antibody host species, were incubated in 5% milk TBS-T for 1 hour. The membrane was washed again 3x in TBS-T before detection of bands an Odyssey Licor system. Primary antibodies used in this study for western blotting are detailed in table 2.15 and secondary antibodies are detailed in table 2.16.

Description	Target	Species	Source	Blocking	Dilution
ERK #4695	ERK	Rabbit	Cell Signaling	BSA	1;1000
pERK (Thr202/Tyr204) #4370	ERK	Rabbit	Cell Signaling	BSA	1;500
AKT	AKT	Mouse	Cell Signaling	BSA	1;500
pAKT (Ser473) #9271	AKT	Mouse	Cell Signaling	BSA	1;500
MEK (Ser217/221) #9122	MEK	Mouse	Cell Signaling	BSA	1:500
pMEK #9154	MEK	Mouse	Cell Signaling	BSA	1:500
pEGFR (Tyr845) #2231	EGFR	Rabbit	Cell Signaling	BSA	1:1000
EGFR #sc-03	EGFR	Sheep	Santa Cruz	Milk	1:500
CRAF #A301-519A	CRAF	Rabbit	Santa Cruz	Milk	1:1000
CI-M6PR	CI-M6PR	Rabbit	Paul Luzio	Milk	1:500
VPS35 #ab10099	VPS35	Goat	AbCam	Milk	1:1000
Cathepsin D #219361	Cathepsin D	Millipore/ Calbiochem	Millipore	Milk	1:2000
HRS #864/3	HRS	Rabbit	Sylvie Urbe	Milk	1:1000
USP4 #A300-830A	USP4	Rabbit	Bethyl	Milk	1:1000
USP8 #HA004869	USP8	Rabbit	Sigma	Milk	1:1000
USP15 #H00009958-M01	USP15	Mouse	Abnova	Milk	1:1000
USP46 #HPA007288	USP46	Rabbit	Sigma	Milk	1:250
BRAP #A302-682A	BRAP	Rabbit	Bethyl	Milk	1:1000
KSR #2234-1	KSR	Rabbit	Epitomics	BSA	1:1000
PHLLP1 #A300-660A	PHLLP1	Rabbit	Bethyl	Milk	1:200
PHLLP2 #A300-661A	PHLLP2	Rabbit	Bethyl	Milk	1:200
Actin #Ab6276	Actin	Mouse	AbCam	Milk	1:10,000
Tubulin #T5168	Tubulin	Mouse	Bethyl	Milk	1:10,000

Table 2.15. Primary antibodies used in this study for western blotting.

Secondary Antibody	Manufacturer	Dilution
Donkey anti-mouse IRDye 800cw #926-32212	Licor Biosciences	1:15,000
Donkey anti-mouse IRDye 680cw #926-32222	Licor Biosciences	1:15,000
Donkey anti-rabbit IRDye 800cw #926-32213	Licor Biosciences	1:15,000
Donkey anti-rabbit IRDye 680cw #926-32223	Licor Biosciences	1:15,000
Donkey anti-sheep IRDye 800cw #926-32214	Licor Biosciences	1:15,000
Donkey anti-sheep IRDye 680cw #926-32224	Licor Biosciences	1:15,000

Table 2.16. Secondary antibodies used in this study for western blotting.

2.3. Cell Biology

2.3.1. Reagents.

The following products were purchased from Invitrogen (Paisley, UK), Oligofectamine transfection reagent (#12252-011), RNAi Max transfection reagent (#13778-075). Genejuice transfection reagent was obtained from (#70967, Merck Chemicals, Millipore, Darmstadt, Germany). Gefitinib (#51025) and AZD6244 (#142886). PI-1O3 (#528100), PDGF (#521225) and moviol (F017), epoxomicin (#324800) was purchased from Calbiochem (Merck, Millipore, Darmstadt, Germany). 16% PFA (#F017) was obtained from TAAB (Reading, UK). All other chemicals were obtained from Sigma Aldrich (Poole, UK) unless otherwise stated. EGF was a kind gift from Dr. J. Smith (University of Liverpool). All plastic ware was sourced from Corning Inc. (NY, USA). All other cell culture reagents were obtained from Invitrogen (Paisley, UK) unless otherwise stated.

2.3.2. Cell culture.

HeLa, U2OS, HEK293t and HCT116 cells were cultured at 37˚C in a 5% CO_2 atmosphere in Dulbecco's Modified Eagles' Medium (DMEM) supplemented with 10% FBS, 1% non-essential amino acids and 1%penicillin/streptomycin sulphate. HeLa (Human cervical cancer), U2OS (Human osteosarcoma), HEK293t (Human embryonic kidney cells) and HCT116 (Human Colon cancer cells) cells reached confluence after 2-3 days. HeLa, U2OS and HCT116 cells maintained by splitting a confluent dishes 1:5 while HEK293t were split 1:10.

2.3.3. Culture of CD8-CI-M6PR and CD8-FURIN cell lines.

CD8-CI-M6PR-HeLaM and CD8-CI-Furin-HeLaM cells (a gift from Dr. Matthew Seamen, Cambridge Research Institute) stably express a chimera of the luminal domain of CD8 fused to the tail of CI-M6PR and Furin[158]. Cells were maintained in DMEM media supplemented with 0.5mg/ml G418. Cells were maintained by splitting a confluent dish every 2-3 days at a ratio of 1:5.

2.3.4. SILAC cell culture.

Stably transfected HeLa S3 cells (G7, WT2, CS3) were grown in DMEM media lacking Arg and Lys (Dundee cell products), 10% Dialyzed FBS (Dundee cell products) and 1% penicillin/streptomycin sulphate. G7 cells were grown in media supplemented with light amino acids (Arg0/Lys0/Pro0), CS3 in medium amino acids GFP-USP46-C44S (CS3) (Arg6/Lys4/Pro0) and WT2 in heavy amino acids GFP-USP46-C44S (WT2) (Arg10/Lys8/Pro0).

2.3.5. Transient transfection of tissue culture cells.

For transient transfection of mammalian expression constructs, all cells were transfected with Genejuice (Merck Millipore). Typically, cells were grown on 22mm^2 coverslips in 6 well plates. Plasmids were incubated with Genejuice in a 1:3 ratio between µg DNA/µl Genejuice, for a 6 well plate 1µg of DNA was incubated with 3µl Genejuice in serum free OptiMEM for 15mins. The mixture was then added directly to the cells in complete DMEM media for 16-24 hours.

2.3.6. siRNA transfection of tissue culture cells.

HeLa cells were transfected with 40nM of siRNA using Oligofectamine (Invitrogen), U2OS and HCT116 cells were transfected with 20nM and 40nM siRNA respectively using RNAi max (Invitrogen). Typically for a 72hour transfection, cells would be seeded in a 6 well plate a density of 1.2x10^5 cells and allowed to adhere to the plate, the next day the medium would be exchanged for serum free medium and treated with siRNA transfection reagent complex to the manufactures instructions. FBS was added 4 hours later to a final concentration of 10% and the media was exchanged the day after. All siRNA was obtained from Dharmacon Inc. (Lafayette, CO, USA), details of siRNA oligonucleotides used in this study are outlined in table 2.17.

Target	Brand	Cat number	Target Sequence
USP4-8	On-Target Plus	J-004974-08	AAACUCAACUCUCGAUCUA
USP8-1	siGENOME	D-005203-02	UGAAAUACGUGACUGUUUAUU
USP8-2	siGENOME	D-005203-03	GGACAGGACAGUAGAUAUU
USP15-1	siGENOME	D-006066-01	GAAGAAGGCUCACCAAGUG
USP15-2	siGENOME	D-006066-02	GAACGCACCUUGGAAGUUU
USP46-6	On-Target Plus	J-006092-06	GAACGAACCUGCGGAAAAU
USP46-7	On-Target Plus	J-006092-07	GAAACUCGAUGCUUGAACU
USP46-8	On-Target Plus	J-006092-08	AAACAUCGCCUCCAUCUGU
USP46-9	On-Target Plus	J-006092-09	CCGCAUGUAUGACUUGGUU
AMSH-3	On-Target Plus	D-012202-02	GAGAAGCCCUCCUUAGAUGUU
BRAP	On-Target Plus Smart Pool	L-006597-00	GGUAUUAUGCACCUAUAUA UGAGAAGUGUGAUAAUCUA CGACGUAAUUGAACAAAUG GGAGAGAAAGUAGCGAUUA
RAF1	On-Target Plus Smart Pool	L-003601-00	ACAGAGAGAUUCAAGCUAU AUUCAAAGAUGCCGUGUUU CAAAGAACAUCAUCCAUAG GUAAAUGGCACGGAGAUGU
VPS35	On-Target Plus Smart Pool	L-010894-00	GAACAUAUUGCUACCAGUA GAAAGAGCAUGAGUUGUUA GUUGUAAACUGUAGGGAUG GAACAAAUUUGGUGCGCCU
NT1	On-Target Plus	D-001810-01	UGGUUUACAUGUCGACUAA

Table 2.17. siRNA Oligonucleotides used in this study.

Name	Target	Species	Source	Blocking	Incubation	Fixation	Dilution
HRS 958/3	HRS	Rabbit	Sylvie Urbe	10% GS	5% GS	Methanol	1;1000
VPS26	VPS26	Rabbit	Abcam	10% GS	5% GS	PFA	1;500
EEA1 243/3	EEA-1	Mouse	Ian Mills	10% GS	5% GS	PFA	1;500
EEA1	EEA-1	Mouse	BD	10% GS	5% GS	PFA	1;500
CD8	CD8	Mouse	Matthew Seaman	DHB	DHB	PFA	1:500
P230	P230	Mouse	BD	10% GS	5% GS	PFA	1:500
CI-M6PR	CI-M6PR	Rabbit	Paul Luzio	10% GS	5% GS	PFA	1:200
FK2	Ubiquitin	Mouse	Millipore	10% GS	5% GS	PFA	1:1000
ERK 4695	ERK	Rabbit	Cell signaling	10% GS	5% GS	Methanol	1;100
pERK 4370	pERK	Rabbit	Cell signaling	10% GS	5% GS	Methanol	1;200
GFP	GFP	Sheep	Ian Prior	2% BSA	2% BSA	Methanol	1;200

Table 2.18. Primary antibodies used in this study for immunofluorescence.

2.3.7. Immunofluorescence.

Cells were typically washed 2x in PBS then fixed in 3-4% PFA (16% w/v stock solution) for 10mins immediately after the experiment (or following a 3min incubation in 0.02% Saponin/PIPES-MTSB, to remove cytosolic staining). Cells were subsequently quenched in 50mM NH_4Cl for 20mins. Some antibodies were not compatible with PFA fixation and were fixed in -20˚C Methanol on ice for 5mins (Primary antibodies used in this study are detailed in table 2.18). Cells were then generally blocked in 10% Goat serum in 0.2% Triton X-100 for one hour. Primary were typically incubated in 5% goat serum in 0.2% triton-X100 facedown on a 100µl drop for 1 hour. Coverslips were then washed 5x in PBS, 3x short 1min washes and 2x 5min wash. Secondary antibodies (detailed in Table 2.19) were incubated in 5% Goat serum in 0.2%Triton X-100/PBS. Cover slips were then washed again and mounted on 40µl drop of moviol (Calbiochem) on a microscope slide,

were necessary 4',6-diamidino-2-phenylindole (DAPI) stain was added to the moviol at 1:10,000. Cell were imaged either SP2 aobs (lecia; 63.0 x 1.4 oil objective) confocal microscope or a Nikon Ti-E (60x Oil N2 N.A. 1x4, W.D.0.13mm) widefield microscope.

Ab name	Species	Source	Dilution
Anti-Mouse AF350 #A10035	Donkey	Invitrogen	1;500
Anti-Mouse AF488 #A21202	Donkey	Invitrogen	1;1000
Anti-Mouse AF594 #A21203	Donkey	Invitrogen	1;1000
Anti-Rabbit AF488 #A21206	Donkey	Invitrogen	1;1000
Anti-Rabbit AF594 #A21207	Donkey	Invitrogen	1;1000

Table 2.19. Secondary antibodies used in this study for immunofluorescence.

2.3.8. Generation of Flp-in cell lines.

Flp-in cells were generated by co-transfection of pEF-FRT vector containing the gene of interest along with pOG44 plasmid encoding the Flp recombinase. Parental HeLa S3 cells containing the FRT recombination sites (generated by Maria Hernández) were seeded into 6 well plates and transfected using Genejuice with the method described in section 2.3.5. with a ratio of 1:9; 100ng of pEF-FRT plasmid and 900ng of pOG44 plasmid. 24 hours after transfection the cells were re-seeded onto 10cm^2 dishes at a density of 1:2 and 1:4. The cells were cultured in the presence of 150µg/ml Hygromycin B to select for positive clones; media was exchanged every 3 days. After 14days colonies were visible colonies formed which were picked and transferred into a 24 well plate. Once the cells had formed large islands (approximately 1 week later) the cells were transferred into a 6 well plate and then into 25cm^2 flasks for 2 passages before freezing down clones. Positive clones were identified through western blotting and immunofluorescence.

2.3.9. Growth factor stimulation and lysis.

Cells were serum starved for 16hours before stimulation with serum free DMEM supplemented with the appropriate concentration of growth factor. Cell are washed 2x in Ice cold PBS and lysed in RIPA buffer (10mM Tris-HCl pH 7.5., 150mM NaCl, 1% Triton X-100, 0.1% SDS, 1% Sodium deoxycholate) supplemented with mammalian protease inhibitors (1:250)(Sigma) and PhosSTOP inhibitors (1 tablet per 10ml)(Roche). Application of growth factor is staggered so that all cells are lysed concurrently. Or alternatively cells were washed x2 in PBS and fixed in 4% PFA or -20˚C methanol.

2.3.10. USP8 rescue experiments.

HeLa cells were transfected 2x with 40nM of siRNA using oligofectamine (Invitrogen) over 96 hours at 0 and 48 hour time point. The cells were transfected with GFP constructs for 66hours using Genejuice (Merck Millipore). After 72 hours cells were seeded 0.4 x 10^6 cells per 22mm^2 or at 6.7x10^5 cells per 6well plate. The cells were then either fixed in 3% PFA or lysed in NP40 buffer.

2.3.11. Epoxomicin treatment.

Cells pretreated with siRNA were incubated with DMEM supplemented with 0.5μM Epoxomicin or 2μl DMSO, for 8hours before and lysis in NP40 buffer on ice for 10mins on ice.

2.3.12. Kinase inhibitor treatment.

HeLa cells were serum starved overnight before incubation in serum free DMEM supplemented with kinase inhibitors (300nM Gefitinib, 150nM PI 103, 300nM AZD6244) for 15mins. Media was then exchanged to serum free DMEM containing the appropriate kinase inhibitor or DMSO and 20ng/ml EGF. Cells were then washed 2x in ice cold PBS before fixation in 4% PFA or lysis in RIPA buffer.

2.3.13. Immuno-precipitation using GFP Nano-Trap.

Stably transfected HeLaS3 cells were lysed in NP40 buffer (0.5% NP40, 25mM Tris pH7.5, 100mM NaCl) and centrifuged at 16,200g (4˚C) to pellet cell debris. Lysates were adjusted to equal concentration using lysis buffer. GFP Nano-Trap antibody[159] was pre-coupled to sepharose beads (Maria Hernández). Beads were incubated with the lysate for 2 hours at 4˚C (5µl beads per 100µg of lysate), the beads were then washed 3x in YP buffer (1%NP40, 25mM Tris pH 7.5, 150mM NaCl, 4˚C) and then 1x in 25mM Tris (4˚C). Proteins were eluted for the beads by incubation in either 1x SDS running buffer at 98˚C for 10mins or for large volumes in 1%SDS at 98˚C for 10mins, the elute was the dried in a speed-vac (RVC 2-25, Christ, Osterode am Harz, Germany) for 16hours at 40˚C and the subsequent pellet was resuspended in 1x SDS running buffer.

2.3.14. CD8 uptake assay.

CD8-CI-M6PR and CD8-Furin cells were either treated with 40nM siRNA twice over a 96-hour time period at 0 and 48 hours. CD8-CI-M6PR and CD8-Furin cells were seeded onto 22mm^2 coverslips at a dilution of 1:4, after 72 hours siRNA treatment. After 96 hours cells were incubated for 15mins on ice cold DHB (serum free DMEM, 25mM HEPES, 0.2% Fatty acid free BSA), then subsequently incubated on a spot of 1µg/ml anti-CD8 antibody in 100µl DHB for 1 hour in the dark. The coverslips were then washed twice in ice-cold

PBS and transferred into 37˚C DMEM. The cells were fixed in 3% PFA at the indicated time points and processed for immunofluorescence.

2.3.15. Cathepsin D secretion assay.

HeLa cells were treated for 96 hours with 40nM siRNA against their respective targets. Cells were seeded at 72 hours cells were seeded into 6 well plates at a density of $6.7x10^5$ cells. 16 hours before the end of the experiment media was exchanged to 1ml serum free OptiMEM. The conditioned media was removed and underlying cells were washed twice in ice-cold PBS and lysed in NP40 buffer. SDS was added to the conditioned media to a final concentration of 0.02% and incubated on ice for 30mins. The media was centrifuged at 16,200g for 30min (4˚C) to remove cell debris. TCA (Trichloroacetic acid) was added to the supernatant to a final volume of 10% and incubated on ice for 1 hour after which it was centrifuged for 30mins at 16,200g (4˚C). The resulting pellet was washed in ethanol:ether (1:1) and resuspended in 1x unbuffered SDS running buffer. Equal loading was determined by Ponceau staining.

2.4. Mass spectrometry

2.4.1. Reagents.

Trypsin Gold (#V5280) was sourced from Promega (Southampton, UK). HPLC grade Acetonitrile (#20060320) and Water (#23595328) were purchased from VWR (Lutterworth, UK). LoBind Eppendorf tubes (#022431081) were sourced from Eppendorf (Hamburg, Germany). All other chemicals were obtained from Sigma Aldrich (Poole, UK) unless otherwise stated.

2.4.2. In-gel digestion.

Immuno-precipitated samples were run in a single lane of a NuPage 4-12% SDS polyacrylamide gel at 190v for 1 hour. The gel was stained with colloidal blue, used to the manufacturers instructions to visualize the bands. Bands were cut from the gel using a scalpel and de-stained in 50mM Ammonium Bicarbonate (Ambic)/ 50% Acetonitrile (ACN). Gel slices were reduced and alkylated by incubating gel slices at 37˚C in 10mM Dithiothreitol for 30mins followed by incubation in 50mM Chloroacetamide for 30mins at room temperature in the dark. Gel slice were then incubated in 100% ACN to dehydrate the gel piece at 37˚C. 20µl of 50mM trypsin was added to the gel slices and incubated for 16hours at 37˚C. 1% formic acid was added to quench the reaction and 100% ACN was added to extract the peptides. The eluted was spun at 16,200g for 10mins to pellet any gel pieces; the supernatant was transferred into fresh tubes and dried in a speed-vac (RVC 2-25, Christ, Osterode am Harz, Germany) at 45˚C for 6 hours. The pellet was resuspended in 0.05% TFA and loaded on LC-MS/MS.

2.4.3. Detection and identification of peptides.

5µl of each sample was loaded on high performance liquid chromatography column coupled to an LTQ-Orbitrap XL (Thermo Fisher) fitted with a Proxeon nanoelectrospray source. Samples were run on a 1-62.5% linear ACN gradient over 21mins. MS spectra were acquired by the Orbitrap at a resolution of 30,000 and MS/MS was performed on the TOP 6 ions in the LTQ ion trap. All spectra were acquired using Xcalibur software (version 2.0.7; Thermo Fisher Scientific). Raw MS spectra were searched against human.ipi.library and analyzed using MaxQuant software 1.3.0.5[160].

Chapter 3 USP15 regulates the MAPK pathway through CRAF.

3.2. Introduction.

Reversible ubiquitylation can govern many signaling processes by regulating the stability of substrate proteins, enzymatic activity and protein-protein interactions. The NFkB pathway is a model for the action of reversible ubiquitylation in the regulation of signaling pathways[161]. However, the role of ubiquitylation had not been as extensively explored in as a regulator of the MAPK pathway. Several components of the MAPK pathway notably, the RAS family of GTPase have been shown to be directly ubiquitylated, which influences localization[162], activity[163] and degradation[164]. The role of deubiquitylases (DUBs) as direct regulators of MAPK pathway components, downstream of the RTKs had been relatively understudied. USP17 has been described as determining the localization of N-RAS through RCE1[165]. While another DUB CYLD has recently been shown to regulate the activity of AKT, by maintaining it's plasma membrane localization and opposing the action of E3 ligases that ubiquitylate AKT[166]. Ubiquitylation prevents the translocation of AKT into the cytosol and it's subsequent inactivation.

One feature of DUBs is that they are often found in complexes together with E3 ligases. This allows for dynamic interplay between E3 ligases and DUBs[166]. One explanation for these associations is that DUBs are required to deubiquitylate E3 ligases that have a tendency to auto-ubiquitylate[167]. Sebastian Hayes performed a directed Yeast two-hybrid screen to look at the interactions between 55 DUBs and 133 RING E3 ligases, to identify E3 ligase DUB partners that could influence signaling pathways. An interaction between BRAP and USP15 was observed, which was of interest because of the described function of BRAP[167].

BRAP is also annotated in the literature as IMP standing for Impedes Mitogenic Propagation. It was identified in a yeast two-hybrid (Y2H) screen

with active H-RAS[168]. Further analysis reveled that BRAP has an inhibitory role in MAPK signaling through a non-catalytic action on the MAPK scaffold KSR[169]. BRAP removes KSR from a complex with the RAF and MEK kinases were it would facilitate their activation[170, 171]. In the presence of activated RAS^{G12V}, BRAP becomes auto-ubiquitylated and is sequestered into Triton-X100 insoluble complexes[169]. This in turn frees KSR allowing it to act as a scaffold increasing signaling through the pathway by enhancing the activation of the RAF/MEK kinases. The effect seen with BRAP was not restricted to EGF activation. Matheny al. (2004)[169] were able to observe a KSR dependent inhibition in MAPK signaling, when over expressing BRAP in KSR-/- MEFs stimulated with PDGF[168].

Following USP15 knockdown, we would predict an increase in signaling with USP15 depletion due to a reduction in the levels of BRAP. However, when the activation of the MAPK pathway was tested with knockdown of USP15 by siRNA, a paradoxical decrease in MAPK activation was observed. To investigate this problem further, U2OS cells were employed as a model to study PDGF signaling. By testing USP15 function in PDGF signaling, it allowed us to test whether this effect was a conserved regulatory step in the MAPK cascade.

3.2. Results.

3.2.1. Establishing Knock down conditions in U2OS cells.

In order to establish conditions to use U2OS cells as a model system to study the effects of USP15 on PDGF signaling. We first sought to assess the knockdown efficiency using RNAi max transfection reagent. As a control A549 cells were included, which had been previously used in the lab and produced efficient depletion by siRNA. Two different concentrations of oligonucleotides were tested, 20nM and 40nM with two individual oligonucleotides. Individual oligonucleotides had been previously verified by deconvolution from the pool of oligonucleotides targeting USP15. We aimed to reduce the amount of

siRNA needed for each knockdown experiment, cutting both cost and off target effects associated with siRNA transfection (Figure 3.1).

Both concentrations of oligonucleotides produced knock down efficiency of over 90% after 72hours, with the higher concentration being marginally more effective in U2OS cells (Figure 3.1.) Interestingly the Scr (scrambled) control caused a slight decrease in the expression levels of USP15 and was omitted as a control for later experiments. The levels of expression were quantitated using the odyssey software and values for USP15 band were normalized to the Actin control.

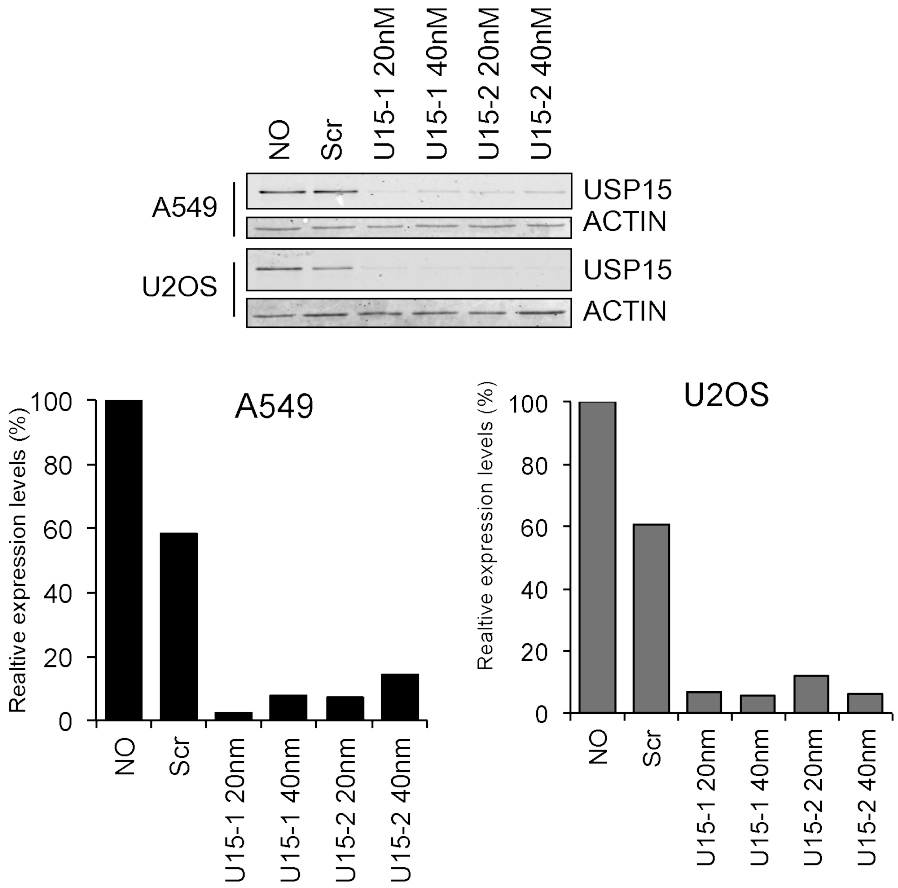

Figure 3.1 Testing knockdown efficiency of USP15 in U2OS cells

U2OS and A549 cells were depleted of USP15 with varying concentration of siRNA for 72 hour using RNAi MAX. The cells were lysed in RIPA buffer and lysates were probed for USP15 and Actin, quantification was performed using Odyssey software. USP15 values were normalised to actin and expressed as relative abundance of no oligo control (%). Representative blot shown.

3.2.2. Titration of the concentration of growth factor required to activate MAPK pathway.

Next we produced dose response curves for PDGF on U2OS cells. In addition to U2OS cells, dose response curves were performed for HeLa and HEK293t cells with EGF for comparison. pMEK (Ser217/221) was used as a readout of MAPK pathway activation. This was preferred to pERK because it is less influenced by cross talk from other signaling pathways than MEK.

Performing a titration ensured that any perturbation of the MAPK pathway would be seen as either an increase or decrease in signal. For example, if you were to stimulate with too high a concentration of growth factor and saturate the system, then the pathway would be already maximally stimulated and no increase in signal would be observed. Equally if the perturbation caused a decrease in signal and you were stimulating the cells in the low end of the activation profile. Then this would reduce the dynamic range of the assay and underestimate any effect seen. For this reason we chose to use a concentration in our experiments at approximately the EC_{50} for a given growth factor (10ng/ml PDGF).

In figure 3.2, HeLa, U2OS and HEK293t cells were grown to confluency on the day of lysis. The cells were serum starved in DMEM for 16 hours before stimulation with the indicated concentration of growth factor for 5mins. Each growth factor reached saturation of the pMEK signal at 20ng/ml while PDGF had a shallower activation curve compared to EGF on HeLa and HEK293t. Interestingly in HEK293t cells, inhibition was observed at 100ng/ml relative to 20ng/ml of EGF. Also of note across the different cell lines tested there was differential activation of MEK isoforms. In Hek293t cells only one band was observed, in U2OS cells and HeLa cells two bands were seen for each. However, in HeLa cells both bands are activated equally whilst in U2OS cells the lower band is stronger than the upper.

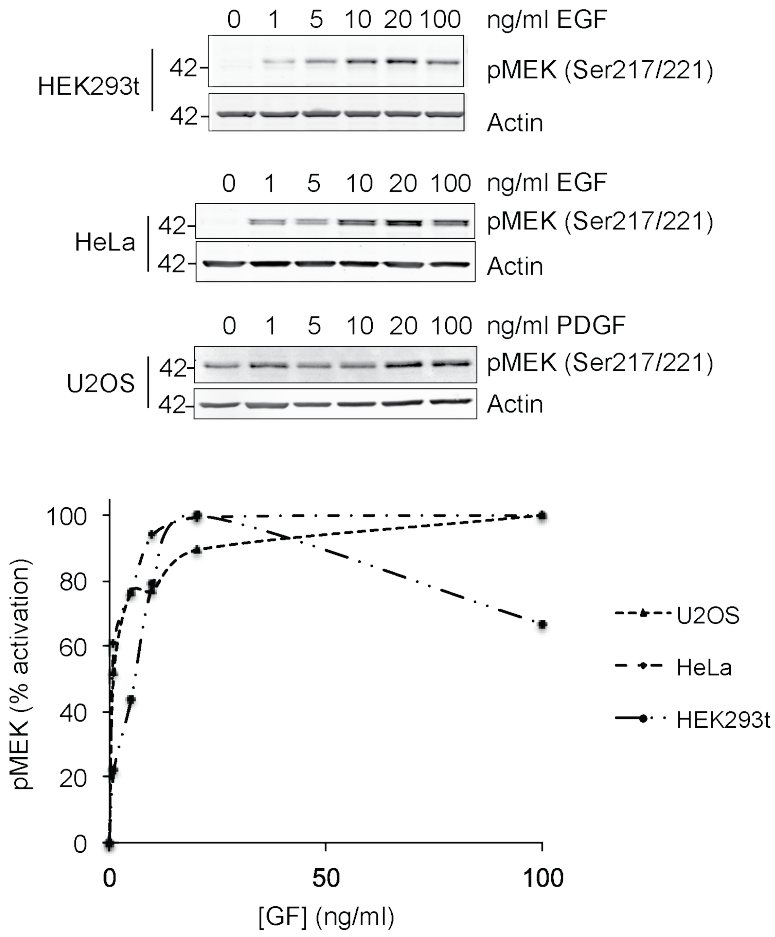

Figure 3.2. Titration of Growth factor for MEK activation.

Hek293t, HeLa and U2OS cells were serum starved overnight before stimulation with increasing concentrations of growth factor (indicated) for 5min. Cells were lysed in RIPA buffer and lysates were probed with antibodies against pMEK and actin. Quantification was performed Image J with values normalized to actin. Representative blot shown.

3.2.3. Time course of MAPK activation.

We next wanted to establish the time course of MAPK activation. Again this was performed in U2OS, HEK293t and HeLa cells. Cells were serum starved in DMEM for 16 hours before stimulation with the concentration growth factor indicated, for a time course between 0 and 60 mins. This would allow us to pick the optimal time point to assess changes in MAPK activation.

All cell lines showed pMEK rising sharply to peak at 5 mins and then declining. U2OS cells had the most sustained activation profile of those tested, consistent with previous reports[172] (Figure 3.3). In contrast to U2OS cells activation, HEK293t cells rapidly declined after 5mins of stimulation.

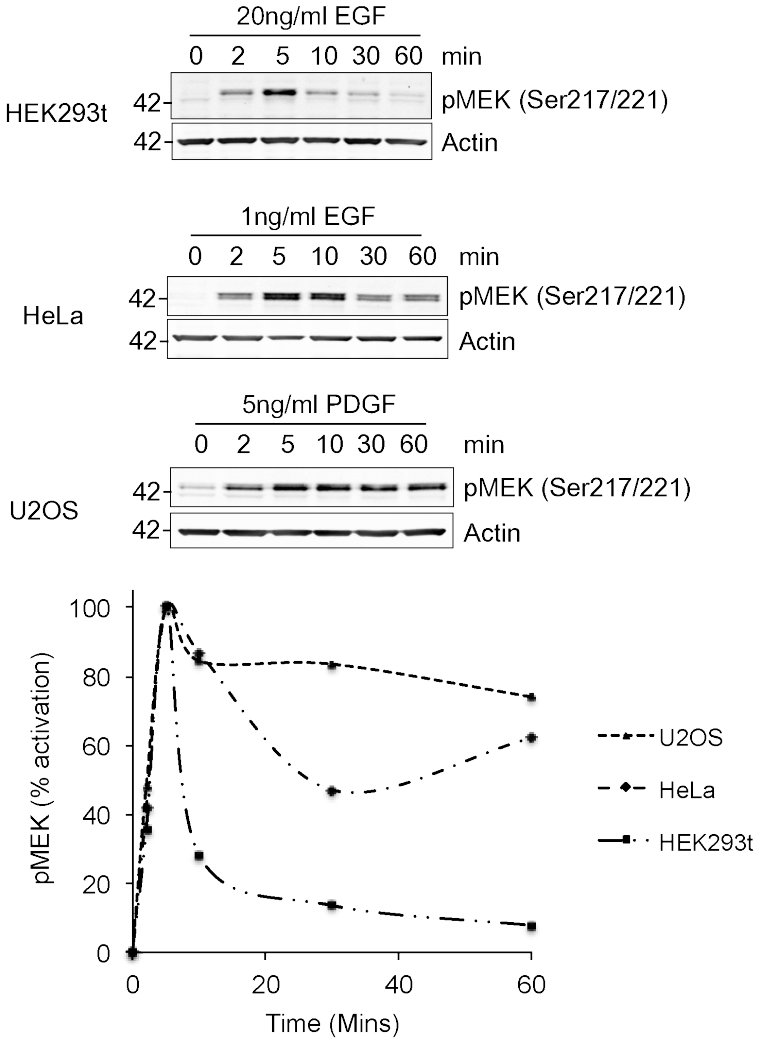

Figure 3.3 Time course of pMEK activation with growth factor stimulation.
Hek293t, HeLa and U2OS cells were serum starved overnight before stimulation with growth factor indicated for a time course between 0 and 60min. Cells were lysed in RIPA buffer and lysates were probed with antibodies against pMEK and actin. Quantification was performed with image J with values normalized to actin. Representative blot shown.

3.2.4. EGF titration against time in HeLa cells.

To further investigate the regulation of the MAPK pathway by EGF. We generated activation profiles for 3 different concentrations of EGF (1ng/ml, 5ng/ml and 20ng/ml) over a time course of 0-60 mins. This was performed on HeLa cells, a commonly used model to study EGF signaling. Lysates were run on the same gel and probed for pAKT and pMEK as readouts of the PI3K and MAPK signaling pathways respectively (Figure 3.4).

By increasing the concentration of EGF there is acceleration in the phosphorylation of MEK and AKT, demonstrated by an increasing signal at the 2min time point. The slope of decay for AKT phosphorylation seems unaffected by the increase in concentration of EGF, which suggests that there is an overriding dephosphorylating activity for AKT even concentration that produces maximal activation of the pathway. However, there is more sustained signaling for MEK activation with increasing EGF. A second peak of MEK activation is observed, which is more evident with the lower doses of EGF and most apparent at 5ng/ml. It is likely at 20ng/ml the second peak is masked by sustained activation.

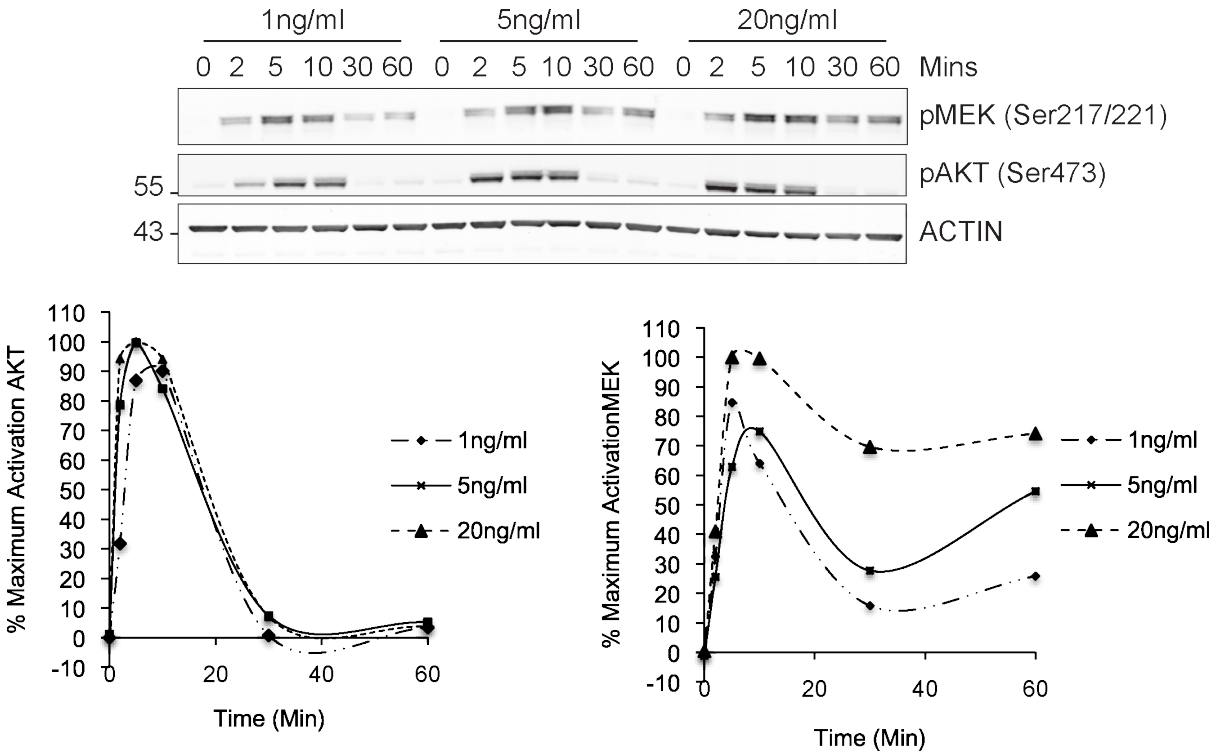

Figure 3.4. The effect of increasing EGF concentration over time on downstream effectors.

HeLa cells were serum starved overnight before stimulation with increasing concentrations of EGF over a time course between 0 and 60 min. Cells were lysed in RIPA buffer and lysates were probed with antibodies against pMEK and pAKT as a measure of activation of downstream effectors. Quantification was performed with Image J with values normalised to actin. Representative blot shown.

3.2.5. USP15 regulates PDGF stimulated MAPK pathway through CRAF.

U2OS cells were treated with siRNA targeting USP15, and BRAP for 72 hours. Control cells were mock treated with RNAi max alone or with siRNA targeting USP4. USP4 is a closely related DUB, also identified in the Y2H screen as binding to BRAP, which has no effect on the stability of BRAP[167]. Cells were serum starved overnight before stimulation with 10ng/ml PDGF for 5 mins (figure 3.5).

We observed a significant decrease in the levels of pMEK (U15-1= 39.8% SE=5.3, student t-test 0.008; U15-2 = 49.8%, SE= 1.9, student t-test p= 0.001, n=3) with USP15 knockdown with 2 individual oligonucleotides. To decipher the mechanism of this inhibition we probed for the critical upstream kinases, CRAF and BRAF. There was a significant decrease in the levels of the CRAF kinase (U15-1= 43%, SE=2, student t-test p= 0.001; U15-2 = 48.6% SE= 3.6, student t-test p= 0.004, n=3) but not the in the levels of the BRAF kinase with USP15 depletion. The decrease in CRAF could be observed with two individual oligonucleotides that corresponded to the decrease in pMEK.

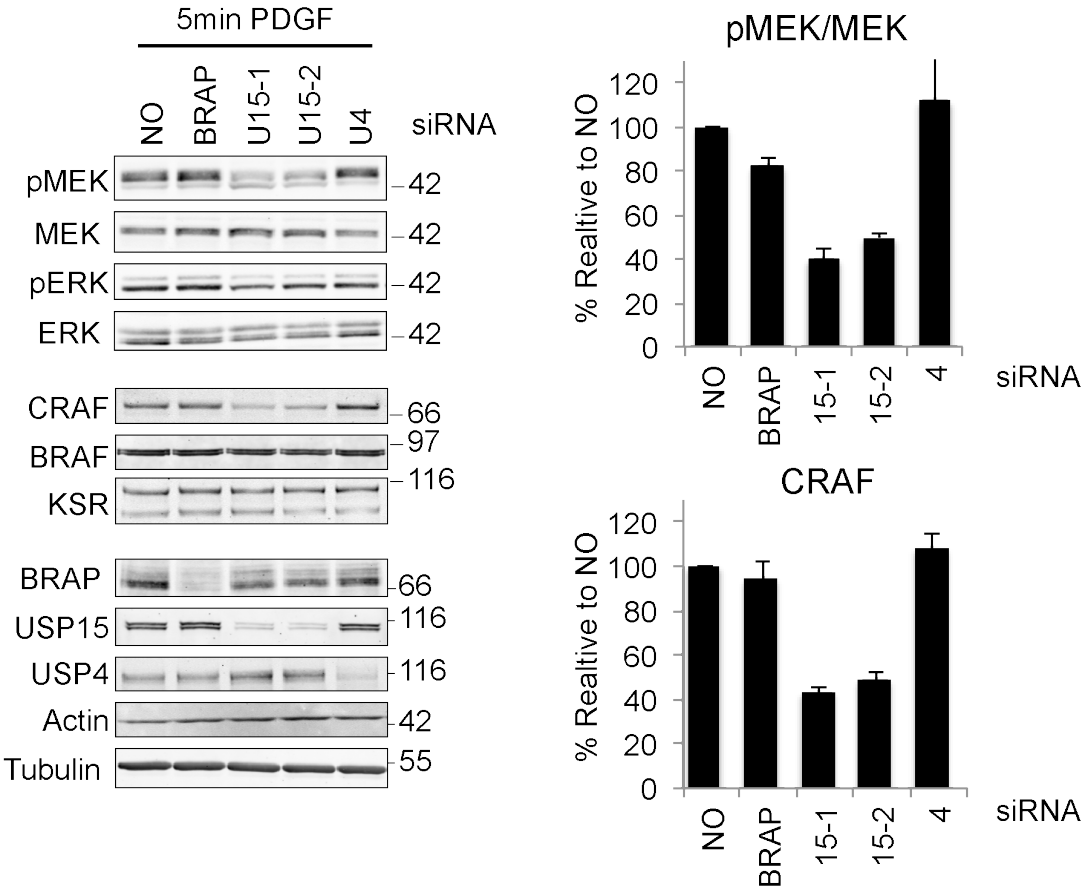

Figure 3.5. siRNA depletion of USP15 causes a decrease in MEK activation and the levels of CRAF.

Depletion of USP15 leads to a reduction MEK activation and concomitant reduction in the levels of CRAF. U2OS cells, treated with siRNA for 72 hours, serum starved overnight then stimulated with 10ng/ml PDGF for 5 mins. Bands were quantified using Image J and bars represent standard error (n=3)

3.2.6. Treatment with epoxomicin fails to rescue loss of CRAF with USP15 depletion.

To investigate whether the loss of CRAF in USP15 depleted cells was due to changes in the ubiquitylation status of CRAF. We employed epoxomicin to inhibit the proteasome, if knock down of USP15 was causing an accumulation of CRAF in an ubiquitylated form. One hypothesis would be that this would lead to its degradation via the proteasome. Inhibition of the proteasome would therefore rescue the levels of CRAF.

U2OS cells were treated with siRNA for 72 hours to deplete USP15 or USP4 as a control. The cells were then treated for 8 hours with 0.5μM epoxomicin before lysis. The intensity of bands was determined using image J software and normalized to the actin control.

There was a loss of CRAF in the USP15 depleted cells but not in the no oligo control or in cells where USP4 has been depleted. Treatment with epoxomicin failed to recue the levels of CRAF in USP15 depleted cells. This indicated that the loss of CRAF in U2OS cells was not due to increased ubiquitylation leading to its degradation via the proteasome.

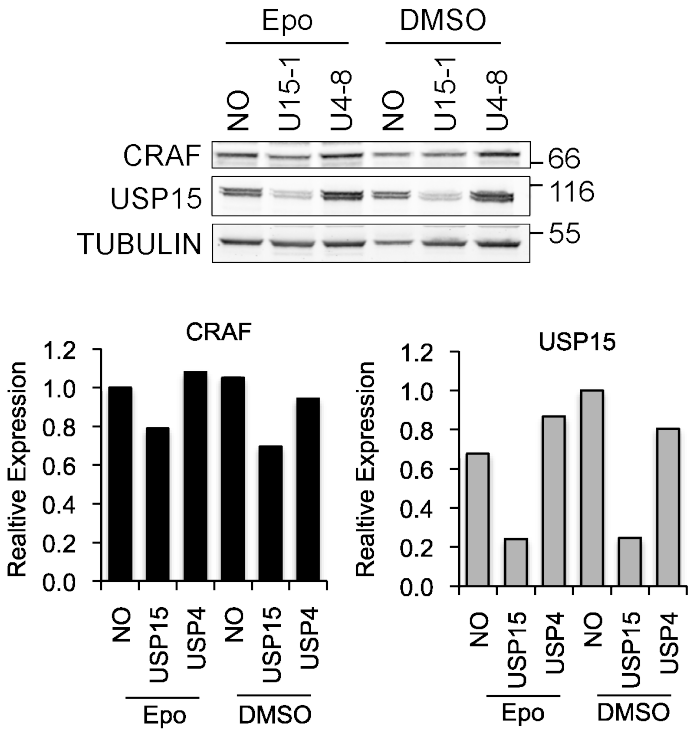

Figure 3.6. Inhibition of the proteasome fails to rescue CRAF levels.

U20S cells transfected with siRNA for 72hours before treatment with 0.5μM epoxomicin. Cells were lysed in RIPA buffer and lysates were immuno-blotted with CRAF, USP15 and Tubulin antibodies. Bands were quantitated using image j and normalised to tubulin, expressed as relative abundance to no oligo control. Representative blot shown.

3.2.7. Knockdown of CRAF phenocopies depletion of USP15.

To investigate what the consequences of CRAF loss are in the MAPK pathway. We depleted CRAF in U2OS cells with USP15 as a comparison. U2OS cells were treated with either a pool of oligonucleotides against CRAF or with individual oligonucleotides targeting USP15. Cells were serum starved overnight before stimulation with 10ng/ml PDGF for the time course indicated. There was a similar reduction in the levels of pMEK with both CRAF and USP15 depletion. Knockdown of CRAF is phenocopying the depletion of USP15.

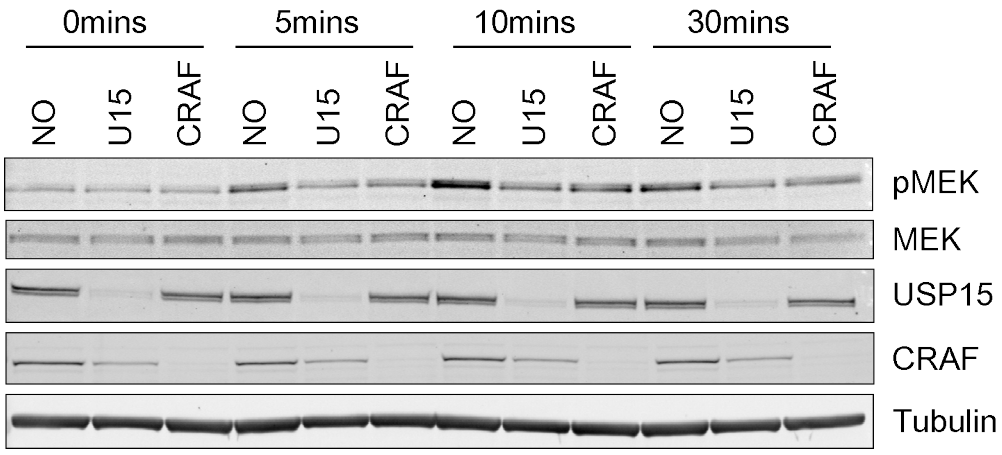

Figure 3.7 USP15 knock down phenocopies knock down of CRAF.

U2OS cells were transfected with siRNA for 72hours, serum starved overnight then stimulated with 10ng/ml of PDGF for a time course between 0min and 30min. Lysates were probed with antibodies against pMEK and CRAF.

3.2.8. Rescue attempt of CRAF levels.

We next asked whether the loss of CRAF was dependent on the catalytic activity of USP15. In order to answer this question I generated siRNA resistant forms (resistant to USP15 Oligo-1) of GFP-USP15* and catalytically inactive form GFP-USP15*-C269S (star denotes siRNA resistance). USP15 constructs were rendered siRNA resistant by introducing silent point mutations into the target sequence of oligonucleotide 1. Mutations were introduced using Quick-change kit (Stratagene), the primers are documented in the materials and methods section 2.5. and 2.6. We made the constructs with the aim of expressing these exogenous forms of USP15 and rescuing the levels of CRAF seen with USP15 depletion. The same loss of CRAF was observed following USP15 depletion in HeLa cells and due to technical difficulties performing rescue experiments in U2OS cells; we concentrated on rescuing USP15 in HeLa cells.

HeLa cells were treated either with USP15 oligo 1, USP4 as a control or mock treated with no oligo for 72 hours. 24 hours prior to lysis cells were transfected with GFP, GFP-USP15* or GFP-USP15*-c269s. The constructs were expressed constructs had the correct molecular weight and a second upper band was observed for GFP-USP15*-c269s that had been previously demonstrated to be an ubiquitylated form of USP15. However, in cells treated with USP15 oligo1 none of the constructs were expressed, indicative that knockdown of USP15 prevented the re-expression of plasmid DNA.

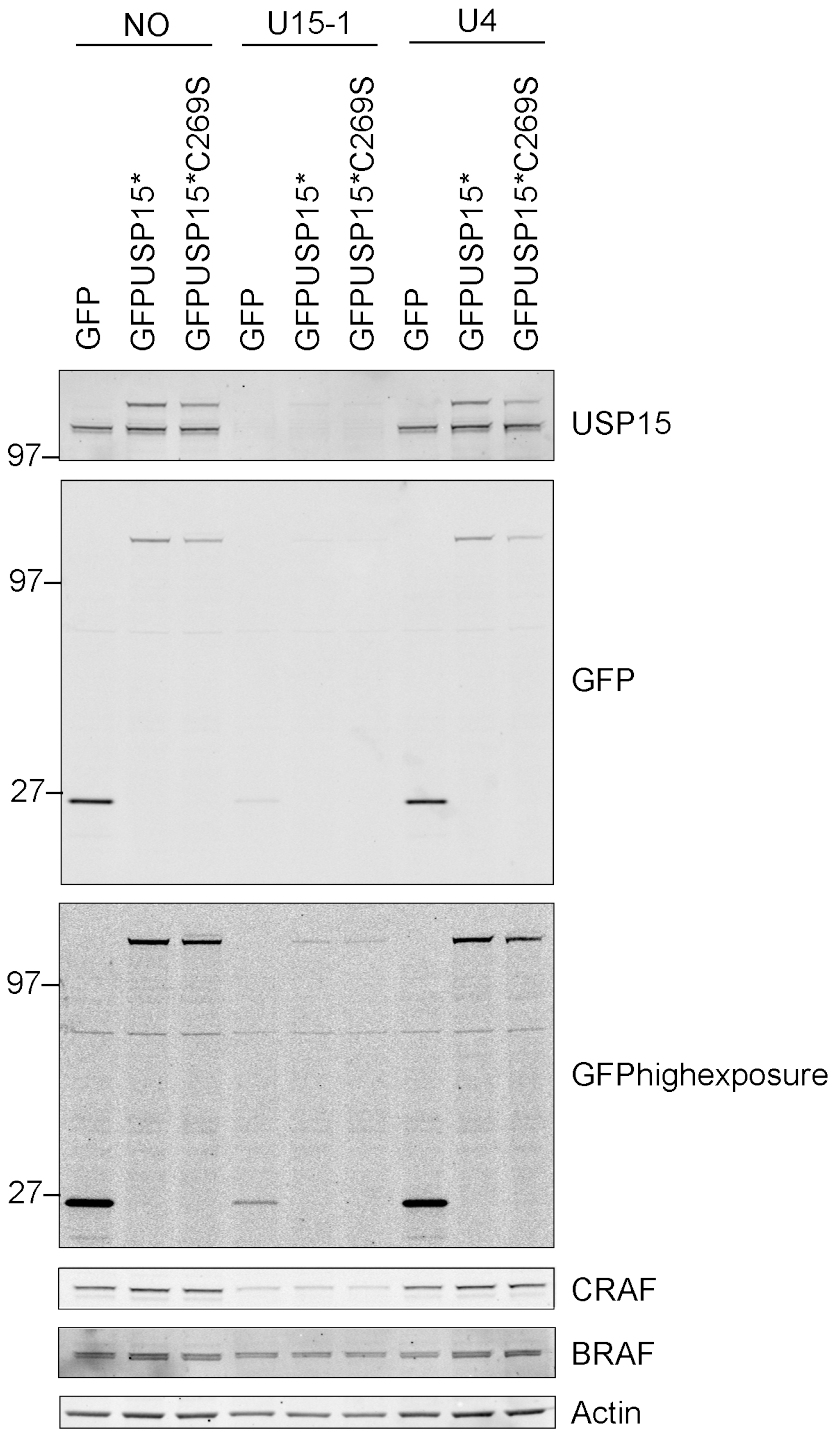

Figure 3.8 siRNA Resistant constructs fail to express in USP15 depleted cells.

HeLa cells were treated with siRNA targeting USP15, USP4 or left as a No Oligo control for 72 hours. 24 hours prior to lysis cells were transfected with siRNA resistant constructs GFP-USP15*, GFP-USP15*C269S or GFP.

3.3. Discussion.

We originally hypothesized that USP15 would have a positive effect on the regulation of the MAPK pathway. This was based on the findings that USP15 depletion led to the destabilization of BRAP, an E3 ligase that had been previously identified as a negative regulator of the pathway. BRAP functions by inhibiting the action of KSR, a scaffold for the RAF/MEK kinases facilitating their activation[168, 170, 171, 173]. The work presented here, together with other data published in Hayes et al. (2012)[167], demonstrated that USP15 has a dual role in the regulation of the MAPK pathway through direct and indirect mechanisms.

We also monitored the signaling kinetics of EGFR with varying concentrations EGF. We analyzed the activation of MAPK and AKT signaling pathways using phospho-specific antibodies. The results indicate that there is acceleration in the activation of AKT signaling with increasing concentration of EGF. While increasing the concentration of EGF delayed the inactivation of MAPK signaling. This fit with a model that AKT signaling is primarily occurring at the plasma membrane while MEK signaling can be sustained from the endosome. EGFR is endocytosed by either clathrin dependent routes with low concentrations of EGF (1ng/ml) or clathrin independent routes with high concentrations of EGF (100ng/ml)[103]. Clathrin mediated endocytosis has been reported to be dispensable in the degradation of EGFR, however is required the prolonged signaling of AKT an MAPK past peak (5mins) stimulation with EGF. Inhibition of non-clathrin dependent endocytosis causes increased post peak stimulation of AKT and MAPK pathways[174]. This would suggest that in at least HEK293t cells stimulated with EGF the predominant route of entry for EGFR is through non clathrin dependent endocytosis.

The effect of EGF concentration on the kinetics of EGF signaling is that well understood. However, one study addressing this issue used micro-western arrays to probe for multiple substrates of EGFR in A549 cells[175]. However, the authors were unable to see the same changes in AKT and MAPK we report here. There are two possible explanations for this, first, that

there are a cell specific effects of EGF activation that can depend on the multiple factors, such as EGFR concentration on the plasma membrane. Secondly, the sensitivity of their assay may not as great as our own due to the nature of micro-western arrays.

It would be interesting to explore which features of EGF signaling kinetics depended on the endosomal localization of EGFR. The activation and termination of the AKT signaling pathway is relatively quick and one could image that this is a mainly dependent signaling complex being localized plasma membrane. However in the case of MAPK pathway, it would be worth exploring the role of endocytosis on late acute signaling. Is the second peak of MAPK activation dependent on the endosomal localization of EGFR, as after 60min acute stimulation one would expect the majority of EGFR to be internalized into intra luminal vesicle (ILV) of the multi vesicular body (MVB). To test this hypothesis one could perform the same experiment with and without perturbation of endocytosis, using for example a dynamin inhibitor.

By using U2OS cells as a model system we have established that USP15 depletion caused a decrease in PDGF stimulated MAPK signaling. This was supported by evidence from HeLa cells and suggested that the effect was a conserved form of regulation[167], as USP15 depletion reduced MAPK signaling, in both EGF and PDGF stimulated cells. This led us to hypothesis that USP15 was regulating a core component of the MAPK pathway. By probing kinases in the pathway, we were able to confirm that this hypothesis held true. There was a reduction in the levels of the CRAF kinase, which was a specific effect as the BRAF kinase levels remained unaffected. Furthermore, the reduction of pMEK seen with USP15 depletion was phenocopied by knock down of CRAF.

This study suggests that USP15 is acting through CRAF to modulate the MAPK pathway. This is supported by additional experiments in W266-4 cells that harbor an activating $BRAF^{V600D}$ mutation. In this genetic background the knockdown of USP15 no longer has an effect as downstream signaling to MEK, as downstream signaling is now dependent on BRAF by passing

CRAF[167]. In contrast, in this context BRAP loss would be expected to have an effect.

Two questions remain outstanding. First, why is BRAP not having an affect on the MAPK pathway? This is partially answered in HeLa cells where it has been observed that serum starvation ablates the action of BRAP. Depleting BRAP in cells grown in full media caused an effect on MAPK signaling, which is abolished by serum starvation before stimulation[167]. In U2OS cells however, we didn't observe this effect. Secondly, are there additional targets for USP15 in the MAPK pathway? Knockdown of CRAF caused over a 90% drop in CRAF levels, which elicited the same response as partial (around 50%) loss with USP15. This raises the possibility that there are other targets for USP15 in the MAPK pathway that we are yet to uncover.

The mechanism of action USP15 on BRAP is direct as it is a bone fide substrate of USP15[167]. The mechanism of action of USP15 remains more obscure. Data from our lab indicate that USP15 is acting at a pre-translational, level influencing the stability of CRAF mRNA, which is dependent on the 3'UTR of CRAF[167]. Although this form of regulation was unexpected for USP15 on CRAF, ubiquitylation has been demonstrated to regulate mRNA stability[176]. From the literature it is also apparent that USP15 can regulate protein levels by multiple mechanisms. A portion of USP15 has been shown to be associated with polysomes and influences the generation of newly synthesized proteins[177]. It has also interacts with multiple components of the spliceosome, where it is possibly influencing the splicing of gene products[178, 179].

This work has helped establish USP15 as modulator of the MAPK pathway. It builds on growing evidence of the importance of ubiquitylation as a regulator of MAPK signaling events, both directly and indirectly. USP15 has now also been established as a mediator of other cancer associated pathways, notably, the TGF-β and BMP signaling pathways[180, 181].

So could USP15 be a viable drug target to treat cancer? With a complex involvement in different signaling pathways it is not clear whether USP15 would make a suitable drug target. Detailed understanding of the signaling functions of USP15 within different genetic backgrounds would need to be explored to confirm this hypothesis.

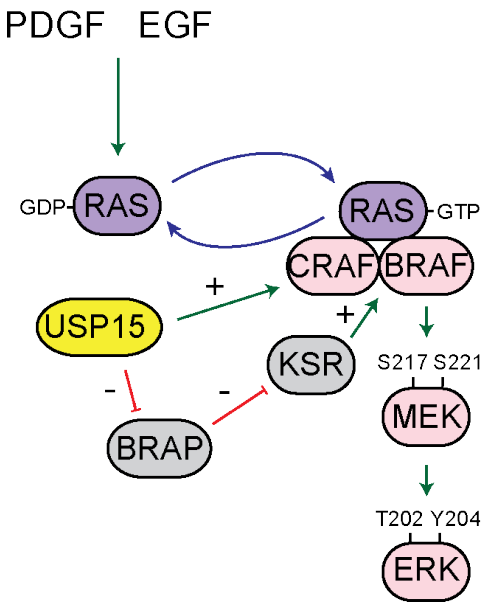

Figure 3.9. Model for the role of USP15 in MAPK signaling cascade.
USP15 has both positive and negative roles in the regulation of the MAPK cascade. Positive by maintaining the levels of the CRAF kinase and negative by deubiquitinating BRAP leading to it's proteasomal degradation. In systems tested in the dominant signaling function of USP15 is through CRAF however, in models where MAPK is not dependent of CRAF, the dominant signaling function of USP15 may signal through BRAP.

3.4. Conclusions

1. USP15 is a positive regulator of MAPK signaling.
2. USP15 maintains the levels of the CRAF kinase.
3. The dominant signaling effect of USP15 in U2OS cells is consistent with CRAF modulation.

Chapter 4 USP46 is a potential effector of EGFR.

4.1. Introduction

EGFR activation occurs at the plasma membrane[19] and the activated receptor if internalized into the endo- lysosomal pathway[13, 182]. The topology of EGFR means that the cytosolic kinase domain remains in the cytosol until it's is enveloped into multi vesicular bodies (MVB). This allows both the plasma and endosomal membranes act as platforms to build EGFR dependent signaling complexes[122, 123]. However, activation of EGFR regulates processes in locations distinct from the receptor. To achieve this downstream signaling, effector proteins can be recruited to separate compartments. The prototypic example of this recruitment is the MAPK (ERK1/2), which translocates from the cytoplasm to the nucleus upon EGFR activation. Translocation allows ERK to activate downstream transcription factors such as ELK1 and through it regulate gene transcription[35].

Phosphorylation is a key mediator of signaling pathways downstream of EGFR. The role of other post-translational modifications, such as ubiquitylation in the EGF signaling pathway is less understood. In 2011 Argenzio et al.[183] identified 285 proteins that changed ubiquitylation status in response to EGF application. This work suggested that ubiquitylation was playing a greater role in EGF signal transduction than previously thought. Ubiquitin is thought to be able to build signaling networks through interactions between ubiquitylated proteins and ubiquitin interacting motifs (UIM), comparable to those built between pTyr and SH2 domains. One may expect, as proteins are becoming ubiquitylated in response to EGF stimulation, that ubiquitylation is involved EGF signal propagation. Because of the dynamic nature of signal transduction, one would also expect DUBs to oppose the action of ubiquitin dependent signaling complexes.

It has been previously shown that USP8, is recruited onto endosomes with EGF application and is cytosolic when cells are serum starved[132]. USP8

regulates the degradation of EGFR through the endo-lysosomal pathway and is an effector of EGF signaling cascade[132, 135]. We devised an assay to identify other DUBs which exhibited EGF dependent localizations, utilizing a GFP-DUB library previously established in the laboratory[184]. We hypothesized that any DUB that changed its localization with EGF stimulation would potentially be an effector of the EGF signaling cascade.

4.2. Results

4.2.1. Identification of DUBs that are post-translationally modified in response to EGFR activation

We wanted to mine the literature for DUBs that are post-translationally modified with EGF stimulation, to guide our own studies. We curated data from 4 separate mass spectrometry experiments, which had identified post-translationally modified proteins with EGF stimulation. The first source was Olsen et al. (2006)[185] who used phospho-peptide enrichment from HeLa cells to create a global picture of proteins that are phosphorylated, in response to EGF. BAP1 was the highest confidence DUB hit in this screen with FLJ14981, A20 and USP54 also having some fluctuations in the phosphorylation status with EGF application.

The second source was Hammond et al. (2010)[186], the experiment sought to identify differences between EGF and HGF signaling in A549 cells. The authors used pTyr antibodies to enrich phosphorylated proteins after EGF/HGF stimulation, 3 DUBs were identified in the EGF IP, CYLD, USP6 and USP9x. The third source was Argenzio et al. (2011)[183] who enriched for ubiquitylated and ubiquitin bound proteins with EGF stimulation from HeLa cells. A number of DUB were identified in that study, ATXN3, JOSD1, USP5, USP11, USP15 and USP34. The final source was from Blagoev et al.(2004)[187] using a similar strategy to Hammond et al. (2010)[186] enriched pTyr pull down with EGF application at 0, 1 and 10min time points from HeLa cells. CYLD was the only DUB identified in this experiment and the only DUB seen in more than one experiment.

Gene	Phospho Peptide enrichment		pTyr IP EGF/HGF	Ub IP With EGF	pTyr IP EGF
	Increasing	Decreasing			
BAP1	Y	-	-	-	-
FLJ14981	Y	-	-	-	-
A20	Y	-	-	-	-
USP54	-	Y	-	-	-
CYLD	-	-	Y	-	Y
USP6	-	-	Y	-	-
USP9X	Y	-	Y	-	-
ATXN3	-	-	-	Y	-
JOSD1	-	-	-	Y	-
USP5	-	-	-	Y	-
USP11	-	-	-	Y	-
USP15	-	-	-	Y	-
USP34	-	-	-	Y	-

Table 4.1 PTM-DUB identified in large-scale proteomic screens.

Data collected from 4 different sources on post-translational modification of DUBs in response to EGF signaling. Column 1 is sourced from Olsen et al.(2006) [185], Column 2 is sourced from Hammond et al.(2010) [186], Column 3 is sourced from Argenzio et al.(2011) [183], Column 4 is sourced from Blagoev et al.(2004) [187].

4.2.2. Validation of model system

We sought to validate HeLa cells as a model by demonstrating that changes in localization could be observed with saturating dose of EGF and that those changes could be visualized following fixation in 4% PFA. As a readout we used the ERK1/2 as it is a prototypic model for protein translocation after EGF stimulation. HeLa cells were serum starved for 16 hours before stimulation with 20ng/ml EGF for 10 mins. Cells were fixed in 4% PFA and stained using antibodies against ERK1/2 and the phospho specific antibodies that target the activated form of ERK1/2 (Thr202/Tyr204). ERK1/2 translocates into the nucleus after 10 mins of stimulation with 20ng/ml EGF stimulation in its activated form (Figure 4.1).

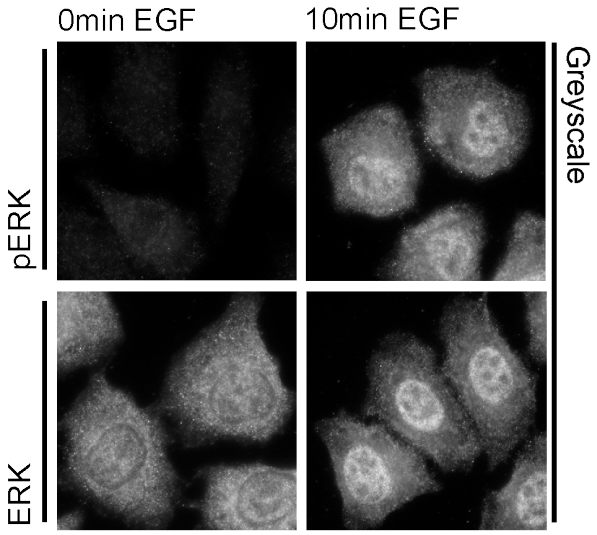

Figure 4.1 Positive controls for EGF dependent translocation.

Validation of model, HeLa cells were serum starved for 16hours before application of 20ng/ml EGF for 10mins and fixed in PFA. Cells were stained with antibodies against the phosphorylated and total ERK.

4.2.3. DUB-EGF screen

We chose to perform the screen in HeLa cells, as the GFP-DUB library had been previously used in this system to assess the basal localization of each construct[184]. This provides an added reference point to assess changes in localization seen with EGF application. Cells were serum starved before stimulation to remove the effect of any other factors present in the serum. 3 time points were used, 0 min representing serum starved conditions, 10 min to capture post-peak stimulation and 30 mins for late signaling events.

HeLa cells were transfected with individual members from the GFP-DUB library. 63 individual DUBs were included in the screen; a break down of the coverage across the families of DUBs is shown in figure 4.2.B. Following detailed visual inspection, changes in distribution were noted for USP8, USP46 and UCHL5. Figure 4.2.A shows representative images for these proteins taken from the screen. USP8 was observed being recruited onto punctate structures in the cytoplasm. This served as a positive control for the screen as the endosomal recruitment of USP8 with EGF stimulation has been previously reported[132]. USP46 was also observed on similar punctate structures in the cytoplasm with EGF stimulation, reminiscent of those changes seen with USP8. UCHL5 was seen in punctate structures in the nucleus under starvation conditions that disappeared with EGF stimulation. The changes seen were all subtle; therefore quantification was performed on USP46 and UCHL5 to increase confidence. As USP8 translocation has been previously reported[132] we didn't follow this up.

Full results are shown in supplementary figures S.1-6. Results are split into DUB sub-families groups with representative images shown for each DUB. Notes from the screen are documented in supplementary table S.1. Some DUBs displayed dual distributions that were not dependent on EGF when further analyzed; this data is summarized in table S.1.

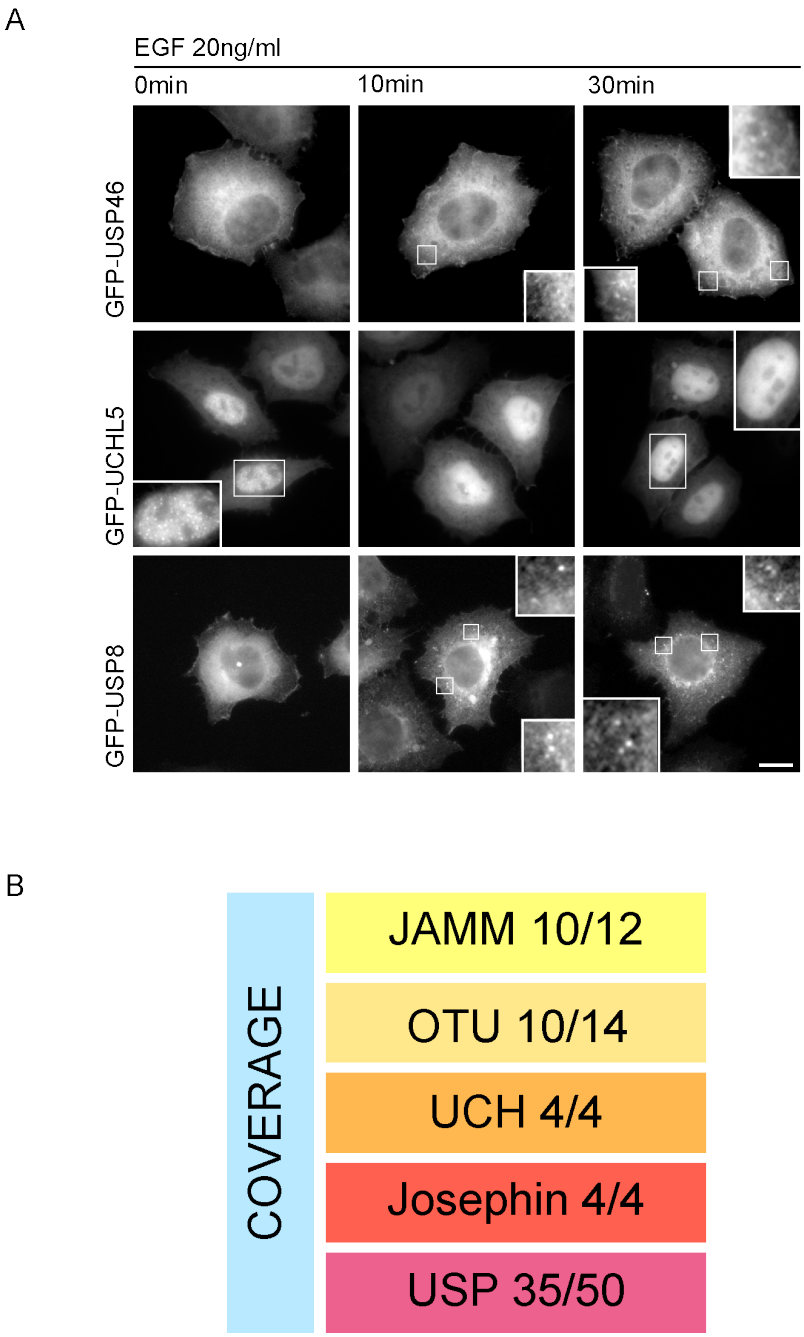

Figure 4.2. Overview of DUB-EGF screen.

A) GFP-DUB library was transfected into HeLa cells, cells were stimulated with 20ng/ml of EGF for a time course of 0min, 10min and 30min. Cells were then imaged using fluorescence microscopy to judge changes in subcellular localization. Representative images shown in panel A. Scale = 10μm.

B) A graphic representation of the coverage of the screen across the different families of DUBs.

4.2.4. Quantification of UCHL5 distribution

There was an enrichment of UCHL5 into punctate structures within the nucleus in serum-starved conditions, which disappeared following EGF stimulation. This observation was quantified by stratifying cells into different bins were there was no punctae (C; red), observable punctae (B; yellow) and prominent punctae (A; green). Each experiment was performed 3 times and approximately 200 cells were counted per condition, cells were counted by eye under the microscope from random fields of view, error bars represent standard deviation. There was a significant dissipation of the punctate structures following EGF stimulation (Figure 4.3).

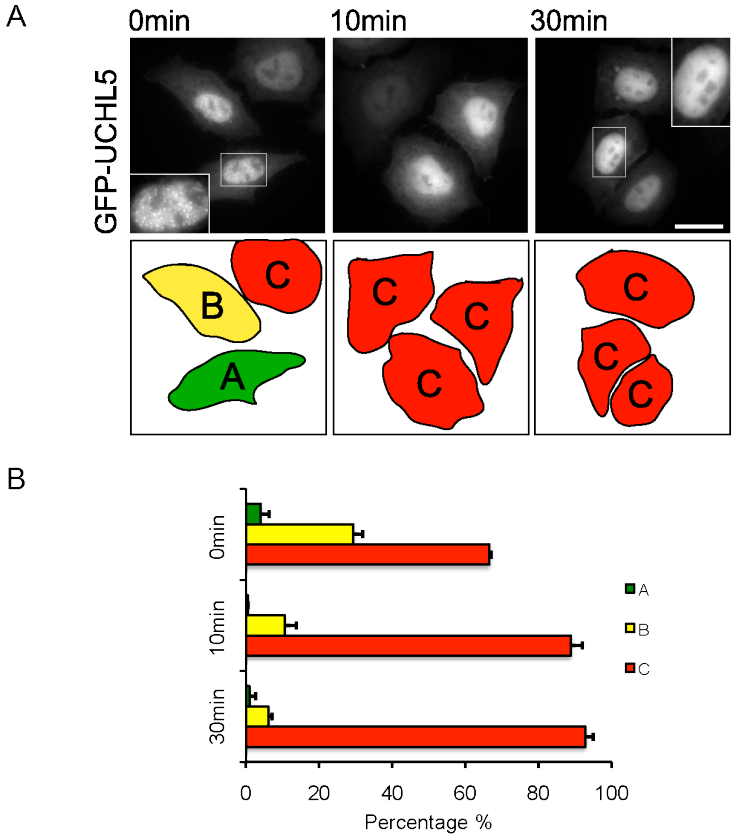

Figure 4.3 Quantification of GFP-UCHL5 nuclear punctae.

HeLa cells were transfected with 1µg GFP-UCHL5, serum starved for 16 hours and then stimulated with 20ng/ml EGF for a time course of 0, 10 and 30 mins before fixation in 4% PFA. A) Represents criteria for stratification A, prominent nuclear punctae B, observable punctae C, No nuclear punctae. Images taken from fig. 4.21. scale bar = 20µm B) Graph showing the results of quantification, results were grouped into 3 bins. Approx. 200 cells were counted per condition, n=3. Bars represent standard deviation.

4.2.5. Quantification of USP46 punctate distribution in HeLa and U2OS cells.

Quantification of USP46 enrichment into cytosolic punctate structures was performed on GFP-USP46 transfected cells. Cells were stratified into 2 categories (i) observable punctae (ii) diffuse cytosolic distribution. Each experiment was performed 3 times and approximately 100 cells were counted per condition, cells were counted by eye under the microscope from random fields of view. Under serum starved conditions 13%±3 of transfected cells displayed punctae, after 10mins 20ng/ml EGF stimulation this increased to 60±11% and fell to 48±11% after 30mins of EGF stimulation (Figure 4.4).

To test whether this effect was specific to EGF stimulation we tested the effect of PDGF stimulation on U2OS cells transfected with the same plasmids. Under serum starvation conditions, 14±6% of transfected cells had a punctae distribution, this rose to 55±4% after 10min stimulation with 20ng/ml PDGF. Representative images from U2OS cells are shown in figure 4.4.B.

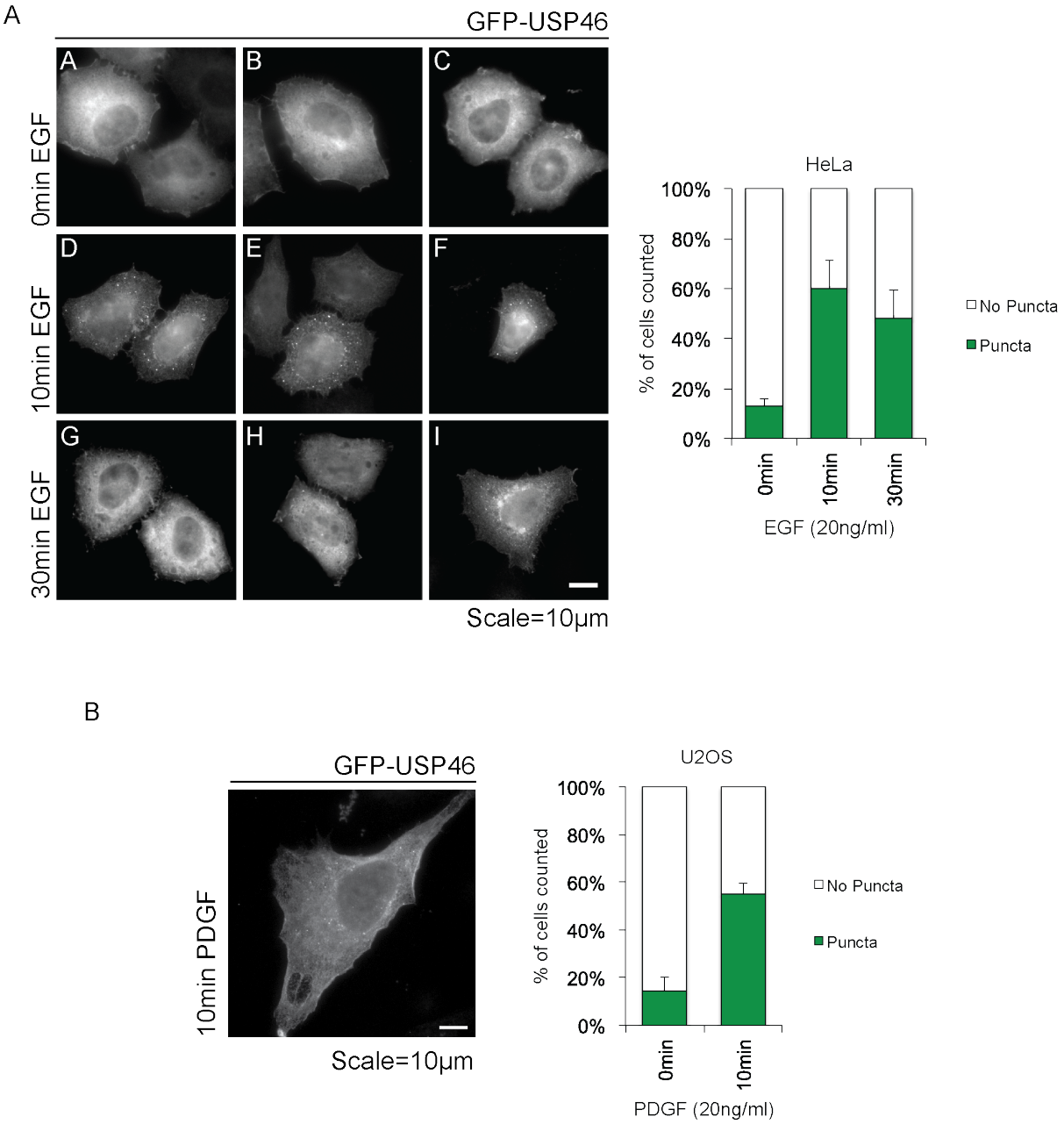

Figure 4.4. Quantification of Punctate Phenotype.

A) Images taken from DUB-EGF screen, images A and G are taken from figure 4.3.1.A. HeLa cells were transfected with GFP-USP46 and stimulated with 20ng/ml EGFR. Scale = 10µm. Cells were stratified as either (i) observable punctae (ii) diffuse cytosolic distribution. Error bars = Std dev. n= approx. 100 per condition.

B) B) U2OS cells were transfected with GFP-USP46, cells were serum starved overnight before stimulation with 20ng/ml PDGF. (i) Observable punctae (ii) diffuse cytosolic distribution. Error bars = Std dev. n= approx. 100 per condition.

4.2.6. Blockade of the EGF receptor activation prevents USP46 translocation.

We next wanted to test if either of the MEK/ERK or PI3K/AKT pathways is required for the translocation to occur. To do this we used a panel of kinase inhibitors, which would block the canonical signaling cascades downstream of the EGFR receptor. Gefitinib that blocks activation of the receptor itself[188], PI103 that inhibits class 1α PI3K[189] and AZD6244 that inhibits MEK[190]. We titrated the concentration of the kinase inhibitors and tested the efficacy using HeLa cells which were incubated for 15 mins with the kinase inhibitors before the media was exchanged for medium containing 20ng/ml EGF + the respective concentration of kinase inhibitor. Cells were then lysed in RIPA buffer and lysates were probed with phospho specific antibodies against the EGFR receptor, AKT and ERK kinases, which identify the active form of each kinase. We noted that with increasing concentrations of the MEK inhibitor we observed a paradoxical increase in the levels of AKT phosphorylation (figure 4.5.A). Gefitinib and AZD6244 were used at a concentration of 300ng/ml and PI103 were used at 150ng/ml.

When the translocation of GFP-USP46 was assessed in the presence of the kinase inhibitors there was a block of the translocation seen with treatment with Gefitinib to similar levels observed (10%±4%) in serum starved cells indicating that the translocation was dependent upon tyrosine kinase activation. There was no effect observed with inhibition of the PI3K signaling pathway (47±1%) compared to the DMSO control (45±5%) and blockade of the MAPK pathway (21±13%) showed a partial blockade of the translocation (figure 4.5.B). This indicated that the translocation effect was downstream of the EGFR receptor regulated, by the MAPK pathway, which corroborates with the observations that PDGF stimulation can also induce the translocation as the PDGF can also activate the MAPK pathway.

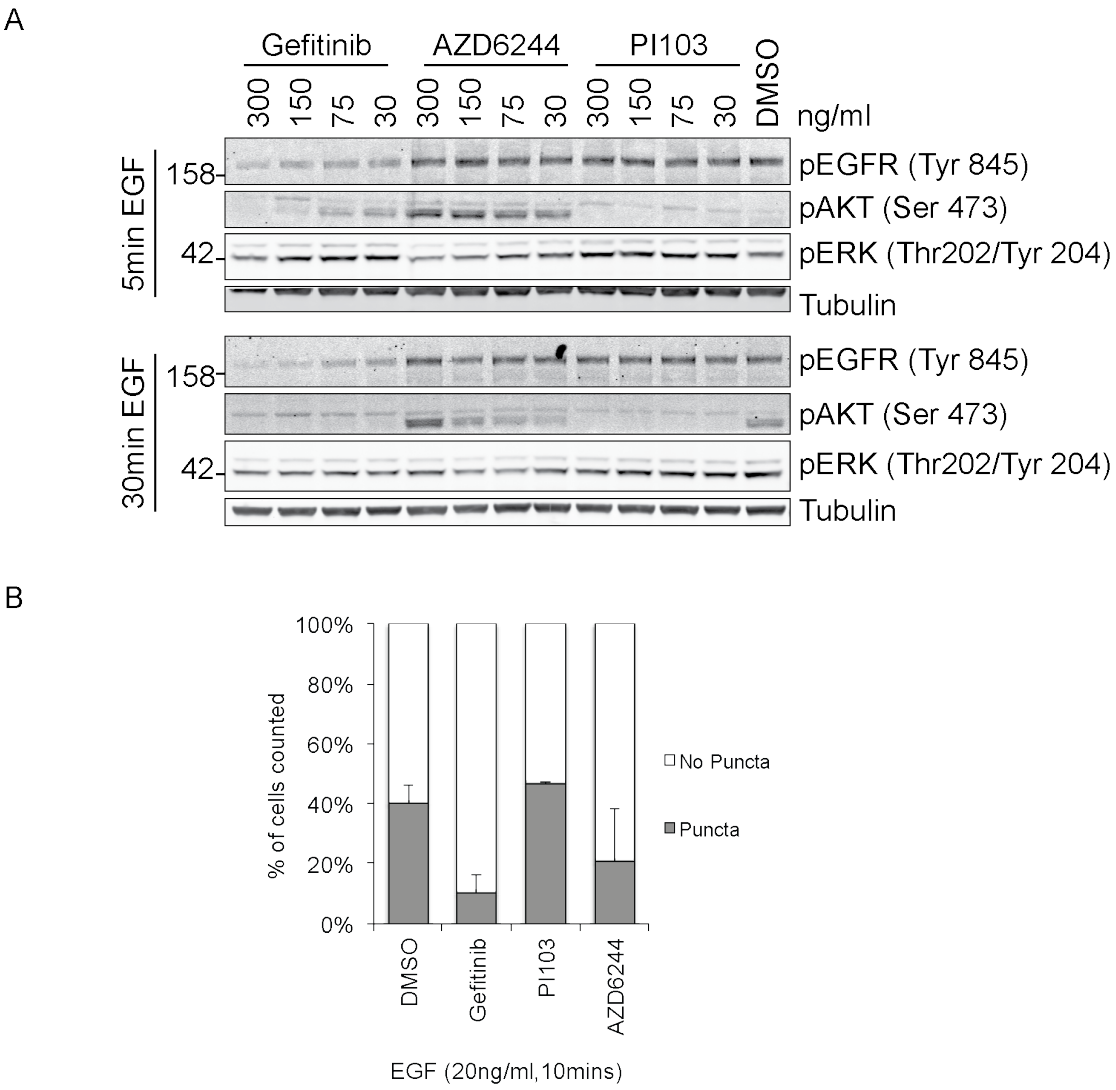

Figure 4.5. Recruitment to punctae is blocked by inhibition of EGFR/ERK pathway.

A) Titration of inhibitors on HeLa cells. HeLa cells were serum starved for 16hours then they were then pretreated for 15mins with the inhibitor at the concentration indicated, then stimulated with 20ng/ml EGF in the presence of the inhibitor. Cells were lysed in RIPA buffer and probed using phospho-specific antibodies.

B) HeLa cells were transfected with GFP-USP46 for 24hours. Cells were serum starved overnight then pretreated with DMSO, 300ng/ml Gefitinib, 150ng/ml PI 103 or 300ng/ml AZD6244. 20ng/ml was then added in the presence of the inhibitor. Transfected cells were stratified into either having punctae or not with approx. 100 cells counted per condition. n=3, error bars represent standard deviation.

4.2.7. USP46 is localized to HRS positive endosomes.

We next sought to identify the punctate structures using confocal microscopy to assess co-localization with a panel of markers for various endocytic compartments. U2OS cells were stimulated with 20ng/ml PDGF and either fixed in methanol or 4%PFA depending on the requirement of the antibodies. There was co-localization with HRS, a protein that decorates the MVB compartment[191]. Concomitant with HRS there was also some overlap with the retromer component VPS26 that is involved in cargo recognition for retrograde transport from the late endosome to the trans Golgi network (Figure 4.6).

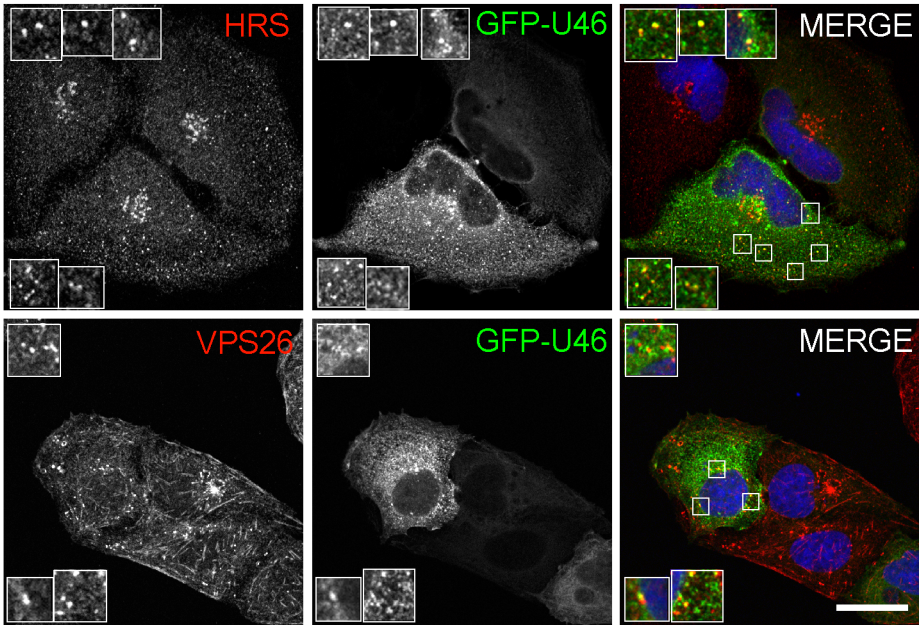

Figure 4.6. USP46 is recruited to HRS positive endosomes.
U2OS cells were transfected with GFP-USP46 for 24 hours then serum starved overnight before stimulation with 20ng/ml PDGF for 10min then subsequently fixed in 4% PFA or 100% methanol. Cells were then labeled with antibodies indicated. Cells were imaged using confocal microscopy. Scale = 20μm.

4.2.8. Knock down of USP46 has no effect on the trafficking of EGFR but causes a delay in the inactivation of EGF signaling.

Given the response to EGF and localization of GFP-USP46 on the multi-vesicular body compartment we wanted to test if knockdown of USP46 had an effect on the degradation of EGFR and downstream signaling. USP46 was depleted using a pool of siRNA oligonucleotides against USP46, using a double hit protocol over a period of 120 hours. Cells were serum starved for 16hours before stimulation with either 1ng/ml or 100ng/ml EGF over a time-course of 0 to 120 mins.

Depletion of USP46 had no effect on the rate of degradation of EGFR was observed (Figure 4.7.A and C). There is a characteristic upshift of the EGFR band with EGF stimulation consistent with hyperphosphorylation of the receptor. At 5 mins hyperphosphorylation is such that it partially prevents the ability of the antibody to recognize EGFR, as the epitope is located in the intracellular domain of EGFR. To better image the later time-points when EGFR is not hyper-phosphorylated, 30µg of sample were run on a gel confirming that there was no effect on EGFR degradation for the time points 0, 30, 60 and 120mins.

Samples stimulated with 1ng/ml EGF were probed with pAKT (Ser473) and pMEK (Ser217/221) as readouts for activation of the two canonical signaling pathways downstream of EGFR (Figure 4.7.B). There was little change in the peak phosphorylation of either pathway, however there was a delay in the inactivation for both pathways seen by increased phosphorylation at the 60 and 120 min time-points.

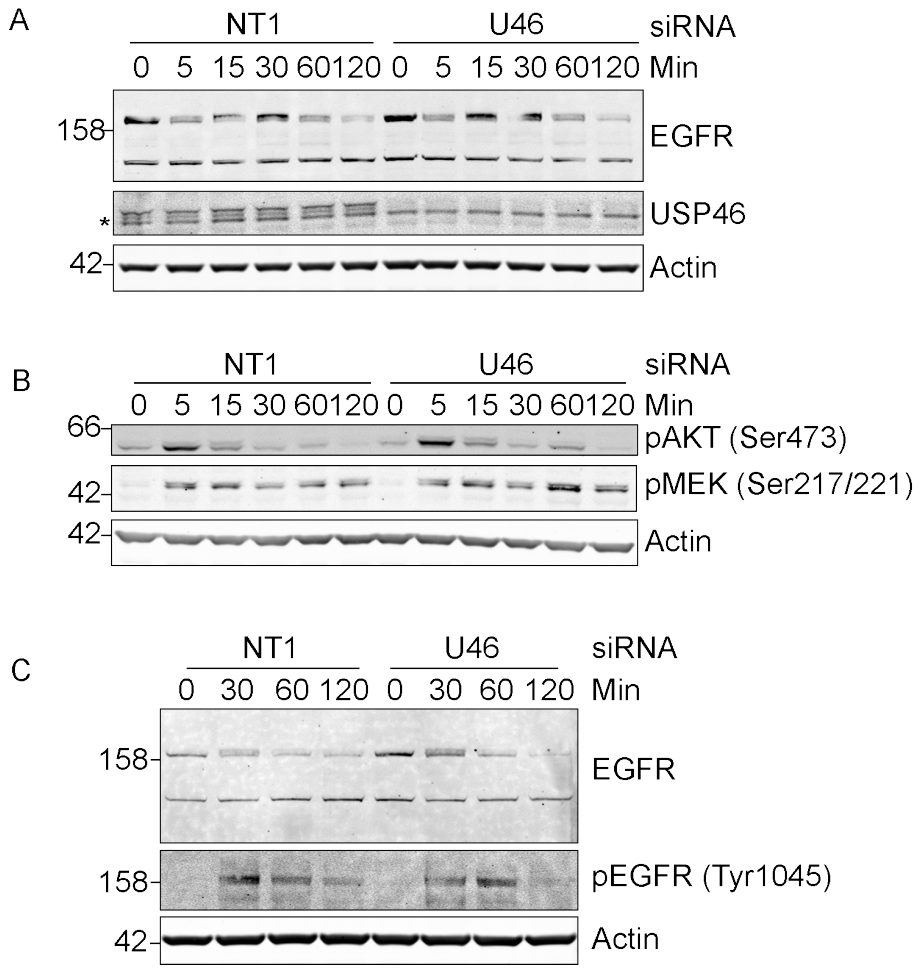

Figure 4.7. USP46 depletion has no effect on the degradation of USP46 but delays pMEK and pAKT inactivation.

HeLa cells were treated with a pool of oligonucleotides targeting USP46 or a Non-targeting oligo for 120 hours. Cells were serum starved for 16hours before stimulation with either 100ng/ml EGF (A and C) or 1ng/ml EGF (B). A and C are the same experiment with lysates run at 15µg and 30µg to improve visualization of EGFR band. * Denotes non-specific band.

4.2.9. Knock down of USP46 delays AKT inactivation.

Next we wanted to test if the signaling phenotype seen with depletion of USP46 was a specific effect of the siRNA. We therefore depleted USP46 using individual oligonucleotides from the pool used in previous experiments. We also tested if the stability of PHLPP1/2 was affected by USP46 depletion. PHLPP1/2 are phosphatases that have been identified as interactors with USP46, and are described as regulating the activity of AKT[58, 178]. A delay in the inactivation of MAPK/AKT pathways was observed when USP46 was depleted, to identify a possible mechanism for this regulation we tested if the depletion of USP46 affected the stability of PHLPP1/2 (figure 4.8).

HeLa cells were treated with siRNA for 72 hours in order to deplete USP46. Non-targeting oligonucleotide (NT1) and No Oligonucleotide mock transfection (NO) was used as controls. Cells were serum starved for 16 hours before treatment with 1ng/ml EGF (approximately the EC_{50} defined in chapter 3) for 5 mins to look at the peak activation and 60mins to look later time point. Of the 4 oligonucleotides, 6, 7 and 8 generated efficient knockdowns while 9 only partially depleted USP46. An increase in pAKT signaling and to a lesser extent with pMEK was seen with oligonucleotides 6 and 7 but not with 8. No changes were seen in the stability of PHLLP1 and an increase in the levels of PHLLP2 was seen with oligonucleotide 6 (figure 4.8).

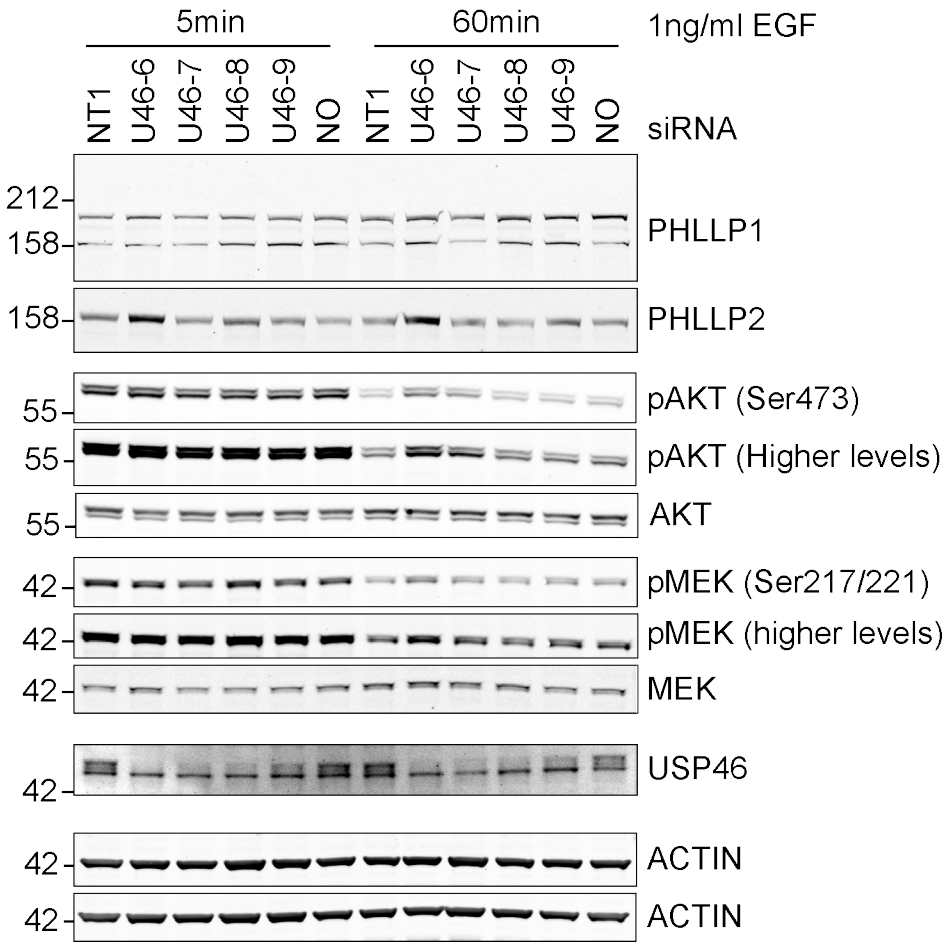

Figure 4.8. Deconvolution of USP46 depletion phenotype on activation of EGF signaling.

HeLa cells were treated with individual oligonucleotides for 72hours. Cells were serum starved for 16hours before treatment with 1ng/ml EGF for 5 and 10mins before lysis in RIPA buffer.

4.2.10. Depletion of USP46 in HCT116 cells.

During the course of this study it was reported by Li et al. (2013)[192] that USP46 was a DUB for PHLPP1. The authors demonstrated that USP46 regulating PHLPP1/2 stability and the phosphorylation of AKT through PHLPP1, in the context of colon cancer cells (HCT116). In light of our results we wanted to use the same model system to look at the stability of PHLPP1 and the attenuation of pAKT signaling. We performed the siRNA depletion experiment in HCT116 cells using oligonucleotides 6 and 7, which gave the greatest knockdown of USP46 in HeLa cells.

We first titrated the concentration of EGF using pMEK as a readout of EGFR activation as to be consistent with previous experiments. The EC_{50} for our EGF on HCT116 cells was approximately 5ng/ml, which was used, in subsequent experiments. The time course of pMEK activation in HCT116 cells displayed interesting kinetics, after peak stimulation there was a long refractory period were pMEK did not return to basal levels of stimulation (Figure 4.9.A).

HCT116 cells with depleted USP46 showed differential activation of the AKT pathway with the two oligonucleotides tested. Oligonucleotide 6 produced a large increase in the levels of pAKT with stimulation over the NT1 control. This effect however was not replicated with the oligonucleotide 7 which had kinetics more similar to the NT1 control. No effects were observed on the stability of PHLPP1 with either oligonucleotide despite both produced efficient knockdowns (Figure 4.9.B).

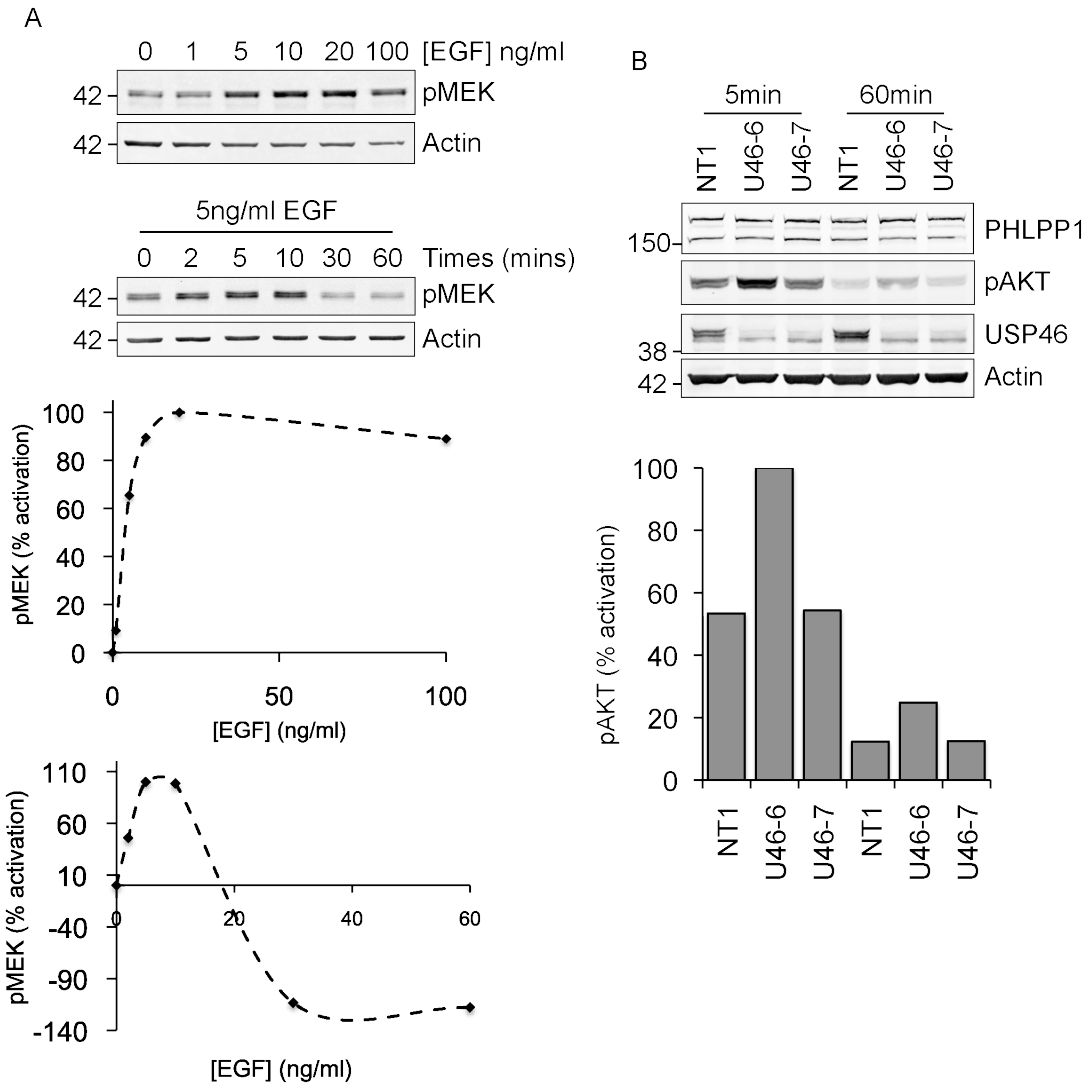

Figure 4.9. Depletion of USP46 in HCT116 cells.

A) HCT116 cells were serum starved for 16hours before treatment with EGF at the concentration and time indicated. Representative blot shown.

B) HCT116 cells were treated with siRNA targeting with USP46 or with a non-targeting control oligonucleotide FOR 72 hours. Cells serum starved for 16hours before treatment with 5ng/ml EGF for the time indicated. Quantification was performed using Image J software; values are normalized to actin control. Representative blot shown.

4.3. Discussion

We devised an assay to look for mobilization of DUBs with EGF stimulation, using a GFP tagged DUB library transiently expressed in HeLa cells. The assay was viable and the redistribution of USP8 could be observed, serving as a positive control that was consistent with reports in the literature[132]. From this screen, we identified a number of candidate DUBs that either changed localization or induced changes in cell shape when stimulated with EGF. 2 DUBs USP46 and UCHL5 were quantified and EGF dependent distributions were confirmed. USP46 was chosen for more detailed analysis, as the changes in distribution were reminiscent of those seen for the EGF effector USP8 and because of the availability of reagents. Using confocal microscopy USP46 was confirmed as an endocytic DUB partially, co-localizing with HRS, a protein that decorates the sorting endosome. A number of DUBs have been associated with endosomes, AMSH[129], AMSH-lp[131], USP8[132], USP2a[193] and USP10[194], all of the which have proposed roles in the trafficking of plasma membrane proteins. AMSH[195], USP8[132] and USP2a[193] have been demonstrated to directly influence the trafficking of EGFR.

USP46 has been shown to play a role in the trafficking of the inotropic GluR1 channel in *C.Elegans.* Knockout worms show a decrease in the expression levels of GluR1 and an increase in the ubiquitylated form of the receptor[142]. This evidence is compounded in mice by a loss of function mutation in USP46 (deletion of Lys92 in mice), which significantly reduced immobile time during forced swimming test (FST) and tail suspension assays (TST)[196]. When animals are subjected to FST and TST they enter a state of behavioral despair, where the animal cannot escape the situation it is in and effectively gives up. This is commonly used to test for anti-depressive effects, as anti-depressive compounds reduce immobility time in these assays[197]. USP46 knockout mice mimic the effect of the mutation and agonists against $GABA_A$ neurons partially increased immobility time. However, these results suggest that USP46 is having multiple levels of action[197], possibly through the regulation of plasma membrane receptors.

In our experiments USP46 didn't regulate the trafficking of EGFR as judged by biochemical methods. These results are consistent with results from Parja et al.[198] who performed a family wide siRNA DUB screen to identify DUBs altering EGFR degradation, using the same assay as here. The non-effect of USP46 depletion on the termination of EGF signaling in figure 4.8 was reproduced with 2 oligonucleotides (figure 4.9) in HeLa cells. We tested the stability levels of PHLPP1/2 because it had been reported that USP46 interacts with PHLPP phosphatases[192,178]. PHLPP1/2 are phosphatases that directly dephosphorylate AKT at Ser473 and have tumor-suppressing effects[58]. USP46 has also been reported to regulate the stability of the PHLPP phosphatases, and theoretically influences the activity of AKT in HCT116 colon cancer cells[192]. However, the results here contradict those published by Li et al. (2013)[192]. Following efficient knockdown of USP46 no effect on PHLPP1 expression levels could be observed, which should reflect protein stability.

We sought to clarify our results with regards to the activation of AKT and PHLPP1/2 by performing USP46 depletion experiments in HCT116 cells (the same used in Li et al. (2003)[192] study). Oligonucleotide 6 produced a pronounced effect on the levels of pAKT while oligonucleotide 7 had no effect, nor did depletion of USP46 have an effect on the stability of PHLPP1. It is of note that the antibody used to detect PHLPP1 was from the same source of Li et al. (2003)[192] and has been well characterized[199]. It is also worth noting that the antibody has also been reported to cross react with β-catenin, which casts further doubt on some of the data published by Li et al. (2013)[192, 199]. The results presented here directly contradict the conclusions in the Li et al.[192] study. There are two possible explanations for this, first, that our depletion was not as effective as that previously employed and the remaining pool of USP46 is sufficient to maintain PHLPP1 levels. In that case the effect seen with oligonucleotide 6 may occur because it has the most efficient depletion. Alternatively as only 1 oligonucleotide is having a significant effect across 2 cell lines (HeLa and HCT116) then the effect seen is an off target effect of the siRNA.

This chapter describes USP46 as a new endosomal DUB responding to EGF activation although we failed to establish a specific endosomal function for USP46. This work has directly contradicted published work describing USP46 as a regulator of EGF signaling through PHLPP1/2.

4.4. Conclusions

- USP46 is an endosomal DUB.
- USP46 is a potential effector of the EGF signaling cascade.

Chapter 5 USP46 interactome

5.1. Introduction

USP46 is a deubiquitylase that has been implicated in the regulation of glutamate receptor (inotropic, GluR1) trafficking[142] and has been identified as drug a target to treat depression[196, 197]. In the previous chapter we have identified USP46 as an endosomal deubiquitylase but could not identify any endosome specific functions of USP46. Interaction datasets have been generated for across the families of DUB including USP46 by Sowa et al. (2009)[178] through immuno precipitation (IP) experiments coupled with LC-MS/MS identification, however, no endosomal proteins were among the high confidence interactors[178]. WDR20 and WDR48 are the 2 best-characterized interactors of USP46[200]. WR20 and WDR48 belong to a family of proteins characterized by the inclusion of WD40 domains. These proteins are believed to behave as interaction hubs that facilitate interactions in protein complexes. Binding of WDR48 and WDR20 to USP46 is required for the deubiquitylating activity[200] and the interaction is required for USP46 function as a histone deubiquitylase[201].

In addition to WDR20/WDR48, the AKT phosphatases PHLPP1/2 have been identified as interactors of USP46[192], reported in 3 separate papers[178, 192, 200]. However, none of these studies have seen this interaction with the endogenous USP46 raising the possibility that it requires overexpression of USP46 to be observed. In the previous chapter we were unable to see any effects on the stability of PHLLP1/2 with USP46 depletion and could not definitively prove an effect on AKT activity. To better understand the functions of USP46 we sought to identify interactors in an unbiased fashion.

We generated cell lines that stably expressed GFP-USP46 and catalytically inactive GFP-USP46-C44S using the Flp-in system. We could IP the exogenous plasmid using GFP Nano-trap antibody, from SILAC (stable isotopically labeled amino acids in culture) labeled cells. This allowed us to

directly compare interactors of GFP-USP46, GFP-USP46-C44S and GFP, in a quantitative manner by using the SILAC ratio to excluded non-specific interactors with GFP[202]. From this experiment we identified several candidate interactors, including FBXO11, a substrate-recognizing component of the SKP-CUL E3 ligase complex[203].

5.2. Results

5.2.1. USP46 antibody is not applicable to IP.

We wanted to establish a method to IP USP46 from cells. We tested the abundance across different cell lines to identify a cell line that expressed high levels of USP46 from which to IP from. 20µg of lysate from of a panel of cell lines was loaded onto a SDS page gel and probed with antibodies against USP46 and USP8, as a reference (Figure 5.1.1). The levels of USP46 varied more greatly across different cell lines, compared to USP8. HEK293t cells had the greatest expression of USP46, while HeLa cell had a relatively low abundance of USP46. We therefore used HEK293t cells to check the efficiency of the anti-USP46 antibody (Sigma) for IP.

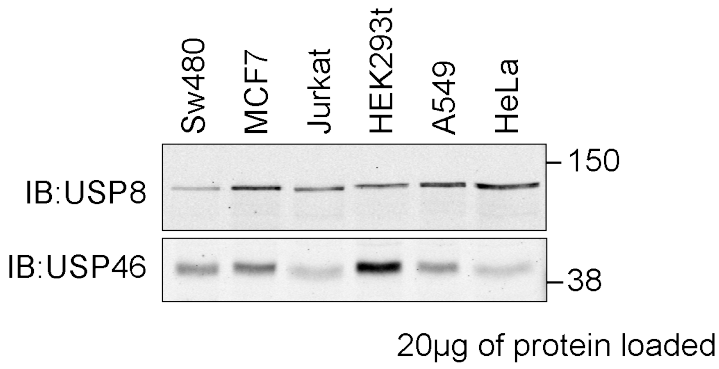

Figure 5.1.1. USP46 expression across a panel of cell lines.
20µg of lysate of each cell line was loaded onto SDS page gel. Even loading was determined by Ponceau staining. Lysates were probed for USP8 and USP46.

We sought to test the efficiency of our anti-USP46 antibody (Sigma) to IP endogenous USP46. HEK293t cells were lysed in NP40 buffer and 750µg of lysate with 0.75µg of antibody for 3 hours at 4˚C (Figure 5.1.2). There was little depletion of USP46 in the unbound fraction compared to both the input and the unbound fraction from the beads only IP. The experiment also highlighted another problem with this approach. There was contamination of the IP with the heavy and light chain of the antibody. As the bands for the heavy and light chain of the antibody were so strong, they would mask the detection any proteins of the same size. We adopted an alternative strategy to overcome these problems using GFP Nano-trap llama antibody that consists only of a 13kDa light chain[159] in a system expressing GFP tagged USP46. The antibody can be produced in the laboratory cheaply and can be coupled to sepharose beads (documented in materials and methods section 2.3.13).

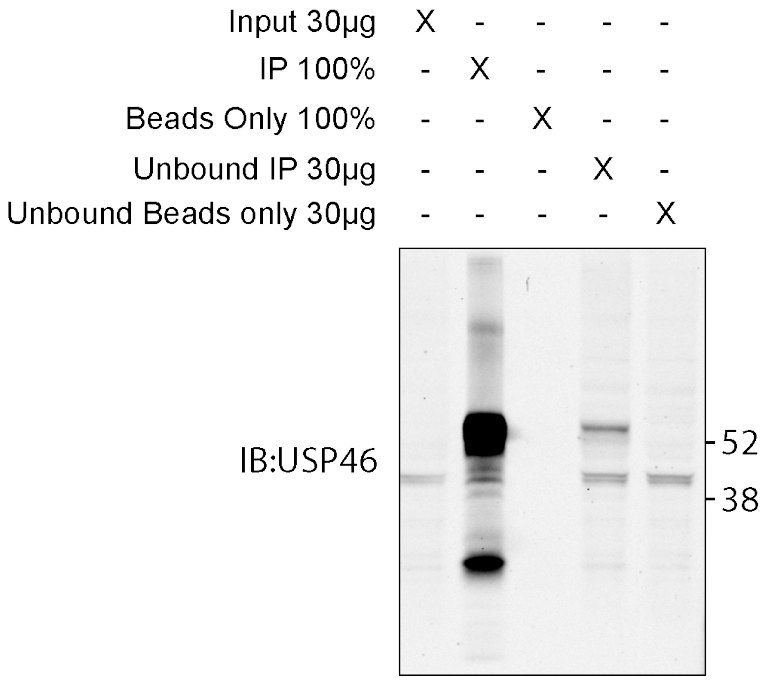

Figure 5.1.2. Endogenous USP46 IP from HEK293t cells.

HEK293t cells were lysed in NP40 buffer. 750µg of lysate was subjected to immuno precipitation (IP) with 0.75µg of anti-USP46 antibody or just beads alone. Input, IP and unbound fractions were loaded onto a SDS page and probed with anti-USP46 antibody.

5.2.2. Generation of USP46 stable cell lines.

In order take advantage of the GFP Nano-Trap system we developed two cell lines that expressed GFP-USP46 and GFP-USP46-C44S. We used the Flp-in system (Invitrogen) to generate the cell lines because it has a number of advantages. First, it has one integration site so each cell should express the plasmid at the same level across separate clones. This allows for direct comparisons of mutant cell lines without variations in expression levels and the artifacts they introduce. The second advantage was that our USP46 cell lines expressed relatively low levels of GFP-USP46 compared to transient transfection; 5 times the levels of endogenous USP46 (figure 5.2.2.).

The Flp-in system takes advantage of Flp Recombination Target sites that are introduced into the genome of the parental cell line. Dual transfection of plasmids containing the gene of interest flanked by FRT sites with pOG44 a plasmid that expresses Flp recombinase, stably introduces the plasmid of interest into the FRT sites in the parental cell genome. A Hygromycin B resistance cassette is included in the expression vector (figure 5.2.1). Once the recombination event has taken place this allows selection of positive clones.

To generate constructs to establish our cell lines, point mutations were introduced into existing GFP-USP46 constructs rendering it inactive by mutating the catalytic cysteine to serine. Both constructs were also made siRNA resistant to oligonucleotide USP46-8 by introducing silent point mutations into the siRNA target sequence. A stop codon was also introduced to prevent the translation of the V5 tag into the open reading frame that is part of the Invitrogen vector. All Point mutations were introduced using the Quick-Change kit (Agilent) and primers are documented in the materials and methods section (2.1.6). PCR derived, linear GFP-USP46 and GFP-USP46-C44S were introduced into pEF-FRT-V5 vector by TOPO recombination. pEF-FRT-V5-USP46 and pEF-FRT-V5-USP46 vectors were transiently transfected into HeLa S3 cells with pOG44 recombinase using Genejuice. The constructs

were incorporated into the genome HeLa S3 cells that had previously had a single FRT site introduced (Maria Hernandez) (Figure 5.2.1).

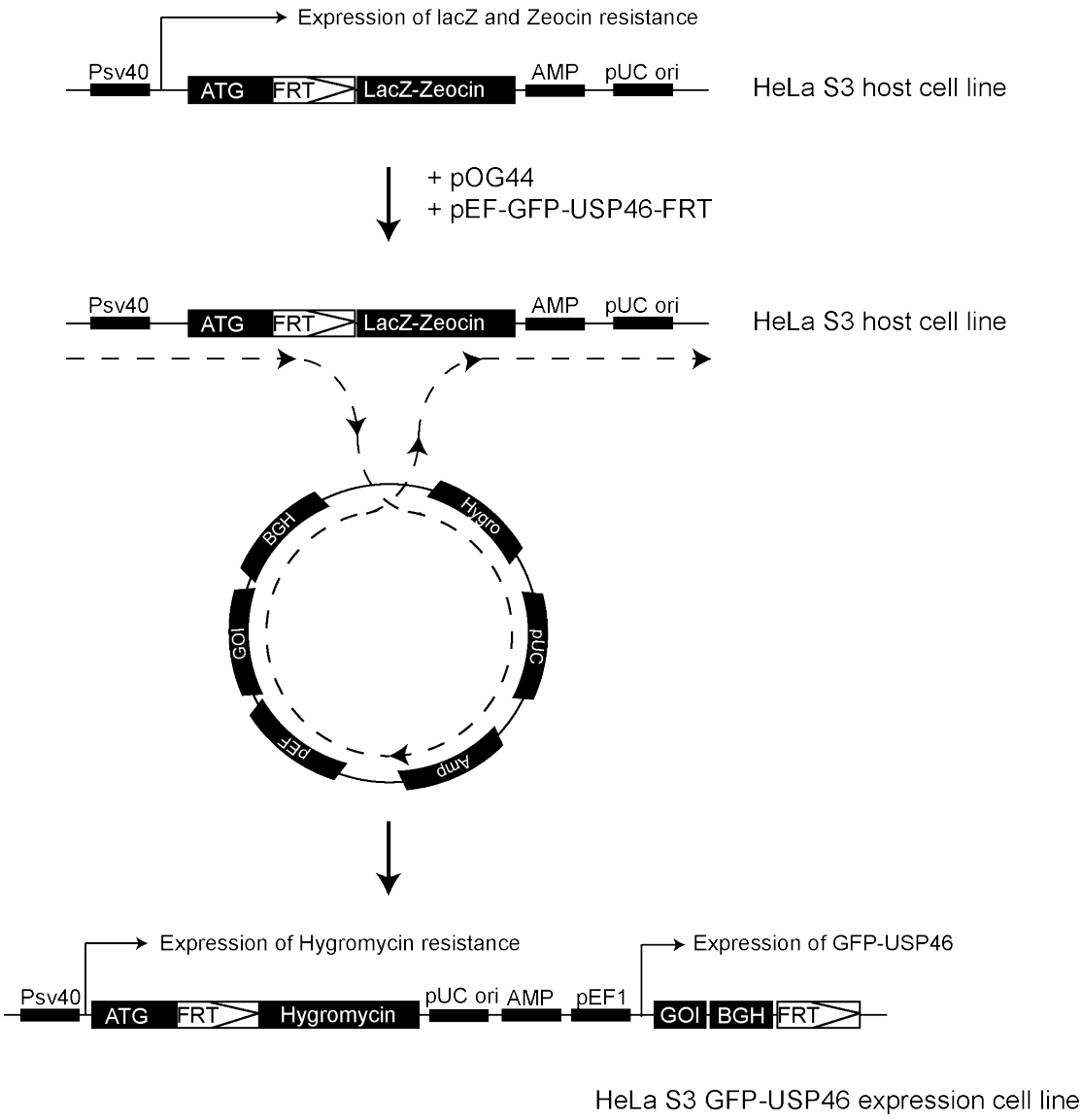

Figure 5.2.1 Schematic for the generation of GFP-USP46 Flp-in Cell lines.
pEF-FRT-GFP-USP46 and pEF-FRT-GFP-USP46-C44S vectors were transiently transfected into HeLa S3 cells with pOG44 recombinase. Through a recombination event the constructs were incorporated into the genome HeLa S3 cells that had previously had FRT site introduced. Figure adapted from Invitrogen handbook.

Colony	Island Morphology
WT1	++
WT2	+++
WT3	+
WT4	++
WT5	++
WT6	+++
WT7	Failed to grow
CS1	++1/2
CS2	++1/2
CS3	+++
CS4	++1/2
CS5	+
CS6	Failed to grow

Table 5.1. Morphologies of USP46 cell line clones.

GFP-USP46 (WT) cells are numbered 1-7 and GFP-USP46-C44S (CS) is numbered 1-6. Morphology was visually judged between + and +++ according to how similar the morphology was to parental cell lines.

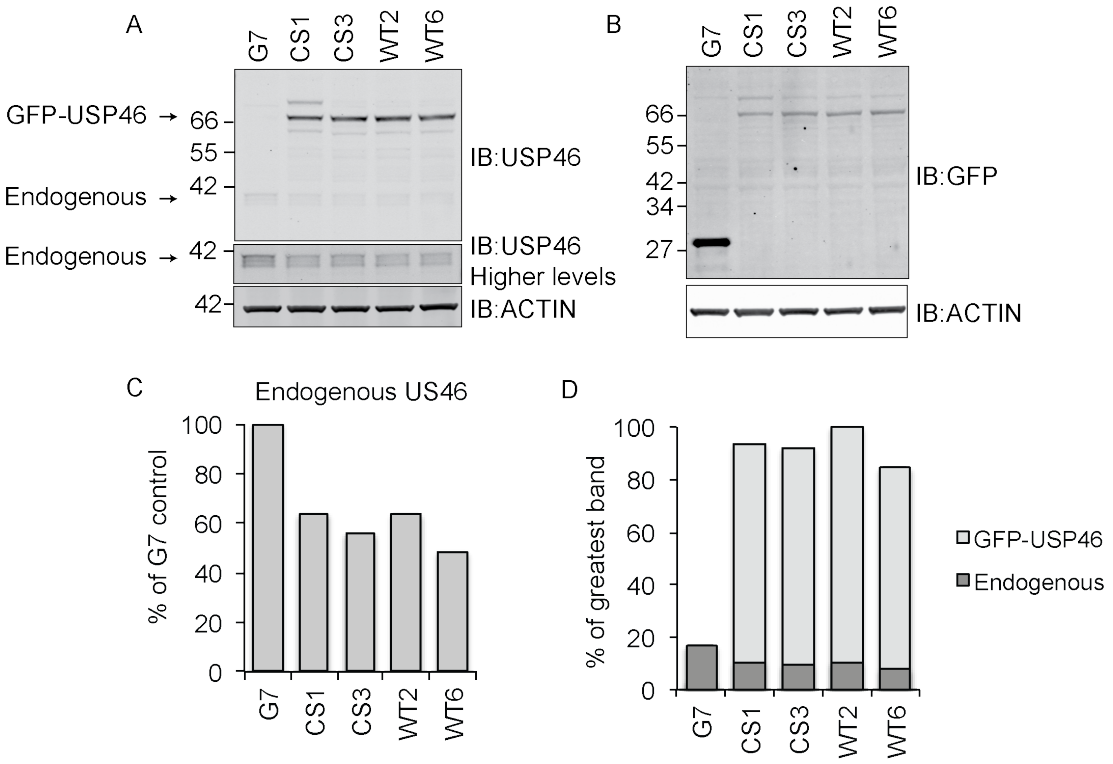

Figure 5.2.2. Lysates from stable cell line clones.

25µg of NP40 lysate were run of SDS-page gels. Cell lysates were probed with A) anti-USP46 and B) anti-GFP. GFP-USPP46 predicted molecular weight = 69kDa GFP =27kDa and USP46=42kDa. Quantification of anti-USP46 blot was performed using Odyssey (Licor) software. C) Quantification of endogenous USP46 levels across cell lines. D) Quantification was expressed a % of the greatest band (WT2) to compare GFP-USP46 band to the endogenous band. Quantification was performed using the odyssey (Licor) software. Representative blots shown.

Transfected cells were maintained in Hygromycin B containing medium to select for positive clones. 7 colonies were picked for wild type cells and 6 colonies were picked for catalytically inactive transfected cells, 2 colonies, WT7 and CS6 failed to grow. Colonies were scored out of 3 based on their morphology (Table 5.1) with WT2, WT6 and CS3 having the morphology most like the parental cells (+++). There was stable expression of the constructs across the different clones and a reduction in the levels of the endogenous protein relative to GFP control Flp-in cells (courtesy of Han Liu) (Figure 5.2.1.C). There was approximately 5 times more GFP-USP46 and GFP-USP46-C44S expressed in our cell lines, compared to the endogenous protein (Figure 5.2.1.D). This expression was within a normal physiological range as HEK293t cells express more that 5 times the levels of USP46 than HeLa cells (figure 5.1.1).

The expression levels of GFP-USP46 in the cell lines were relatively low making them difficult to image. Therefore we counter stained the GFP-USP46 (WT2) and GFP-USP46-C44S (CS3) cell lines with anti-GFP antibody to increase the fluorescence signal (Figure 5.2.3). Cells were either stained under basal conditions or alternatively cells were serum starved for 16 hours and either stimulated with 20ng/ml for 10 mins before pre-permeabilization (pre-treatment) in 0.02% Saponin/MTSB (microtubule stabilizing buffer) for 3 mins to extract cytosolic background before fixation in 100% methanol (-20˚C) before labeling with anti-GFP and anti-HRS antibodies to asses co-localization.

GFP-USP46 and GFP-USP46-C44S had a fine punctate distribution that was resistant to Saponin permeabilization. The punctate structures displayed little co-localization with HRS and there was no change in the distribution of GFP-USP46 and GFP-USP46-C44S with EGF stimulation.

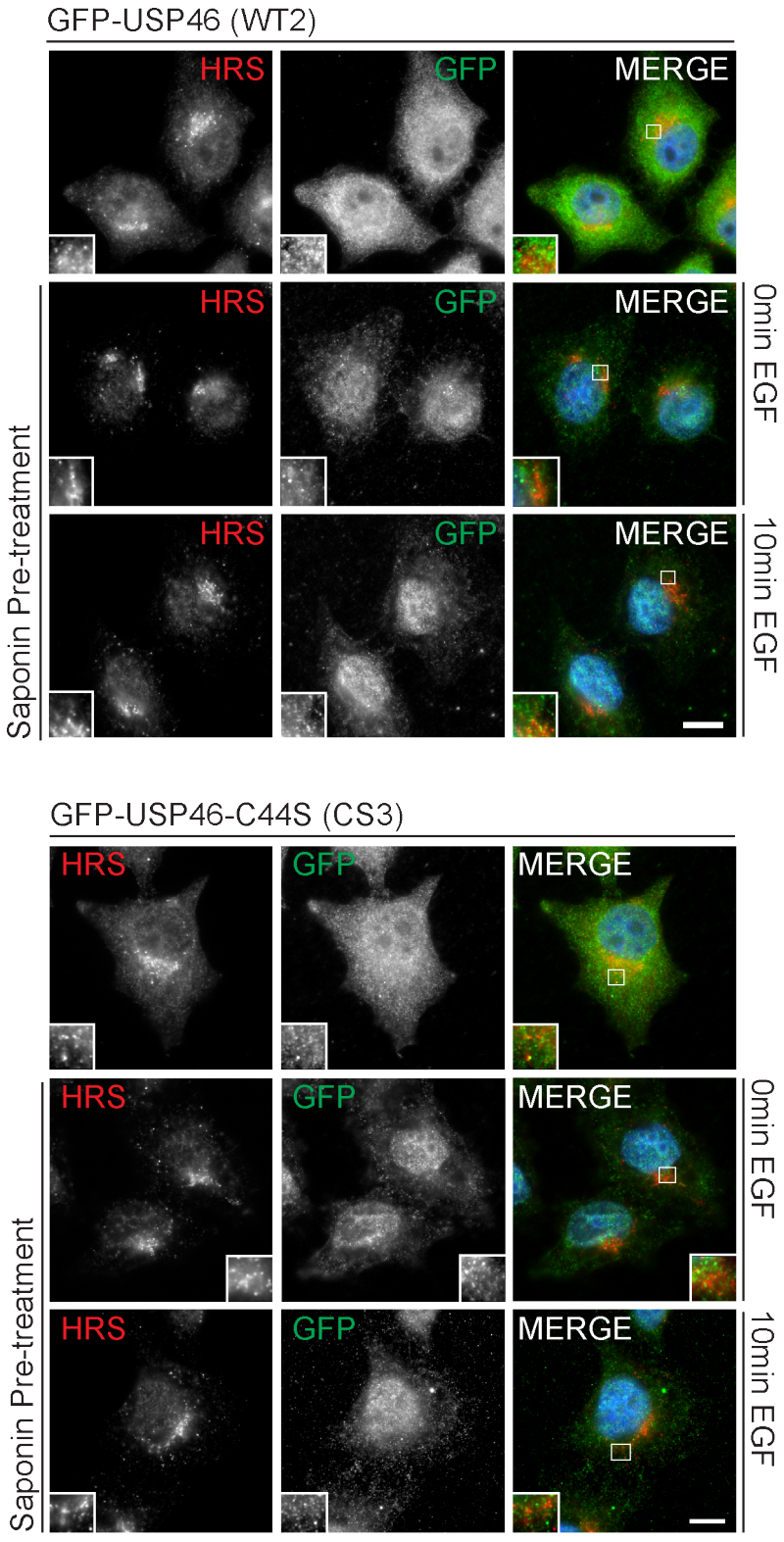

Figure 5.2.3. Images of GFP expressing cells.

GFP-USP46-C44S (CS3) and GFP-USP46 (WT2) cells were fixed in 4% methanol and stained with anti-GFP and anti-HRS antibodies with and without pre-treatment with 0.02% Saponin to remove cytosolic background and +/- 20ng/ml EGF. Images were taken at the same exposure. Scale bar = 10.

5.2.3. Signaling response of USP46 stable cells to EGF.

We next wanted to test the response of each of the stable cell lines to EGF stimulation. GFP (G7), GFP-USP46 (WT2) and GFP-USP46-C44S (CS3) cell lines were serum starved for 16 hours before stimulation with 1ng/ml EGF over a time course between 0 and 60 mins. The cells were lysed in RIPA buffer and lysates were probed for pMEK and pAKT as readouts of activation of the MAPK and AKT signaling pathways respectively.

Cell expressing GFP-USP46 (WT2) had greater levels of pAKT at all time points compared to the GFP expressing (G7) control cells. Cells expressing the catalytically active form of GFP-USP46-C44S (CS3) had a similar activation peak as WT2, but the increase late pAKT signaling in the WT2 was not observed in CS3 cells (figure 5.3). In WT2 and CS3 cells there was a decrease in the activation of the MAPK pathway compared to the G7 cells.

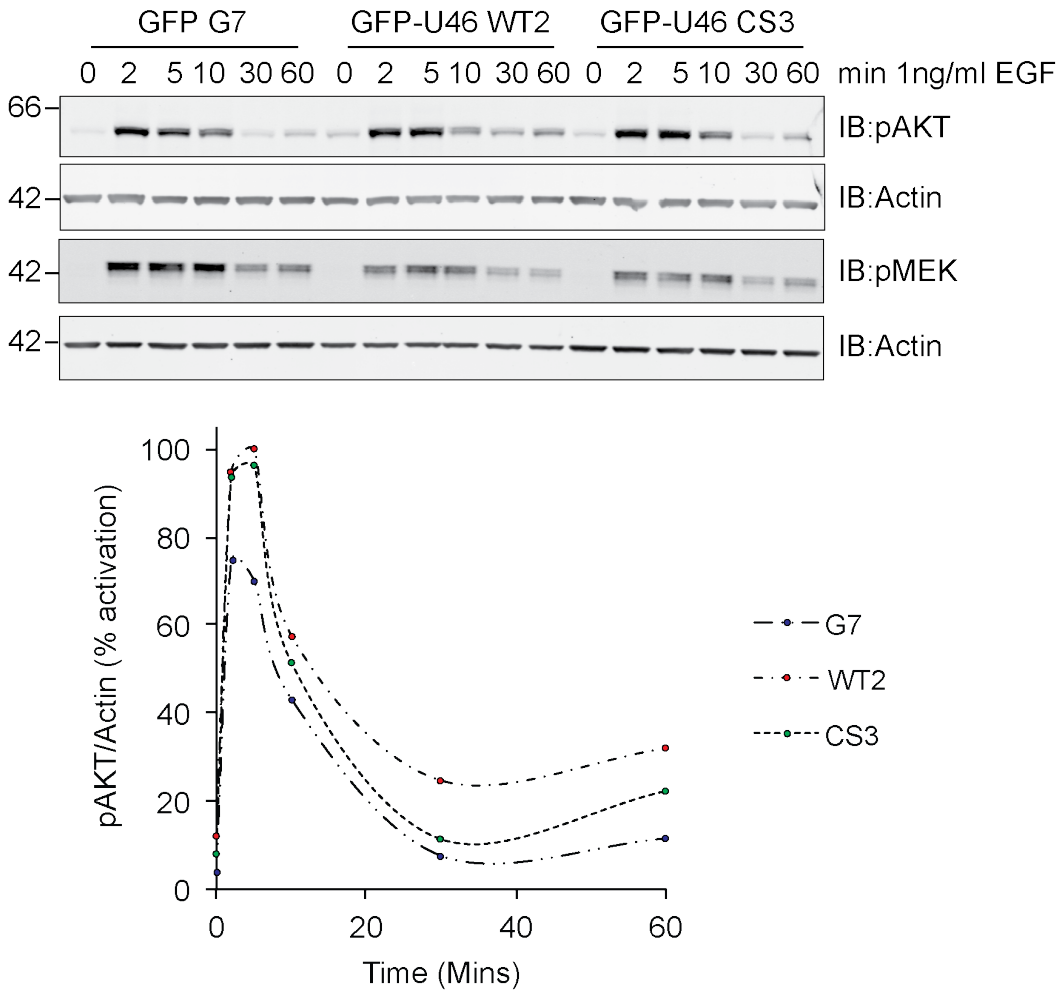

Figure 5.3. EGF signaling response of stable cell lines.

GFP (G7), GFP-USP46 (WT2) and GFP-USP46-C44S (CS3) cells were serum starved overnight before stimulation with 1ng/ml EGF. Cells were lysed in RIPA buffer and probed with pAKT (Ser473) and pMEK (Ser217/221) antibodies as readouts for AKT and MAPK pathway activation respectively. Quantification was performed using Image J, pAKT levels were normalised to Actin control. Representative blots shown.

5.2.4. Optimizing IP conditions for GFP Nano-Trap antibody.

We sought to determine the optimal conditions to use the GFP Nano-trap antibody to IP GFP-USP46 from our cell lines. We wanted to establish conditions that had effective depletion of the GFP-USP46 constructs from cells, while having the minimal amount of antibody in the IP to reduce non-specific binding of the antibody and the beads. The antibody was pre-coupled to the sepharose beads (Maria Hernandez). 5µl of antibody beads complex was added to increasing amounts of GFP-USP46 lysate. The most effective depletion observed was when 5µl of antibody:bead complex was incubated with 100µg of lysate. Depletion could be quantitated using densitometry, demonstrating that there was a 70% depletion compared to the input, when 5µl of bead/antibody complex was incubated with 100µg of lysate (Figure 5.4). We chose not to use a higher concentration of antibody to minimize non-specific binding.

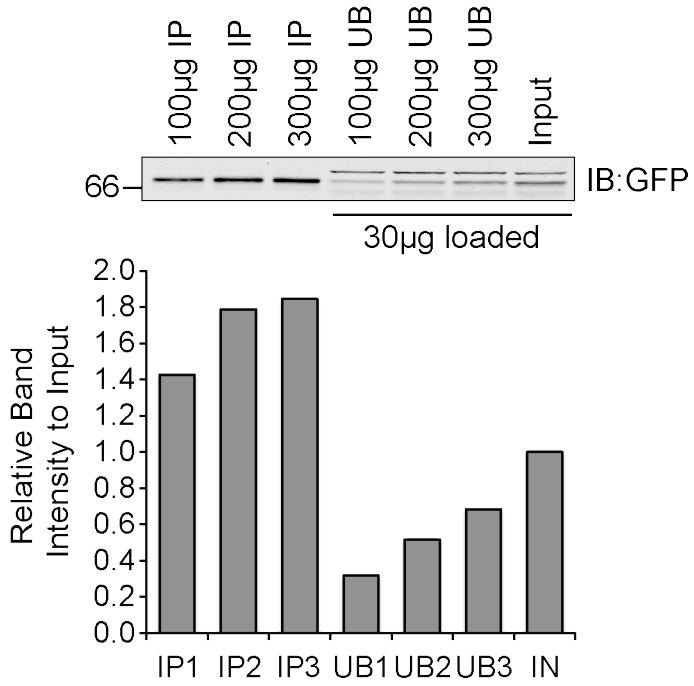

Figure 5.4. Testing GFP Nano-trap antibody.

GFP-USP46 (WT2) cells were lysed in NP40 buffer. GFP-USP46 was immuno-precipitated (IP) with 5µl of GFP-Nano trap coupled beads from a range lysate from 100µg-300µg, 30µg of lysates were loaded from the input and unbound fractions. Quantification was performed using Image J software. Representative blots shown.

5.2.5. Mass spectrometry identification of USP46 interactors.

To identify interactors of USP46 we performed IP from USP46 stable cell lines cultured in SILAC media, using GFP expressing cells as a control. Cells were grown in media containing "heavy" amino acids l-Lysine-$^{2}H_4$ (Lys 4, 4Da heavier), l-arginine-U-$^{13}C_6$ (Arg 6, 6Da heavier), l-Lysine-U-$^{13}C_6$-$^{15}N_2$ (Lys 8, 8Da heavier) and l-Arganine-U-$^{13}C_6$-$^{15}N_4$ (Arg10, 10Da heavier). There will cause a shift in the molecular weight of the peptide, which has incorporated a heavy amino acid, which can then be identified by mass spectrometry. Producing the peptides using trypsin, which will cut at carboxyl side of Lys and Arg, can ensure the production of heavy peptides. This strategy allows you to directly compare the abundance of proteins from different samples by comparing the peak intensity between "heavy" peptides to the "light".

Individual IPs were performed from 3mg of lysates derived from GFP, GFP-USP46 and GFP-USP46C44S cell lines. GFP cells were grown in "light" (Arg0/Lys0), GFP-USP46-C44S was grown in "medium" (Arg6/Lys4) and GFP-USP46 was grown in "heavy" (Arg10/Lys8) (Figure 5.5.1). The elute from each IP was mixed and dried in a speed-vac the resulting pellet was re-suspended in sample buffer and run in a single lane on a Nu-page (Invitrogen) 4-12% SDS gel, as the first phase of chromatography (Figure5.5.1). The gel was processed using in gel digestion on bands cut from the gel[204]. The subsequent samples were then loaded on a reverse phase liquid chromatography column, run on a 1-62.5% linear ACN gradient over 21 mins coupled to a LTQ-OrbitrapXL (Thermo Fisher) fitted with a Proxeon nanoelectrospray source. The top 6 most abundant peptides were selected for MS/MS identification and raw MS/S data was processed using MaxQuant software[160]. Sample peptide MS1 data for USP46 and FBXO11 peptides identified by MaxQuant are show in figure 5.5.2. Samples of MS/MS fragmentation data are shown in figure 5.5.3. Fragmentation peaks were checked by eye against a theoretical fragmentation for each peptide, generated by MS-product software.

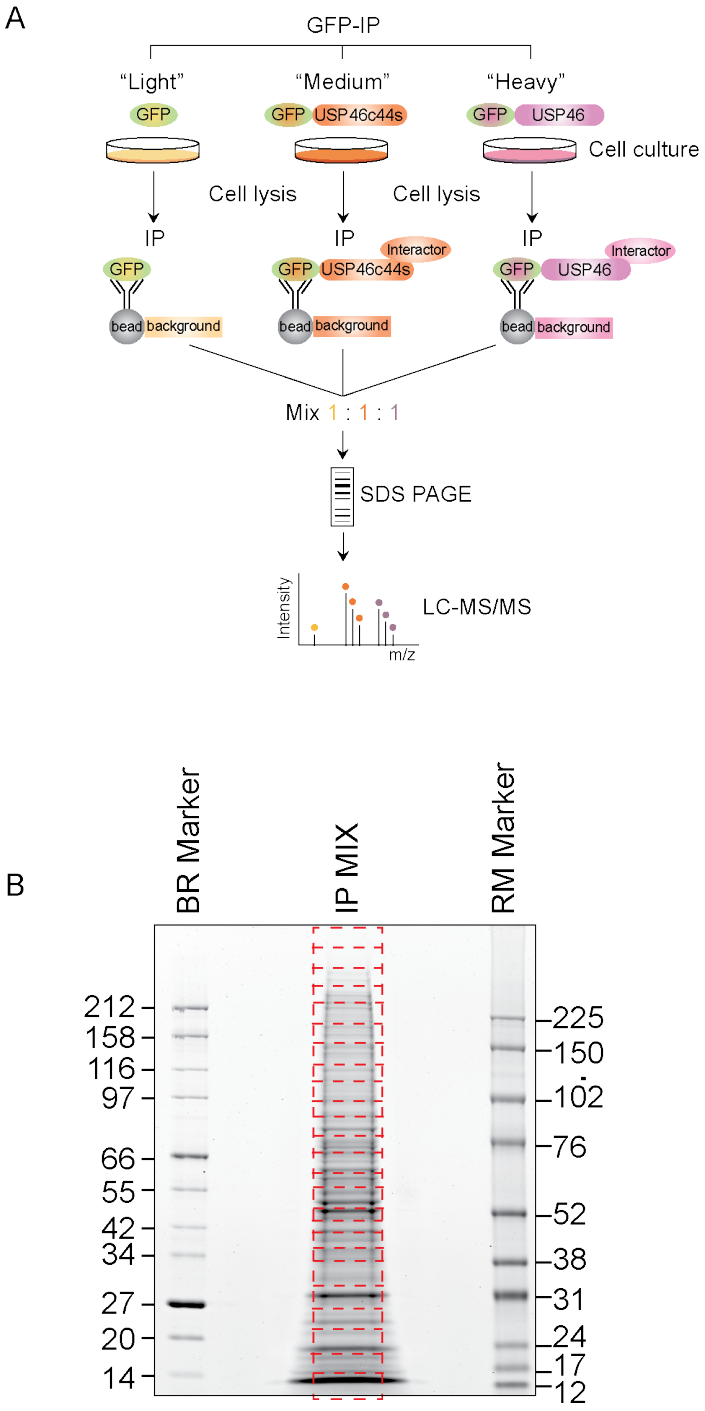

Figure 5.5.1. SILAC configuration for large scale USP46 immuno-precipitation.

A) SILAC labeled GFP (G7) (Arg0/Lys0/Pro0) GFP-USP46-C44S (CS3) (Arg6/Lys4/Pro0) and GFP-USP46-C44S (WT2) (Arg10/Lys8/Pro0) were lysed in NP40 buffer and were subjected to immuno-precipitated (IP) using GFP Nano-trap antibody. IP elute was mixed in a 1:1:1 ratio and run on a SDS page gel, the bands were cut from the gel (B) and subjected to in gel digestion. Peptides were detected by LC-MS/MS and identified using MAX-Quant software.

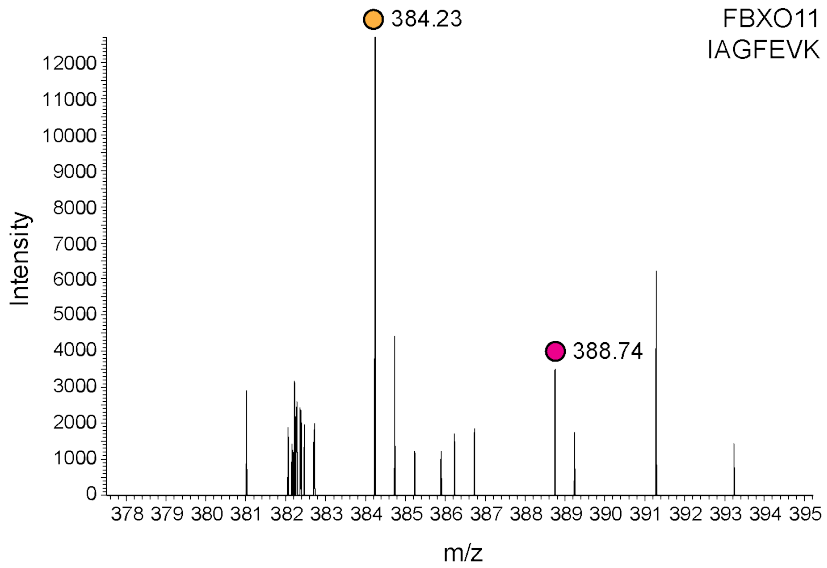

Figure 5.5.2. Sample MS1 spectra.

Sample spectra derived from USP46 and FBXO11 with peaks labeled the medium (yellow) and heavy (red) condition.

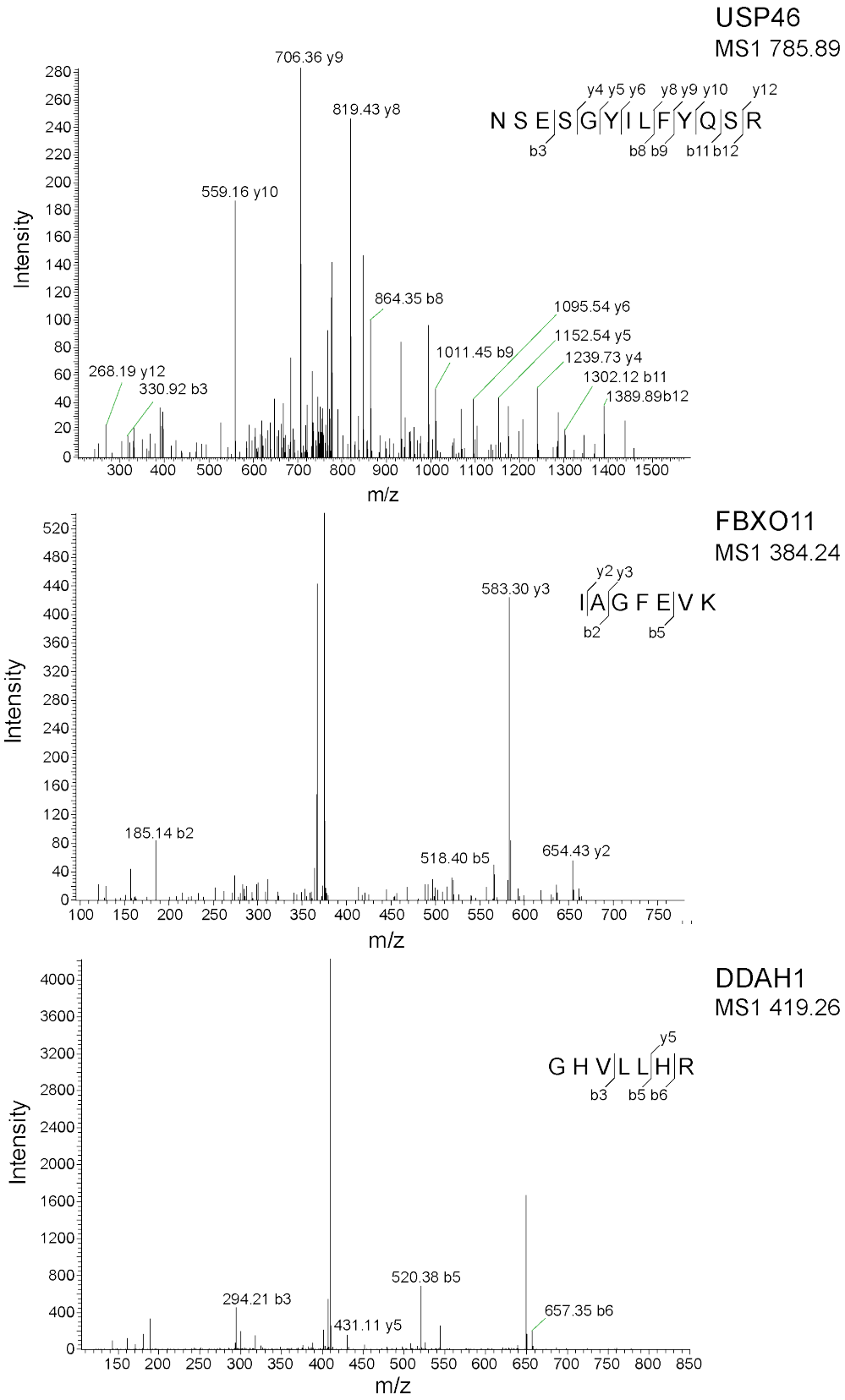

Figure 5.5.3. Sample peptides from MS/MS identification.

Peptides from MaxQuant identification, y and b fragments ions are indicated for each peptide and the corresponding raw peaks are labeled as such.

150 proteins were identified in the experiment, 10 of which were known contaminants such as Keratin and were removed from further analysis. We then performed 2 levels of exclusion, first removing proteins that were part of the BEADome; known "sticky" proteins that are commonly seen in IP experiments established by Trinkle-Mulcahy et al. (2008)[202], this included many histone proteins. Despite USP46 having been demonstrated to be a Histone deubiquitylase[201] we removed them from our list as we did not have the expertise in the lab to follow them up and could not be sure of the reliability of these hits, as they are known "sticky" proteins. The second level of exclusion was to remove any proteins seen in IP experiments from our lab, using the same strategy of IPing GFP tagged constructs from Flp-in cells established from the same parental cell line. A full list of identified peptides including those expelled from either first or second exclusion is provided in supplementary table 2.

In figure 5.5.2-3, graphs of residual proteins are plotted as intensity to LOG_{10} against LOG_2 of ratio. In figure 5.5.2, graph A, ratios are calculated between GFP-USP46/GFP and in graph B, GFP-USP46-C44S/GFP. In figure 5.5.3 ratios are calculated as GFP-USP46/GFP-USP46-C44S providing a comparison between the interactors of the wild type and catalytically inactive form of USP46. Data points were labeled in red for proteins that were enriched greater or equal to 1.5 fold in either GFP-USP46 or GFP-USP46-C44S against GFP. WDR48 and WDR20 are known binding partners of USP46[205] and are thought to regulate the deubiquitylase activity of USP46, and have been labeled in grey as a known protein complex. Neither WDR20 nor WDR48 showed a significant preference for the wild type or catalytically inactive form.

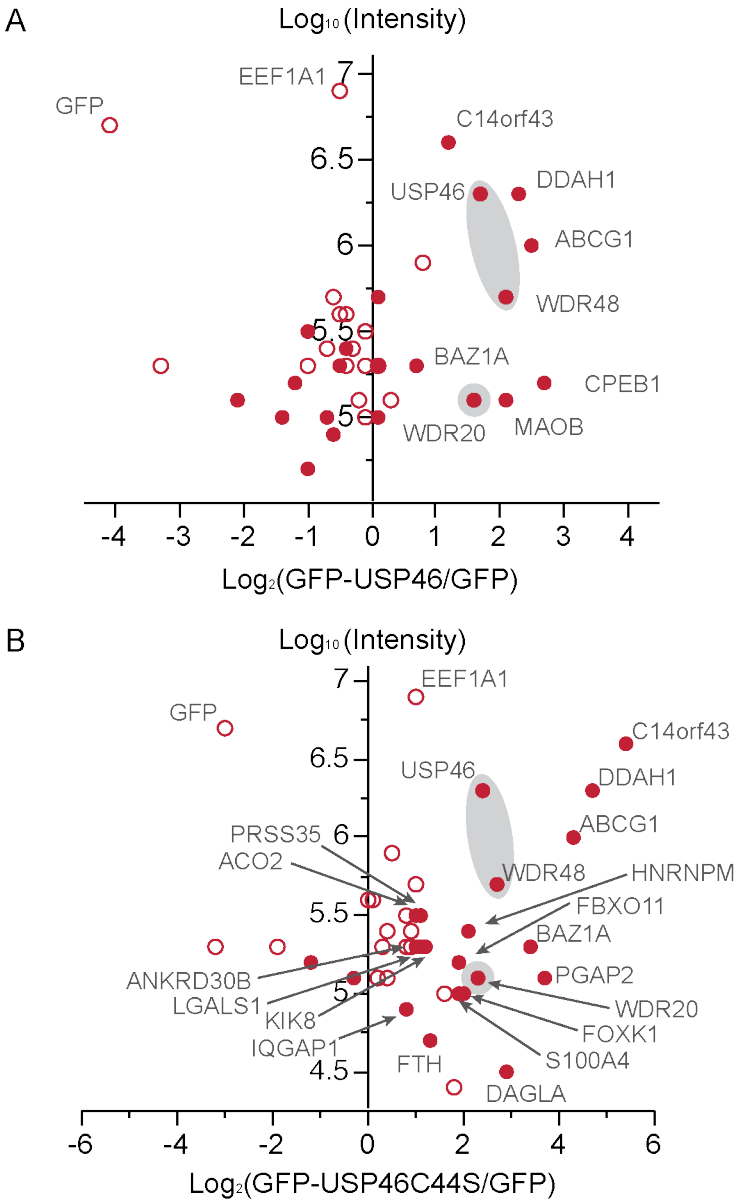

Figure 5.5.4. Comparison of USP46 interactors compared to GFP control.

SILAC ratios were generated between GFP and GFP-USP46/GFP-USP46-C44S using Max Quant. Ratios were transformed to a LOG_2 scale and plotted against the LOG_{10} of the intensity of the peptide signal. Points that have a positive ratio represent proteins that are found more in the GFP-USP46/GFP-USP46-C44S IP. Grey circles denote USP46 complex.

GFP was enriched in the GFP IP compared with either GFP-USP46 or GFP-USP46-C44S presumably because of the higher expression of GFP compared to either USP46 construct. Ubiquitin (UBB) preferentially bound to the catalytically inactive mutant of USP46 over the wild type. It is not clear if the ubiquitin detected derives from USP46 itself and/or from substrate proteins. There was a bias in the experiment towards the catalytically inactive form of USP46 as more proteins were identified in the “medium” condition figure 5.5.4). This suggests that the catalytically inactive form may act as a substrate trap; further experiments would be needed to confirm this. Notably we did not detect PHLPP1/2 in our experiment.

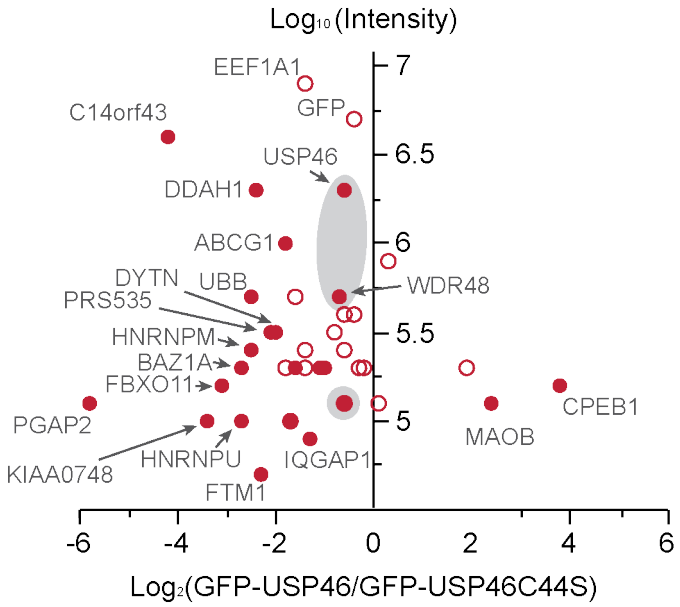

Figure 5.5.5. Comparison of USP46 interactors between wild type and catalytic inactive mutant.

SILAC ratios were generated between GFP-USP46/GFP-USP46-C44S using Max Quant. Ratios were transformed to a LOG_2 scale and plotted against the LOG_{10} of the intensity of the peptide signal. Points that have a positive ratio represent proteins that are found more in the GFP-USP46 IP while negative points represent proteins found in the GFP-USP46-C44S IP. Grey circles denote USP46 complex.

5.2.6. Confirmation FBXO11:USP46 interaction.

We chose to selectively confirm interactions based on novelty and interest. DDAH1 was chosen as it was seen with in both the wild type and catalytically inactive IP and had a similar ratio and intensity to USP46 and WDR48. DDAH1 has also been described in the literature as a regulator of the AKT and NO signaling pathways and an effector RAS[206]. FBXO11 was chosen, as it is part of the Scf-E3 ligase complex[207], given that DUBs and E3 ligase are often found in complexes together we chose to follow this up. 3 separate IPs were performed on 1mg of lysate derived from GFP, GFP-USP46 and GFP-USP46-C44S cell lines using the GFP Nano-trap antibody for 3 hours at 4˚C. Verification of the interaction was confirmed using antibodies against the endogenous protein. No band could be detected for DDAH1 in any of the IP lanes (Figure 5.6).

FBXO11 could be detected at the right molecular weight for FBXO11 in both the WT and CS IP and was not present in the GFP IP. Interestingly there is a second higher molecular weight band that is more highly enriched relative to the lower band, presumably another isoform of FBXO11.

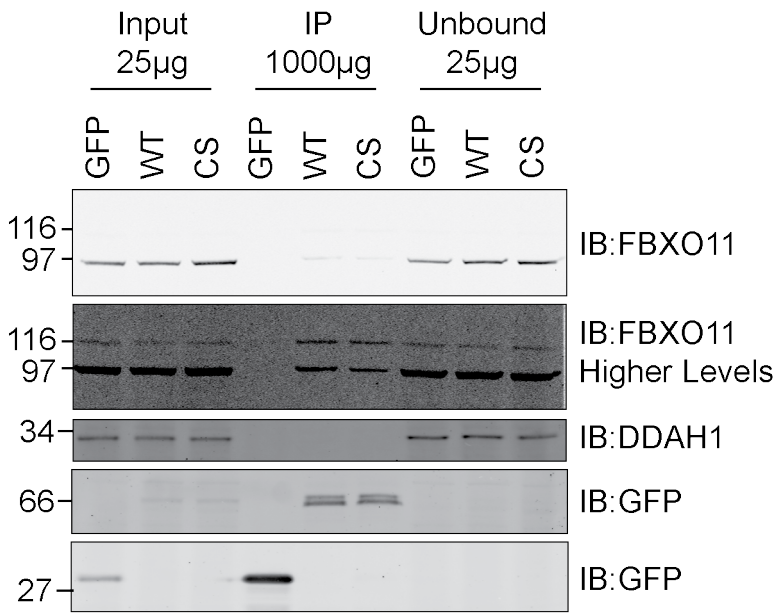

Figure 5.6. Confirmation of USP46:FBXO11 interaction.

GFP (G7), GFP-USP46 (WT2) and GFP-USP46-C44S (CS3) cells were lysed in NP40 buffer. 1mg of lysate was subjected to immuno-precipitation with GFP Nano-trap, 25µg of the input and unbound fractions were run along side the IP fractions. Samples were probed with anti-FBXO11, anti-DDAH1 and anti-MAOAB antibodies.

5.2.7. Depletion of USP46.

We next wanted to test whether the stability of FBXO11 and DDAH1 was affected by USP46 depletion. Despite the interaction between USP46 and DDAH1 not being confirmed, we wanted to test the possibility that USP46 could still affect its stability. DUB substrate interactions are low affinity and it is possible that they could be difficult to detect with 1mg of lysate. USP46 was depleted in HeLa cells over 72hours with 4 individual oligonucleotides. The experiment was set up twice and lysed in NP40 to mimic the IP condition and in RIPA buffer in case USP46 affected a NP40 insoluble fraction.

The levels of DDAH1 decreased with one oligonucleotide (USP46-6) but there was no effect with any of the other oligonucleotides. FBXO11 showed a small decrease in the stability of FBXO11 with multiple oligonucleotides compared to the NT1 control but not compared to the no oligo control (NO) (Figure 5.7).

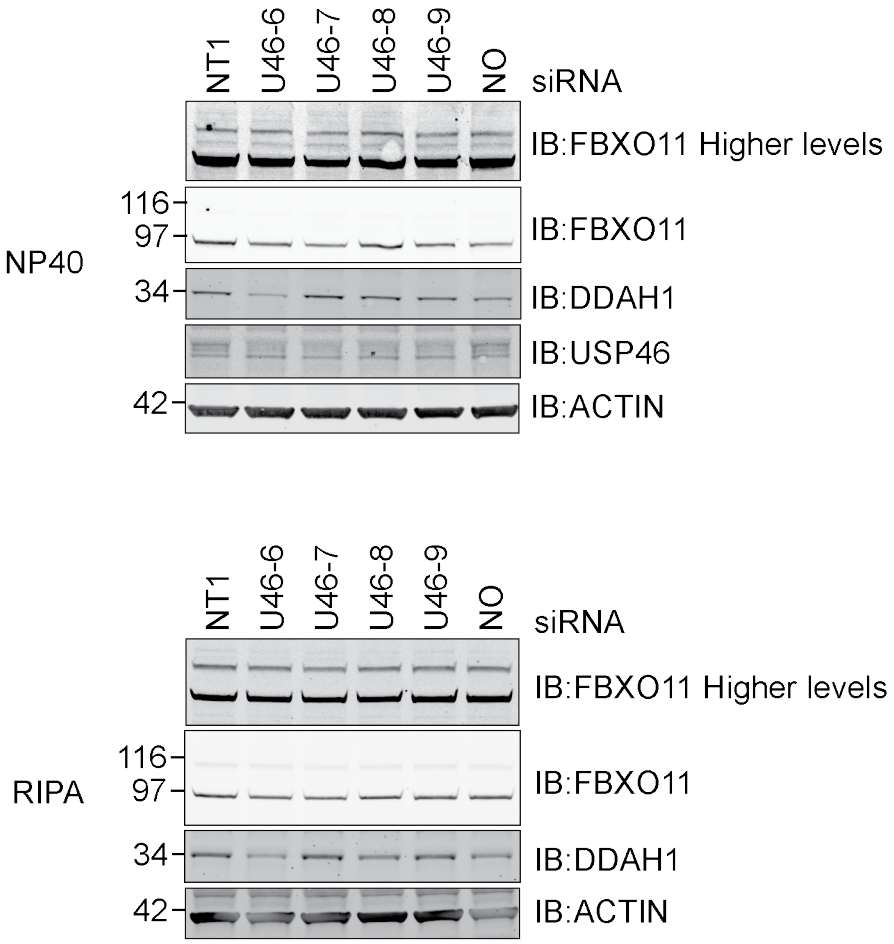

Figure 5.7. Depletion of USP46 causes a modest reduction in the levels of FBXO11 and DDAH1.

HeLa cells were treated with individual oligonucleotides against USP46 for 72 hours. The cells were then lysed in either NP40 or RIPA buffer and run on an SDS-page gel. Samples were probed with anti-FBXO11, anti-DDAH1 and anti-MAOAB antibodies.

5.2.8. Epoxomicin rescue of FBXO11 and DDAH1.

One would expect that if DUB interacts with protein and the protein levels decrease with depletion of said DUB, then this effect would be due to increased ubiquitylation of the protein leading to its proteasomal degradation. To test whether the possible effect on DDAH1 and FBXO11 stability were due to proteasomal degradation, we depleted USP46 in HeLa cells, then either treated the cells with 0.5μM epoxomicin for 8 hours to block proteasome activity or DMSO as a control. In cells treated with USP46-6 oligonucleotide there was a decrease in the levels of DDAH1, however there was no change in the levels of DDAH1 after epoxomicin treatment, suggesting that the effect is pre-translational and likely an off target effect of the oligonucleotide (Figure 5.8). In NT1 cells treated with epoxomicin there was a small increase in the levels of FBXO11. The increase in FBXO11 levels with epoxomicin was greater in cells treated with USP46-6 oligonucleotide. This suggests that FBXO11 protein levels are rapidly turned over via the proteasome; depletion of USP46 did caused a proportionate enhancement FBXO11 levels over the control.

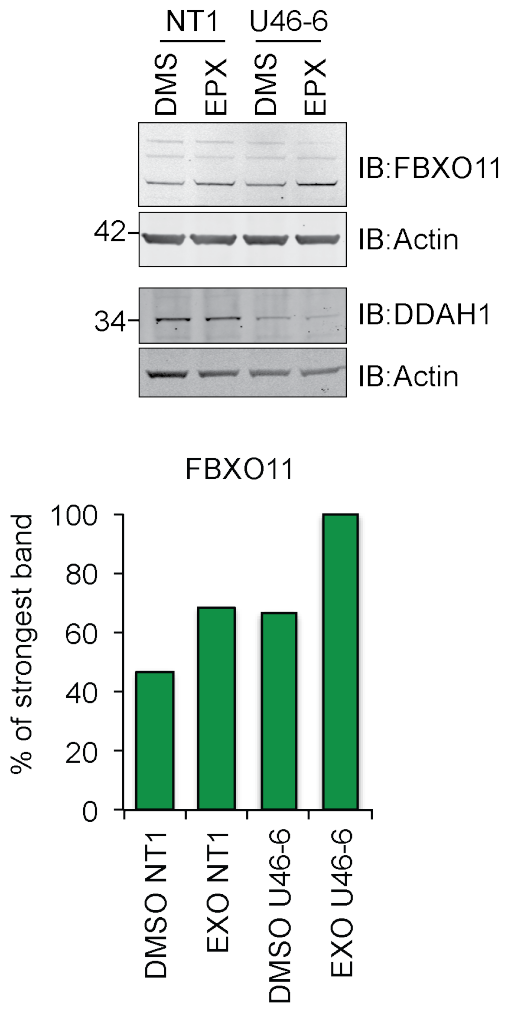

Figure 5.8. Epoxomicin rescue of USP46 depleted cells.

HeLa cells were treated with individual oligonucleotides against USP46 for 72 hours. Cells were treated for 8 hours with 0.5μM epoxomicin before lysis in NP40 buffer.

Lysates were run on SDS-page gel and samples were probed with anti-FBXO11 and anti-DDAH1. Representative blots shown.

5.3. Discussion

We sought to identify interactors of USP46 in an unbiased fashion. To do this we generated two cell lines stably expressing GFP-USP46 and a catalytically inactive GFP-USP46-C44S. We identified a strategy to discover USP46 interactors by IPing the stably expressed constructs via their GFP tags using the GFP Nano-trap llama antibody, to identify proteins that co-precipitated using LC-MS/MS. We selectively followed up hits from our interaction dataset based on interest, novelty and availability of reagents. We were able to confirm an interaction between USP46 and FBXO11. A higher molecular weight isoform of FBXO11 showed increased affinity for USP46.

Furthermore, there was differential activation of the AKT and MAPK signaling across our cell lines, suggesting that USP46 regulates these pathways. An effect on late AKT was observed, which was dependent on the catalytic activity, as neither USP46 nor the catalytically inactive mutant or the GFP expressing cells displayed the same phenotype. The reduction in MAPK signaling was not dependent on catalytic activity of USP46, suggesting that USP46 may be playing some scaffolding role in the formation of signaling complexes downstream of EGFR.

The increase in late AKT signaling was reminiscent of the changes seen with USP46 depletion in HeLa cells (Figure 4.9) with both knockdown and overexpression displaying the same phenotype. One possibility is that USP46 is required for the formation of signaling complexes that terminate AKT signaling, were loss of USP46 would prevent assembly of this complex, while overexpression of USP46 has a dominant negative effect. The data presented here demonstrates that stable USP46 overexpression influences acute EGF signaling. In our cell lines there is an increase levels of AKT signaling in GFP-USP46 cells compared to the GFP control. These results are is contradictory to results published in Li et al. (2013)[192] were the authors demonstrated that there was a decrease in AKT signaling mediated through PHLPP1/2 when USP46 is overexpressed[192]. Taken at face value these

results suggest that USP46 is having multiple roles in the regulation of the pathway that we presently do not understand. Although it will be necessary to confirm that these results are not due to clonal variation by testing the EGF signaling of other clones.

We were unable to confirm the localization experiment from Chapter 4. A proportion of USP46 was localized to punctate structures in the cytoplasm that had little co-localization with HRS. We were also unable to observe EGF stimulated recruitment onto these punctate structures. There are several possible reasons for this observation. The expression levels of GFP-USP46 introduced through transient transfection are above physiological levels and vary from cell to cell. Overexpression of proteins can cause mislocalization and unanticipated artifacts.

We were initially interested in the interaction between USP46 and FBXO11, as it is a F-Box protein that forms the substrate-recognizing component of the SCF E3 ligase complex[203]. One feature of SCF substrates is that they exhibit phosphodegron-dependent interaction with F-Box proteins, which facilitates their degradation through ubiquitylation. However this feature is not universal and in the case of FBXO11, recognition of one of its substrate, CDT1 is blocked by phosphorylation[208, 209]. FBXO11 mutations (E491L) have been identified in Jeff mice[210], homozygous mice are lethal while heterozygous mice display abnormalities in epithelial development, being born with open eyes similar to mice injected with EGF[210]. Jeff mice display increased pSMAD2 activation and a low molecular weight isoform of FBXO11 binds to pSMAD2[210]. The nature of the interaction is unclear and it is not understood how mutations in FBXO11 contribute to increased pSMAD2 signaling. AKT and MAPK are parallel pathways to SMAD2 downstream of TGF-beta receptor. Further analysis is needed to understand how FBXO11 mutations contribute to an increase in pSMAD2 and if USP46 counteracts the SCF^{FBXO11} complex.

Another possibility is that USP46 is directly regulating the stability of FBXO11. There are now numerous examples of DUBs and E3 ligases being

found in complexes together[167]. One function of DUBs is to regulate the stability of E3 ligases, which can become auto-ubiquitylated, thus protecting them from degradation. However in this case, there was no dramatic decrease in the levels of FBXO11 with USP46 depletion. Although, it is possible that USP46 affects the FBXO11 under specific conditions such as during the cell cycle in a more dramatic fashion that we have not tested. USP46 may also function in tandem with FBXO11 to dynamically influence ubiquitylation status of substrates. Several substrates have been described for SCF^{FBXO11}, notably CDT2[209] and BCL6 that influence cell-cycle exit and apoptosis respectively. FBXO11 is beginning to emerge as a tumor suppressor[207] and could potentially explain the anti-proliferative effects of overexpressing USP46[192] by opposing the effects of FBXO11.

FBXO11 has been reported as a nuclear localized protein. In our stable cell lines a proportion of GFP-USP46 was localized to the nucleus, making it unlikely that the USP46:FBXO11 interaction is taking place on the endosome. Co-localization studies using FRET probes would need to be preformed in order to confirm were this interaction is taking place. In Uniprot there are 6 isoforms of FBXO11 annotated (as of September 2013) and there is relatively little information available on the functions of the different isoforms. Our results show that the higher molecular weight isoform of FBXO11 has a relatively increased binding preference to USP46 that the lower molecular weight isoform. It would be interesting to follow up which of the known FBXO11 functions depend on the higher molecular weight isoform and the sub cellular localization of the different isoforms.

Our dataset found overlapping interactors in WDR20 and WDR48. The interactions between USP46 and WDR20 and WDR48 seem to be fundamental to the action of USP46 but the mechanism of action is unclear[200]. It is thought that the WD40 containing proteins act as scaffolds for protein interactions possibly bringing USP46 into contact with the substrate[200]. Crystal structures of USP46 in a complex with WDR20 and WDR48 would be able to shed light on this mechanism. The detection of these proteins in our study provided a positive control for the experiment. Ubiquitin (UBB) preferentially

associated with the catalytically inactive form of USP46. It is unclear whether this is due to ubiquitylation of USP46 itself (which was not consistently seen) or that USP46 was bound to ubiquitylated substrates. If the latter is the case then performing IPs with catalytic inactive DUBs could be a successful strategy to identify new substrates. In our dataset there were more proteins identified in the catalytic mutant IP suggesting that GFP-USP46-C44S may act as a substrate trap. However, this would need to be verified through additional experiments. The identification of true substrates through this method will inevitably be limited by need to use traditional methods such as using antibodies that can be expensive and difficult to source.

We were unable to confirm the interaction between USP46 and PHLPP phosphatases. The methodology used here differed from the Sowa at al. (2009)[211] in that they purified HA-USP46 that was expressed by retroviral vector in HEK cells. The expression levels driven through the retroviral vector are likely to be higher and non-uniform across cells, different cells will express different levels of HA-USP46 depending on the multiplicity of infection by the virus. No interaction between USP46 and PHLPP1/2 has been demonstrated for endogenous USP46 raising the possibility that the interaction depends on high levels of USP46 to be seen.

The results presented here have contributed to the USP46 interactome and confirmed a novel interaction with FBXO11. The work has also provided a provision of new tools to study USP46. Future work will focus on the function of the USP46:FBXO11 interaction.

5.4. Conclusions

- Generation of a new model to study USP46.
- USP46 interacts with FBXO11.

Chapter 6 USP8 regulates retrograde trafficking of CI-M6PR.

6.1. Introduction

A proportion of trans-membrane proteins undergo retrograde transport from the endo-lysosomal system to the trans-golgi network (TGN)[147]. The archetypal cargo for retrograde transport is the cation-independent mannose 6-phosphate receptor (CI-M6PR). The function of CI-M6PR is to bind newly synthesized lysosomal hydrolases in the TGN to be trafficked into the endo-lysosomal system[147]. Once in the endo-lysosomal compartment, the acid hydrolases dissociate from the receptor due to the acidic environment and then are trafficked into the lysosome by bulk flow[147].

Cathepsin D is a lysosomal hydrolase that is trafficked by CI-M6PR. It is synthesized on membrane bound ribosomes and translocates into the lumen of the ER. It becomes N-glycosylated in the ER and then subsequently phosphorylated in the cis-Golgi network. It is through these post-translational modifications that Cathepsin D associates with the receptor[212]. The ligand bound receptor is packaged in AP1 clathrin-coated vesicles, which then fuse with endosomes. A proportion of the receptor is trafficked to the plasma membrane via the secretory pathway and is retrieved through endocytosis[213]. Once the cargo bound receptor reaches the endo-lysosomal system, progressive acidification of the compartment through the v-ATPase pump, induces the maturation of the Cathepsin D into an active form. Cathepsin D maturation is achieved through limited proteolysis first from a 53kDa precursor protein into a 47-kDa intermediate form (also known as a Pro form) in the endo-lysosomal system through an autocatalytic mechanism. The intermediate protein is transferred into the lysosomes where it is processed into a 31kDa active hydrolase in the lysosome[212] and processed through an unknown mechanism[214].

CI-M6PR is then retrieved back to the TGN via the retrograde transport. This process is mediated by the retromer complex, a cargo recognizing trimer unit comprising VPS35, VPS26 and VPS29 and membrane-deforming unit composed of SNX1 and SNX2[215]. However, there are also other mechanisms for retrograde transport. Furin is a trans-membrane endopeptidase that also undergoes retrograde transport passing through the late endocytic compartment. However, unlike CI-M6PR it does not require the retromer complex for retrieval to the TGN[216]. Additionally retrograde trafficking is dependent on the F-actin nucleating complex WASH, which assembles actin filaments required for the extraction of vesicles from the late endosomal membranes[148].

In 2013, Hao et al.[157] identified an E3 ligase regulating retromer dependent retrograde transport, MAGE-L2-TRIM27. Mechanistic studies demonstrated that MAGE-L2-TRIM27 built K63 chains on WASH at K220, which were necessary for vesicle formation[157]. As ubiquitylation was required for normal retrograde trafficking we hypothesized that this would be a reversible process. We therefore screened for disruption of retrograde trafficking of CI-M6PR with depletion and over-expression of 4 endosomal DUBs, USP8, USP46, AMSH and AMSH-lp.

6.2. Results.

6.2.1. Depletion of USP8 causes mislocalisations of CI-M6PR.

We used CI-M6PR distribution as a readout for perturbed retrograde trafficking. Under steady-state conditions in HeLa cells, CI-M6PR is localized to the TGN. If there is a disruption of retrograde trafficking, then CI-M6PR will accumulate in the endo-lysosomal compartment, as it can no longer make the return journey to the TGN. HeLa cells were treated for 72 hours with single siRNA oligonucleotides that have been previously characterized in the lab and are targeting 3 endosomal DUBs, USP8, AMSH, and USP46. VPS35 the core component of the retromer was targeted using a pool of siRNA oligonucleotides and a non-targeting siRNA were used as controls.

In figure 6.1, cells treated with NT1 control show an overlapping distribution between p230 (TGN marker) and CI-M6PR. In cells that were treated with AMSH and USP46 this distribution is unaltered. There was a change in distribution of CI-M6PR in cells depleted of USP8 with 2 individual oligonucleotides. CI-M6PR was trapped in a compartment distinct to p230. Cells treated with VPS35 also showed a change in distribution with the pattern of CI-M6PR distribution appearing more disperse.

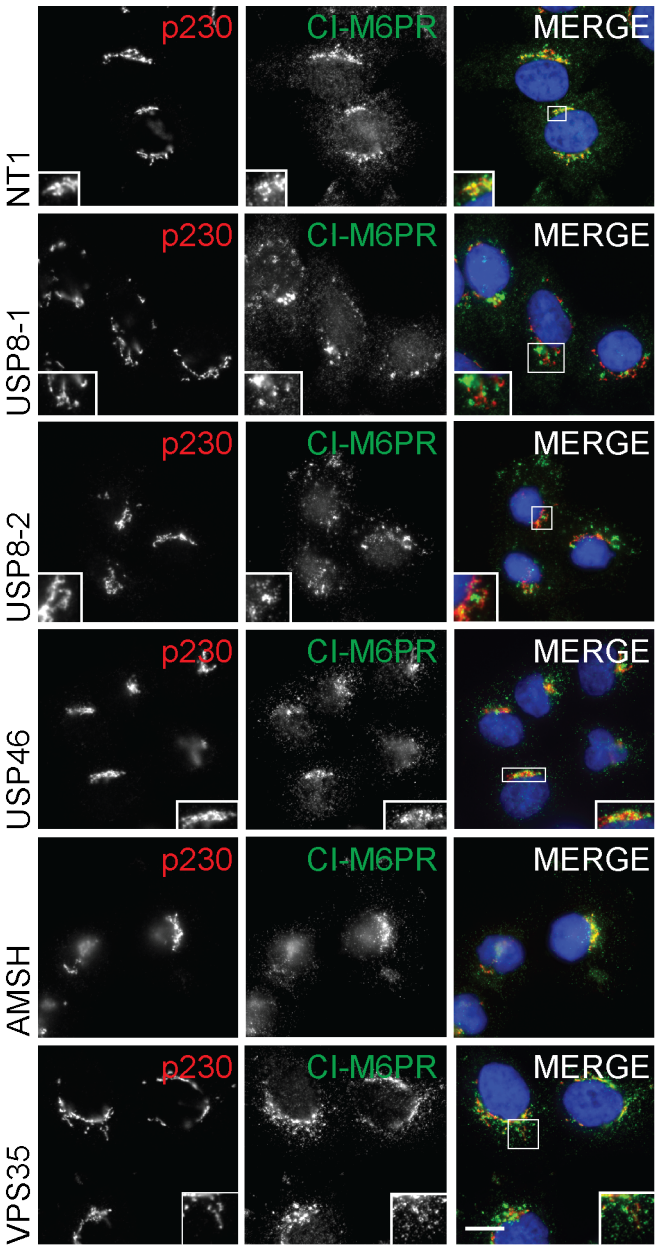

Figure 6.1. Depletion of USP8 causes mislocalization of CI-M6PR.

HeLa cells were treated with siRNA for 72 hours. Cells were fixed and labeled for p230 (TGN) and CI-M6PR. Under steady state conditions CI-M6PR is localized to the TGN. USP8 depletion causes CI-M6PR to accumulate in a compartment separate to p230.

Scale bar=10μm.

6.2.2. USP8 depletion causes an accumulation of CI-M6PR in aberrant endosomes.

As USP8 depletion was causing a mislocalization of CI-M6PR from the TGN, one may predict that CI-M6PR is accumulating in the endosomal system. HeLa cells were depleted of USP8 with 2 individual oligonucleotides or treated with oligonucleotides targeting NT1, AMSH and VPS35 as a control. The cells were stained with EEA1 (early endosome antigen 1) as a marker of early endosomes and CI-M6PR. In figure 6.2.1.A, NT1 and AMSH siRNA treated control cells, show little overlap between EEA1 and CI-M6PR, with the majority of CI-M6PR accumulating in a peri-nuclear compartment. In USP8 knockdown cells, EEA1 positive endosomes show an altered distribution, they appear aggregated and contain CI-M6PR.

Previous work has demonstrated that there is an accumulation of ubiquitin on aberrant endosomes in USP8 depleted cells[132]. To confirm this USP8 depleted cells were stained with anti-ubiquitin FK2 antibody that recognizes mono and poly-ubiquitylated proteins (Figure 6.2.1.B). There was an accumulation of ubiquitylated proteins on endosomes consistent with previously reported results[132].

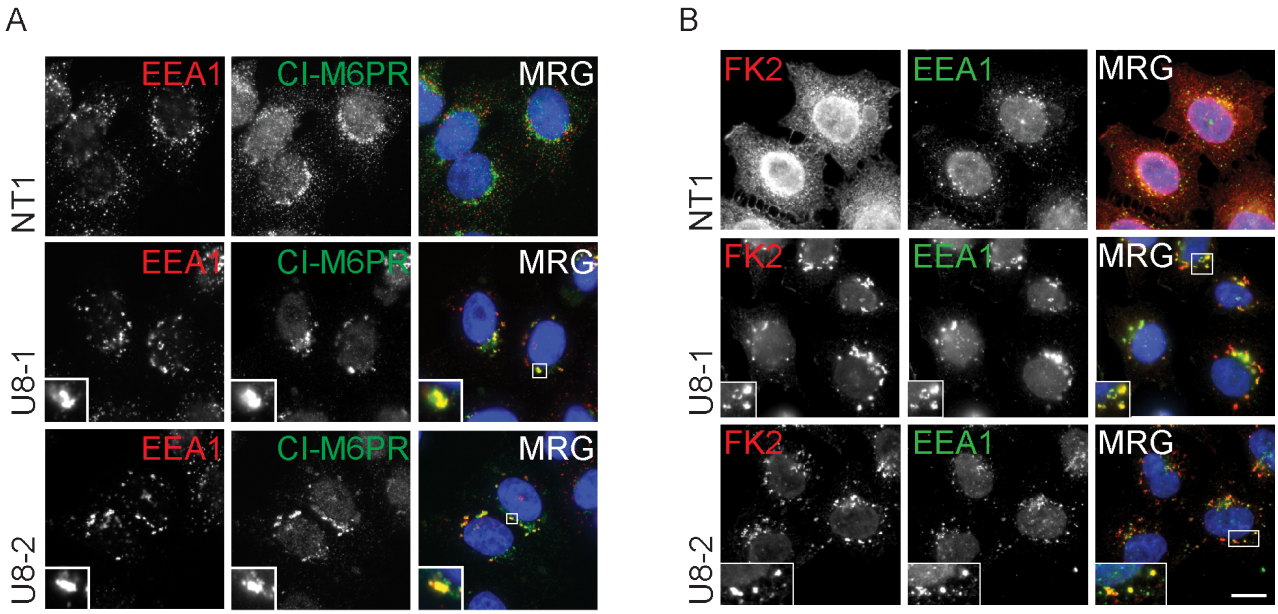

Figure 6.2.1. Depletion of USP8 leads to an accumulation of CI-M6PR in aberrant endosomes.

HeLa cells were treated for 72hours with siRNA. Cells were fixed and labeled with antibodies against A) EEA1 (early endosomes) and CI-M6PR B) FK2 (poly- mono- conjugated ubiquitin) and EEA1. Depletion of USP8 causes an accumulation of CI-M6PR in an EEA1 positive compartment. Scale bar = 10μm.

Lysates from the knockdown samples were probed with antibodies against USP8 and VPS35 (Figure 6.2.3) confirming that the knockdown had been successful. There was no change in the stability of CI-M6PR upon depletion of USP8 or VPS35.

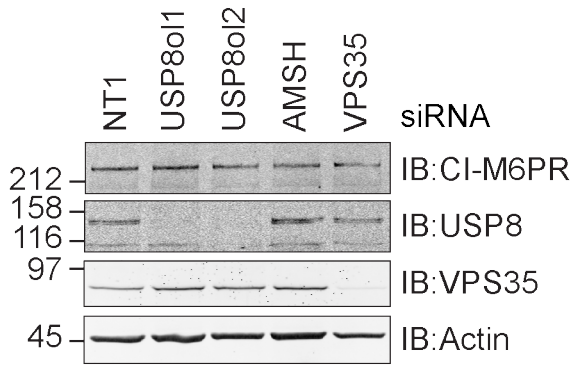

Figure 6.2.3. USP8 depletion dose not cause a change in levels of CI-M6PR.
HeLa cells were treated with siRNA for 72hours. Cells were lysed in NP40 buffer and lysates were probed with antibodies against USP8, VP35, CI-M6PR and Actin. Cells treated with USP8 and VPS35 siRNA showed efficient depletion of their target proteins. Neither knockdown of VPS35 nor of USP8 had an effect on the levels of CI-M6PR.

6.2.3. USP8 depletion causes a delay in CD8-CI-M6PR uptake.

To confirm the disruption of CI-M6PR trafficking with USP8 depletion we employed an assay to look at the uptake of CI-M6PR from the plasma membrane. A proportion of CI-M6PR is lost via the secretory pathway to the plasma membrane. This can be exploited using a CD8-CI-M6PR chimera stable cell line. These cells can be labeled with an anti-CD8 antibody on ice for 1 hour, the cells are then warmed up to 37˚C to promote the internalization of the receptor-antibody complex. The trafficking of the receptor:antibody complex can then be visualized, by fixing the cells and then labeling with fluorescent secondary antibodies at different time points. The cells were counter-stained with EEA1 as a reference point for CD8-CI-M6PR transition through the endosomal compartments. In figure 6.3.1 CD8-CI-M6PR-HeLa cells were treated with siRNA over 96 hours. A delay in the retrograde transport of CD8-CI-M6PR is observed when cells were depleted with USP8 and this effect was consistent using 2 individual oligonucleotides. This is in contrast to control NT1 treated cells where after 48mins at 37˚C, the majority of CD8-CI-M6PR has accumulated in a peri-nuclear compartment. Interestingly in USP8 depleted cells some of the CD8-CI-M6PR still reaches

the TGN indicating that USP8 depletion does not completely block, but rather delays retrograde transport.

The assay failed in VPS35 knockdown cells. There were few cells labeled with the CD8 antibody possibly because VPS35 knockdown efficiently blocked retrograde transport of CI-M6PR, trapping it in the endosomal system. In figure 6.4.2 NP40 lysates from the experiment were probed with antibodies against USP8 and VPS35 demonstrating effective depletion.

NT1
U8-1
U8-2
EEA1
CD8
MERGE
8min
16min
24min
32min
40min
48min

Figure 6.3.1. Depletion of USP8 causes a delay in CD8-CI-M6PR uptake.

CD8-CI-M6PR stably transfected HeLa cells were treated at 0 and 48 hours with siRNA over 96hours. Plasma membrane CD8-CI-M6PR was labeled with an anti-CD8 monoclonal antibody for 1 hour on ice. Cells were subsequently warmed to 37˚C and fixed at various time points over 48mins. The cells were then labeled with EEA1 and fluorescent secondary antibodies to visualize the internalization of CD8-CI-M6PR through the endosomal network. CD8-CI-M6PR trafficking is delayed in USP8 knockdown cells compared to NT1 control. Scale bar=10μm.

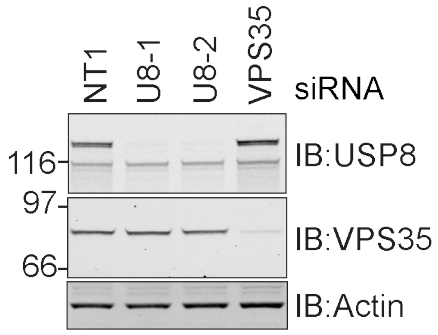

Figure 6.3.2. siRNA treatment efficiently depletes respective targets in CD8-CI-M6PR stable cells.

CD8-CI-M6PR cells from figure 6.4.1 were treated twice with siRNA over 96hours and subsequently lysed in NP40 buffer. Immuno blotting demonstrates efficient depletion of target proteins.

6.2.4. USP8 depletion causes a delay in CD8-Furin uptake.

A delay in the uptake of CD-CI-M6PR was caused by depletion of USP8. To test the hypothesis that this effect was dependent on disruption of the retromer complex, we employed a CD8-Furin uptake assay. Furin is transported through the late endosomal compartment to the TGN, like CI-M6PR, however it's retrograde transport is not dependent on the retromer complex. Stably transfected CD8-Furin-HeLa cells were treated with siRNA twice over 96 hours. Using the same experimental procedure as in figure 6.4.1, the transport of CD8-Furin to the TGN was monitored. Preliminary data had indicated that the transport of CD8-Furin was more or less completed by 32 mins, so the 48min time point was dropped from the assay.

In cells depleted of USP8 a delay in CD8-Furin transport to the TGN was observed with CD8-Furin accumulating in aberrant endosomes, reminiscent of the delay observed for CD8-CI-M6PR. VPS35 depletion had no effect on the retrograde transport of CD8-Furin with the majority of CD8-Furin reaching the peri-nuclear compartment after 32mins in both VPS35 and NT1 treated cells.

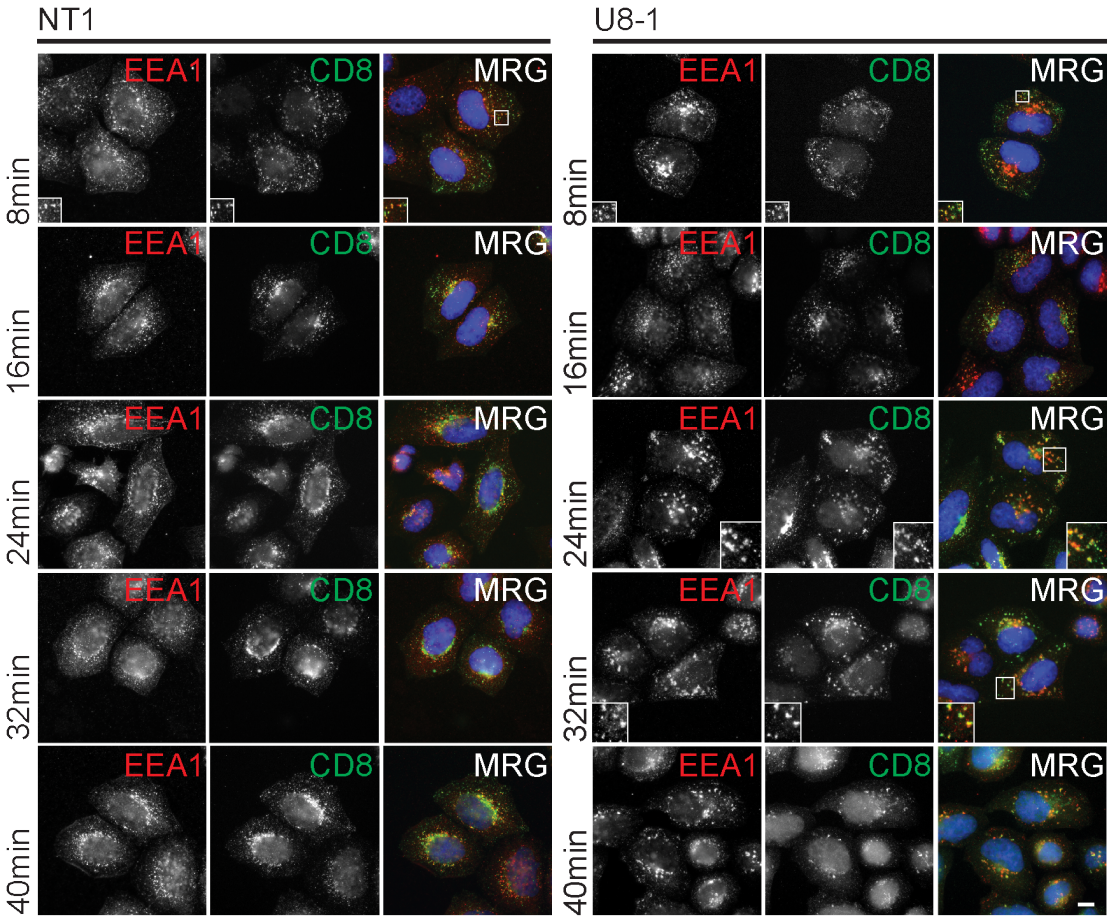

Figure 6.4.1. Depletion of USP8 causes a delay in CD8-Furin uptake part 1.

HeLa cells stably transfected with CD8-Furin were treated twice with siRNA over 96hours. Plasma membrane CD8-Furin was labeled with an anti-CD8 monoclonal antibody for 1 hour on ice. Cells were subsequently warmed to 37˚C and fixed at the indicated time points over 48mins. The cells were then labeled with EEA1 and fluorescent secondary's antibodies to visualize the internalization of CD8-CI-M6PR through the endosomal network. CD8-Furin trafficking is delayed in USP8 knockdown cells compared to NT1 treated control cells. Scale bar=10μm.

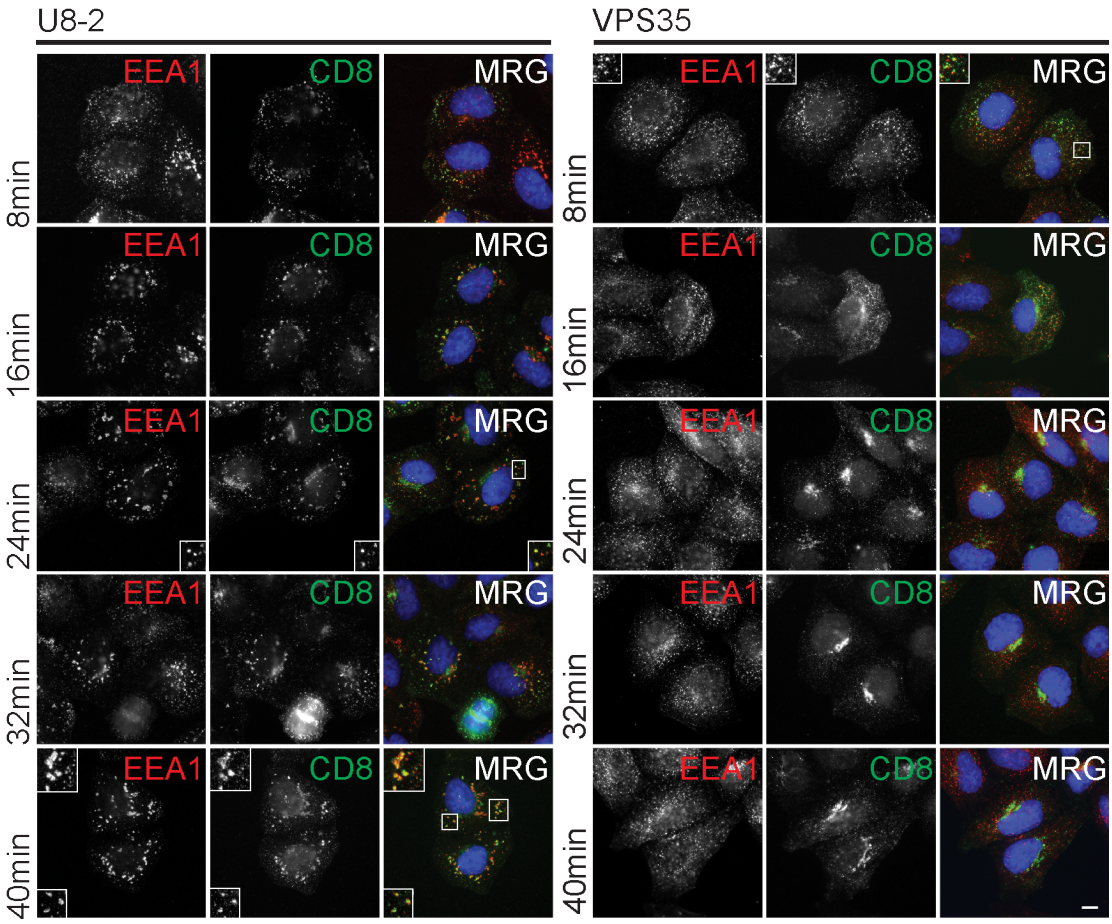

Figure 6.4.2. Depletion of USP8 causes a delay in CD8-Furin uptake part 2.

HeLa cells stably transfected with CD8-Furin were treated twice with siRNA over 96hours. Plasma membrane CD8-Furin was labeled with an anti-CD8 monoclonal antibody for 1 hour on ice. Cells were subsequently warmed to 37˚C and fixed at the indicated time points over 48mins. The cells were then labeled with EEA1 and fluorescent secondary's antibodies to visualize the internalization of CD8-CI-M6PR through the endosomal network. CD8-Furin trafficking is delayed in USP8 knockdown cells compared to NT1 treated control cells. Scale bar=10μm.

6.2.5. Overexpression of exogenous USP8 does not increase CD8 uptake.

USP8 depletion inhibited the uptake of USP8 we therefore wanted to test if overexpression of USP8 increases the rate of CD8-CI-M6PR transport to the TGN. The same assay as used in figure 6.4.1 was employed with transient expression of GFP-USP8, GFP-USP8-C786S or EGFP as a control for 24hours.

In figure 6.5, GFP-USP8 was observed in both the cytosol and on endosomes while GFP-USP8-C786S accumulates on endosomes. There was no increase in the rate of CD8-CI-M6PR observed over the control GFP or to untransfected cells at 8min for either the GFP-USP8 or GFP-USP8-C786S. Nor could any effects been seen on the retrograde trafficking of CD-CI-M6PR at any other time points.

GFP
GFP-USP8
GFP-USP8-C786S
CD8
GFP
MERGE
USP8
USP8CS
8min
16min
40min
48min

Figure 6.5. Overexpression of GFP-USP8 does not effect CD8-CI-M6PR uptake.
HeLa cells stably transfected with CD8-CI-M6PR were transfected with GFP, GFP-USP8 and GFP-USP8-C786S for 24hours. Plasma membrane CD8-CI-M6PR was labeled with an anti-CD8 monoclonal antibody for 1 hour on ice. Cells were subsequently warmed to 37˚C and fixed at indicated time points over a period of 48mins. The cells were then labeled with EEA1 and fluorescent secondary antibodies to visualize the internalization of CD8-CI-M6PR through the endosomal network. There is no effect on the trafficking of CD8-CI-M6PR with overexpression of GFP-USP8 over the GFP control however there is a delay in the trafficking with overexpression of GFP-USP8-C786S. Scale bar = 10μm.

6.2.6. Overexpression of other endosomal DUBs has no effect of CD8-M6PR retrograde trafficking.

Ubiquitylation of the WASH complex was a critical step for retrograde transport[157]. One would predict that overexpression of a DUB that targeted WASH would inhibit the action of WASH. Overexpression of USP8 was having no effect on retrograde trafficking; we therefore sought to identify other endosomal DUBs, which may disrupt this process. We overexpressed 3 other endosomal DUBs (AMSH, AMSH-lp, USP46) in the CD8-CI-M6PR HeLa-M cells. In figure 6.6 in cell transfected with GFP constructs there was no effect on the trafficking of CD8-CI-M6PR for any of the DUBs tested compared to untransfected cells. Co-localization between AMSH, AMSH-lp and CD8-CI-M6PR is observed in a peri-nuclear compartment, which may correspond to the TGN, based on co-localization experiments previously conducted by Monika Chojnowska-Monga[217].

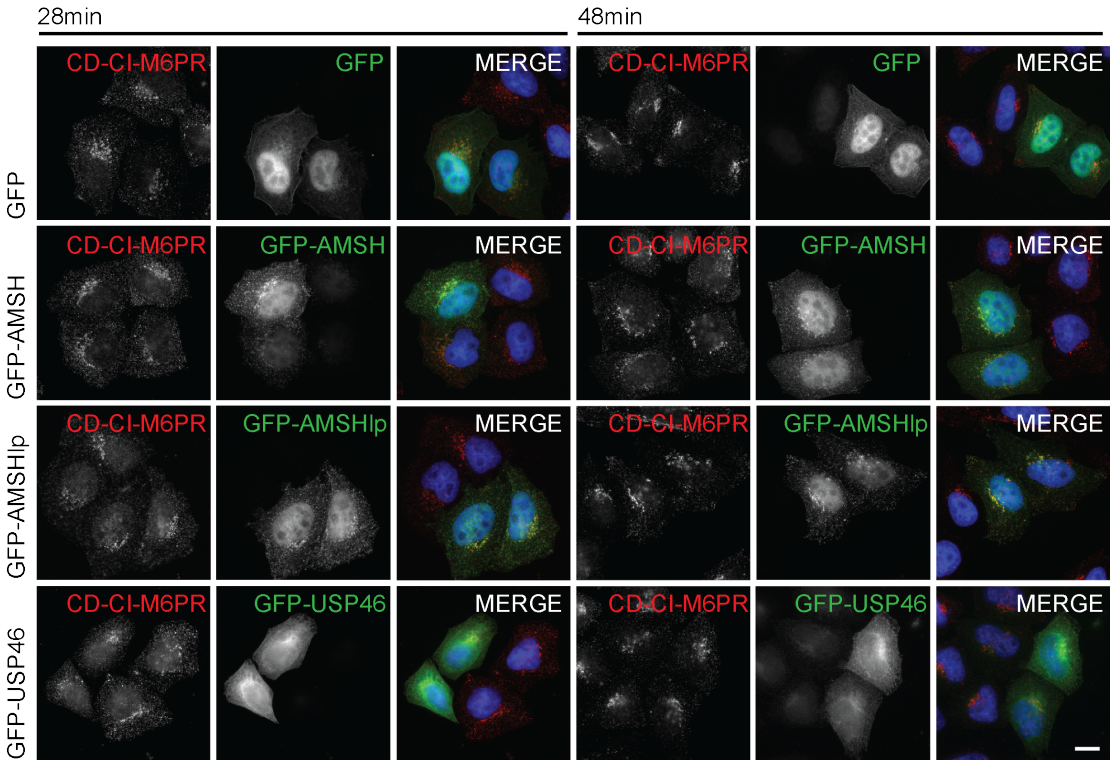

Figure 6.6. Overexpression of endosomal DUBs, USP46, AMSH and ASMH-lp do not disrupt CD8-CI-M6PR retrograde trafficking.

HeLa cells stably transfected with CD8-CI-M6PR were transfected with GFP, GFP-USP46, GFP-AMSH and GFP-AMSH-lp for 24hours. Plasma membrane CD8-CI-M6PR was labeled with an anti-CD8 monoclonal antibody for 1 hour on ice. Cells were subsequently warmed to 37˚C and fixed at the indicated time points over 48mins. The cells were then labeled with EEA1 and fluorescent secondary antibodies to visualize the retrieval of CD8-CI-M6PR to the TGN. Scale bar = 10μm.

6.2.7. Re-expression of GFP-USP8 rescues CI-M6PR mislocalization.

In order to test if the mislocalization of CD8-CI-M6PR is a specific effect of USP8 knockdown or an off-target effect caused by the siRNA, we re-expressed exogenous USP8 to rescue the effect of depletion. Three USP8 constructs that are resistant to USP8-1 siRNA were expressed in either NT1 or USP8-1 siRNA treated cells: wild type GFP-USP8, catalytically inactive GFP-USP8-C786S and GFP-USPΔMIT that lacks microtubule interacting transport domain (MIT) that allows USP8 to associate with endosomes[135]. HeLa cells were treated twice either with NT1 or USP8-1 siRNA over 96 hours with re-expression of exogenous USP8 constructs or pEGFP control for 66hours. By comparing the overlap between p230 TGN marker and CI-M6PR judged mislocalization was assessed.

In figure 6.7.1, NT1 siRNA treated cells displayed an overlapping distribution between CI-M6PR and p230 in all conditions. In USP8 depleted cells, CI-M6PR was mislocalized, consistent with previous results. The re-expression of GFP-USP8 rescued the mislocalization whereas expression of GFP-USP8ΔMIT and EGFP failed to rescue the phenotype and a similar distribution is observed in untransfected cells. In cells transfected with GFP-USP8-C786S there is also no rescue of the CI-M6PR phenotype and CI-M6PR accumulates in aberrant endosomes positive for GFP-USP8-C786S.

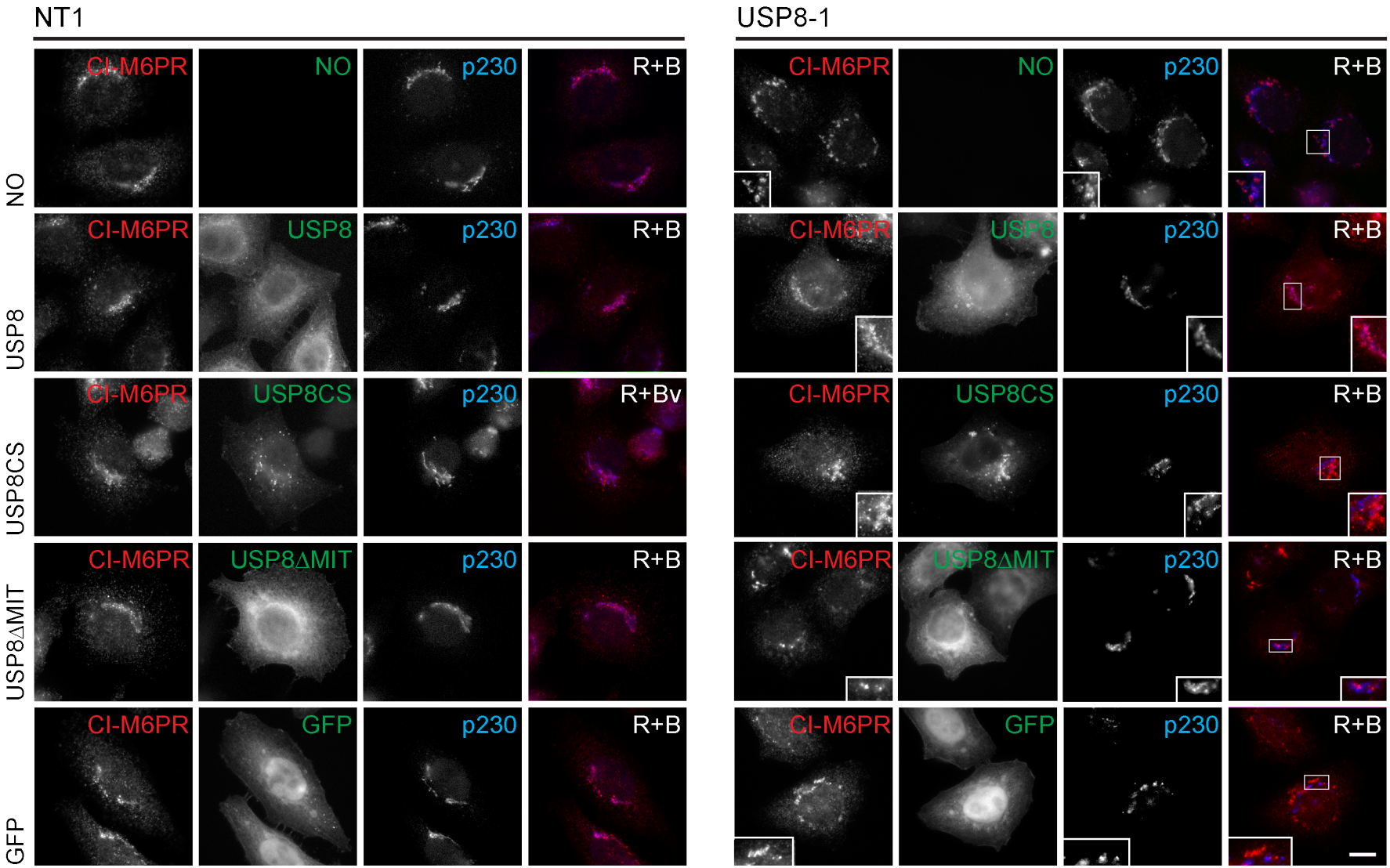
NT1
USP8-1
NO
USP8
USP8CS
USP8ΔMIT
GFP
CI-M6PR
NO
USP8
USP8CS
USP8ΔMIT
GFP
p230
R+B
R+Bv

Figure 6.7.1. Re-expression of USP8 rescues CI-M6PR mislocalization.

HeLa cells were treated twice over 96 hours and transfected with GFP, GFP-USP8, GFP-USP8-C786S (CS) or GFP-USP8ΔMIT for 66hours. Cells were subsequently fixed and labeled with CI-M6PR and p230 (TGN). Exogenous expression of GFP-USP8 rescues CI-M6PR mislocalization caused by USP8 depletion while expression of GFP-USP8ΔMIT does not. Expression of GFP-USP8-C786S accumulates in the same compartment as CI-M6PR and does not rescue the mislocalization phenotype. Merged images are a composite of CI-M6PR (594) and p230 (350). Scale bar = 10μm.

USP8 re-expression rescued the aberrant endosome phenotype of USP8 depletion (figure 6.7.2). In cells depleted of USP8 there was an increase in ubiquitylated substrates on aberrant endosomes consistent with the results in figure 6.22. In cells where GFP-USP8 had been re-expressed the depletion phenotype is rescued and there were reduced levels of ubiquitylated proteins compared to non-transfected proteins in the same field of view. This rescue was dependent on the endosomal localization of USP8 as re-expression of GFP-USP8ΔMIT failed to rescue this phenotype.

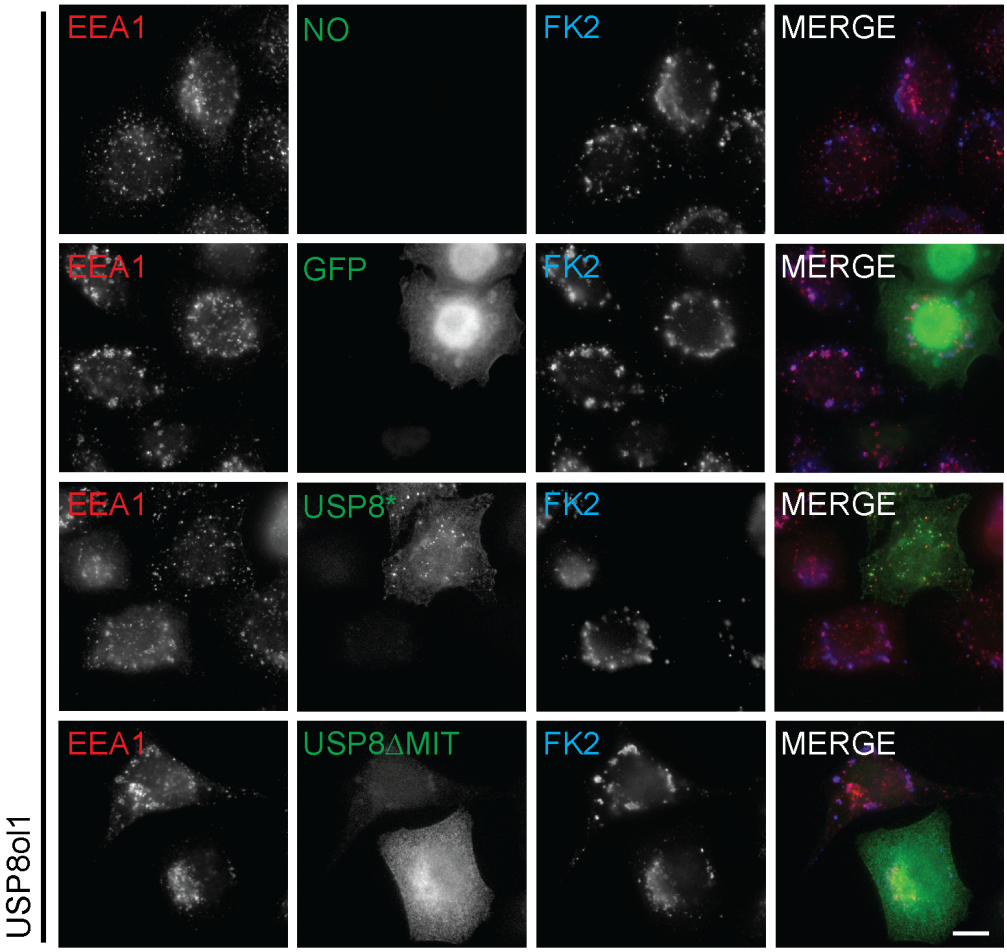

Figure 6.8.2. Re-expression of USP8 rescues aberrant endosome phenotype.
HeLa cells were treated twice with U8-1 siRNA over 96 hours and transfected with GFP, GFP-USP8, GFP-USP8-C786S or GFP-USP8ΔMIT for the last 66hours. Cells were subsequently fixed and labeled with the anti-Ubiquitin antibody FK2 and EEA1 (early endosome). Exogenous expression of GFP-USP8 rescues FK2 accumulation caused by USP8 depletion while expression of GFP-USP8ΔMIT does not. Scale bar = 10μm.

Lysates from the experiment shown in Figure 6.7.3. were run on a SDS-page gel confirming the knockdown of USP8 and the expression of siRES constructs (figure 6.7.3). The GFP-USP8 and GFP-USP8-C786S constructs were expressed at low levels compared with the endogenous USP8 however, this was sufficient to see a significant rescue of HRS, loss of HRS has been demonstrated previously with USP8 depletion[135]. Note that the transfection efficiency was estimated at 20% for this experiment.

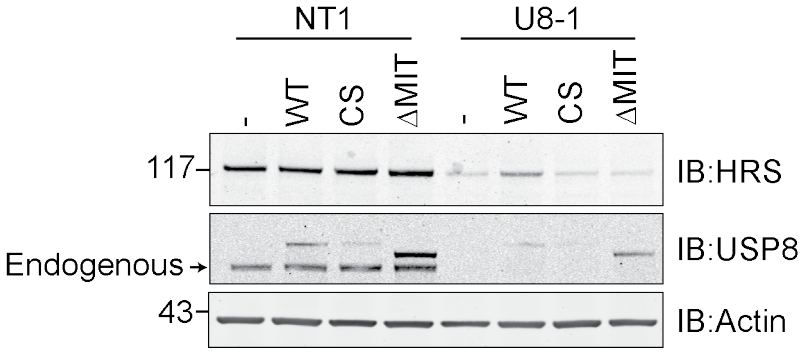

Figure 6.8.3. Re-expression of USP8 rescues HRS loss.

HeLa cells were treated twice with siRNA for 96 hours and transfected with GFP, GFP-USP8, GFP-USP8-C786S or GFP-USP8ΔMIT for 66hours. Cells were lysed in NP40 buffer and probed for HRS, USP8 and Actin. Expression of WT GFP-USP8 rescues the loss of HRS despite low expression levels while GFP-USP46-C786S and GFP-USP8ΔMIT do not.

6.2.8. USP8 depletion causes secretion of Cathepsin D

To test the disruption of CI-M6PR trafficking using a biochemical assay we employed an assay to look at the secretion of Cathepsin D. When CI-M6PR retrograde trafficking is perturbed it can no longer reach the TGN to actively sort newly synthesized hydrolases such as Cathepsin D. In this situation Cathepsin D is missorted and follows the secretory pathway out of the cell into the extracellular environment. The secretion of Cathepsin D can be tested biochemically by TCA precipitating proteins from the media and Cathepsin D levels can then be detected using a conventional western blot.

HeLa cells were treated twice with siRNA targeting USP8 at 0 hours and 48 hours over a 96hour time course. 16 hours before the end of the experiment the media as exchanged to Opti-MEM, after which it was collected and the proteins were TCA precipitated. The underlying cells were lysed in NP40 buffer to determine the cellular levels of Cathepsin D. I observed a marked increase in the levels of Cathepsin D in the media compared to control cells and a concomitant decrease in the mature form of Cathepsin D in cells.

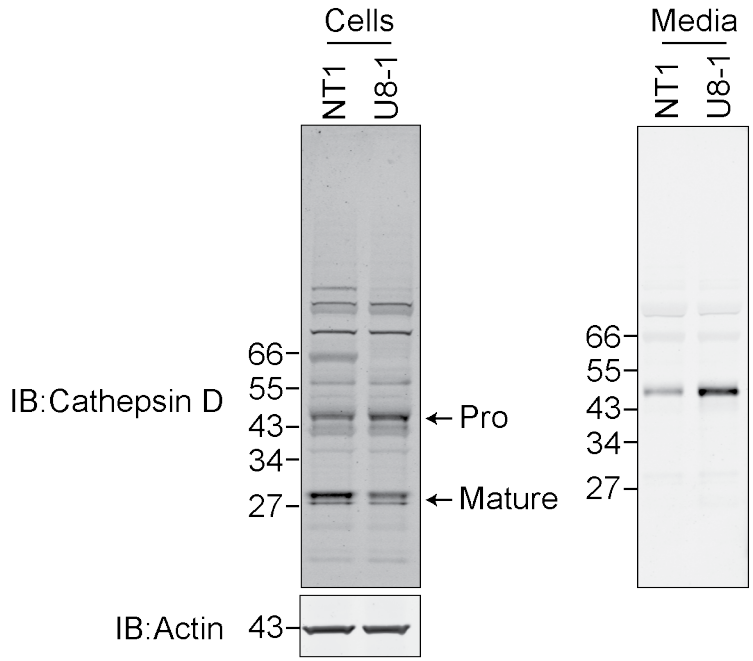

Figure 6.9. Depletion of USP8 causes missorting of Cathepsin D.

HeLa cells were treated twice with siRNA over 96 hours. Media was exchanged to Opti-MEM 16 hours before the end of the experiment. The media was collected and subjected to TCA precipitation. The cells were lysed in NP40 lysis buffer and the samples were probed with Cathepsin D antibody.

6.3. Discussion

Ubiquitylation mediates retrograde trafficking from the late endosomes to the TGN[157]. The work presented in this chapter aimed to identify DUBs that regulate this pathway, by employing a number of assays that monitor the trafficking of CI-M6PR, an archetypal substrate for retrograde transport. We identified USP8 as a novel regulator, which when depleted delayed the transport of CI-M6PR. Furthermore, depletion of USP8 caused a secretion of Cathepsin D, an enzyme trafficked by CI-M6PR to endosomes from the TGN. There was a concomitant decrease in the mature form of the enzyme in cells (Figure 6.10). USP8 required both catalytic function and an endosomal localization domain to mediate these effects as neither GFP-USP8-C786S nor GFP-USP8ΔMIT could rescue CI-M6PR mislocalization. These results indicate that USP8 depletion causes the accumulation of CI-M6PR in aberrant

endosomes and delays trafficking to the TGN, which in turn disrupts lysosome biogenesis.

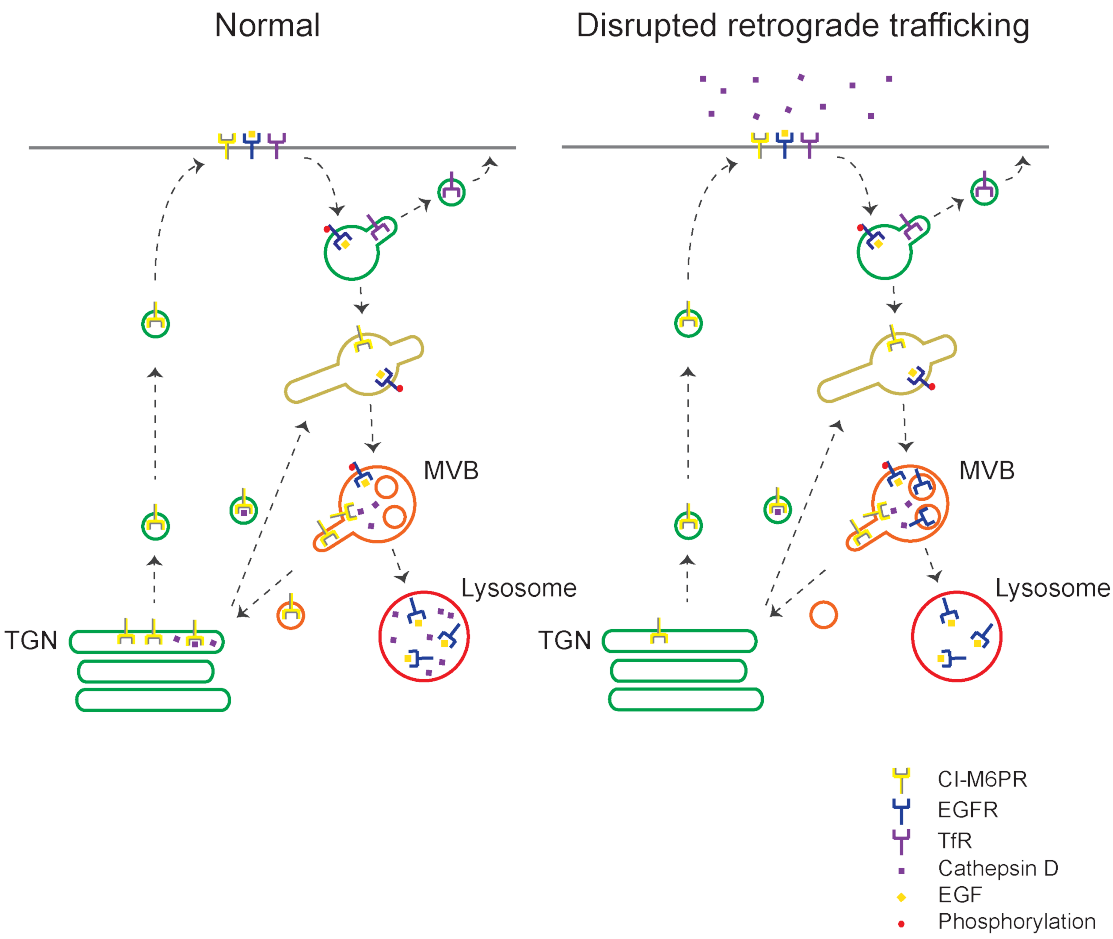

Figure 6.10. Model for retrograde transport in USP8 depleted cells.
USP8 is required for efficient retrograde transport of CI-M6PR and Furin. In USP8 depleted cells CI-M6P^ and Furin accumulate in aberrant endosomes that may prevent recycling from to the TGN. This in turn leads to secretion of newly synthesized acid hydrolases and as a consequence leads to a decrease in lysosome biogenesis.

The nature of the aberrant endosomes has also been addressed on an ultrastructural level. The clusters seen by light microscopy are MVBs that contain EEA1 antigen and are tethered to together by electron dense linkers. Depletion of USP8 produces a mixed phenotype on these endosomes, with some having a reduced number of internal vesicles while others have an increase and others are swollen[132, 137]. With USP8 depletion there is also a

delay in the sorting of EGFR into intra luminal vesicles of MVBs after 30mins. However, most EGFR eventually reached the lumen of late endosomes or lysosomes[137].

Both CI-M6PR and Furin trafficking are disrupted by USP8 depletion. It is also likely that other proteins passing through the late endosomal compartment en-route to the TGN will also be delayed. As such, it is unlikely that USP8 depletion directly disrupts the retromer, although that has not be formally tested and it is possible that USP8 depletion could disrupt retrograde trafficking thorough multiple mechanisms. There are two alternative mechanisms by which USP8 could function. The first is that USP8 depletion causes a loss of the ESCRT0 complex, STAM through proteasomal degradation[132] and it's partner protein HRS through an unknown mechanism[132, 135]. Recently two papers have identified a requirement of HRS for retrograde transport of amyloid beta precursor protein (APP)[218] and Shiga toxin[219]. HRS has also been shown to interact with SNX1[220], which is a component of the retromer complex. Taken together, these studies suggest that HRS may play a role in retromer mediated retrograde trafficking and that USP8 knockdown could disrupt trafficking by through the associated loss of HRS. However, as USP8 can also disrupt the trafficking of Furin this suggests that the mechanism is not retromer dependent. So either HRS could have an effect on multiple routes of retrograde trafficking or USP8 is functioning in another manner. USP8 depletion is partially phenocopied by depletion of HRS causing enlarged endosomes which have fewer internal vesicles[221].

An alternative explanation is that depletion of USP8 causes the formation of aberrant endosomes. An increase in such endosomes is coupled with an increase in ubiquitylated proteins on the endosomes and loss of ESCRT0 complex. Incoming ubiquitylated proteins to the endosome may not be efficiently sorted which could lead to a "traffic jam" of proteins on the limiting membrane of MVBs. Molecular crowding on the membrane of the sorting endosome could impact on other proteins transiting this compartment, whether or not they have been ubiquitylated. This would cause a build up of proteins waiting to be trafficked out of the MVB compartment, effectively

clogging up the system. One way to test this hypothesis would be to acutely inhibit USP8 using an inhibitor and then look at CD8-CI-M6PR retrograde trafficking. If this hypothesis holds true one would predict that acute inhibition would have little effect on a single pass of CI-M6PR trafficking. Supporting this idea is the observation that during the CD8-CI-M6PR trafficking assay there is not a complete blockade of CI-M6PR during a single pass of the endocytic system. However, when we monitor the steady state distribution of CI-M6PR in USP8 depleted cells, there is an altered distribution suggesting the equilibrium of CI-M6PR distribution has been shifted by this delay and that this takes time to establish.

As a consequence of CI-M6PR mistrafficking in USP8 depleted cells there will be a knock-on effect on lysosome biogenesis due to missorting of newly synthesised acid hydrolases. USP8 has been implicated in the regulation of various trans-membrane proteins by preventing their lysosomal degradation. KCa3.1[222], ENaC[223], Fz[224], MET[135] receptor and EGFR[132] are a few well characterized examples. However, the reason why degradation of trans-membrane proteins is inhibited by USP8 depletion is currently unclear. Our results indicate that deficiencies in lysosomal biogenesis may be a contributory factor to inadequate lysosomal degradation of trans-membrane proteins. This effect will be augmented by inefficient sorting into intra-luminal vesicles caused by the loss of ESCRT0 complex.

USP8 has been also implicated in the recycling of the WNT receptor Fz[224]. WNT signaling is initiated by the binding of WNT proteins to the receptor Fz and its co-receptor LRP5/6/Arrow. WNT ligands are morphogens determining the differentiation of tissues; differentiation is controlled through the formation of WNT signaling gradients across tissues. These are maintained through the secretion of WNT proteins via the receptor Wntless and the availability Fz of the receptor on the plasma membrane. Both of these factors are controlled through the endocytic pathway: Fz is ubiquitylated, internalized and sorted at the MVB and USP8 directly deubiquitylases Fz acting as a proofreading step that determines

whether the receptor is committed to degradation in the lysosome or recycled back to the plasma membrane[224]. The Wntless receptor is trafficked through the retrograde pathway, which is dependent on VPS35[225-228]. Recycling of the receptor is required to maintain gradients of secreted WNT ligands. In light of the results presented here, USP8 may have a dual regulatory role in regulating WNT signaling by determining the secretion of the ligand and the plasma membrane levels of the receptor, which would generate the same knockout phenotype.

Inhibition of USP8 can overcome Gefitinib resistance exhibited in some lung cancer cell lines[138] and USP8 has also been identified as a target for the treatment of multiple myeloma[229]. However, the mechanism for overcoming Gefitinib is not known and is presumed to be through defects in the trafficking of EGFR. Byun et al. (2013)[138] found there was a down regulation of several RTK including EGFR with inhibition of USP8. However, siRNA mediated depletion of USP8 induces a delay in the degradation of EGFR. It could be that there are two phenotypes based on long-term depletion and acute inhibition. Long-term inhibition causes the formation of aberrant endosomes that delay EGFR degradation while acute inhibition could enhance degradation by preventing recycling of EGFR. These effects may need to be considerated for administration regimes of any drugs used in patients targeting USP8.

The results presented in the chapter raises another possible explanation for the action of USP8 as an anti-cancer drug target. As USP8 function is integral to MVB function, targeting USP8 may function as a de facto lysosome inhibitor, raising parallels to the use of proteasomal inhibitors. Another feature of USP8 biology that has potential anti-cancer effects is through its regulation of the cell cycle[230]. It would be interesting to explore how these effects are mediated through USP8 and if these effects are mediated through a general disruption of trafficking or via a specific disruption of EGFR trafficking.

6.4. Conclusions

- USP8 regulates retrograde trafficking.
- USP8 is required for lysosomal biogenesis.

Chapter 7 Discussion

This chapter aims to summaries the findings of this thesis and discuss future directions for work.

I found that there is a decrease in MAPK signaling in USP15 depleted cells that correlate with a decrease in the protein levels of CRAF kinase. Work presented here and published in Hayes et al. (2012)[167], has shown that dominant signaling function of USP15 in MAPK signaling, at least in U2OS and HeLa cells, is consistent with the requirement for maintenance of CRAF levels. Future directions would address the suitability of USP15 as an anti-cancer drug target, in disease states that are driven through hyperactivation of MAPK pathway. Despite a significant effect on the activation of MAPK there was relatively little effect on the activation of the downstream ERK kinase this is likely because there is extensive input from other signaling pathways to activate ERK. It would be worth exploring different cancer cell lines to establish what the effects of USP15 are on MAPK dependent proliferation.

Translating our observation into *in vivo* model is not a straightforward issue. USP15 is playing a dual role in MAPK signaling influencing CRAF and BRAP and the extracellular environment dictates the extent of USP15s influence[167]. This effect was demonstrated in HeLa cells were no effect is seen for depletion of BRAP in serum-starved cells before growth factor application, whereas cells kept in complete media before growth factor stimulation exhibit BRAP influenced MAPK signaling[167]. It would be interesting to see how these effects are translated *in vivo,* were there will be considerable heterogeneity in the extracellular environment between different cancer types. Additionally, USP15 has been identified as a regulator of several cancer associated pathways[177, 180, 181]. Making it difficult to predict what the phenotypic output of USP15 inhibition will be *In Vivo*. Although, another viewpoint would be that if USP15 is regulator of many key processes in the cell, therefore inhibition may kill cancer cells, as they have higher metabolic stress than normal cells. The proteasomal inhibitor Bortezimib has been used

successfully in the treatment of cancer despite proteasomal inhibition having many cellular effects[231].

This study identified USP46 as an endosomal DUB. The consequences of this finding are not fully understood. There is an increase in late AKT signaling associated with depletion and overexpression of USP46 that was dependent on the catalytic activity of USP46. This would suggest that USP46 is enhancing EGFR recycling and maintaining its plasma membrane levels. However when tested through biochemical means, we saw no effect on the degradation rate of EGFR. Previous work has identified USP46 as a regulator of AKT signaling by influencing the stability of PHLPP1/2[192] but this study has not been able to recapitulate these findings neither through depletion experiments nor through an unbiased approach to identify interactors of USP46.

We generated a new set of tools to study USP46 by establishing cell lines expressing GFP-USP46 and GFP-USP46-C44S. Using the GFP tag to IP the exogenous proteins from our cell lines, we generated a dataset of potential interactors for USP46. We were able to confirm one interaction between USP46 and FBXO11, but the significance of this interaction is not presently known. We were initially interested in FBXO11 because it is the substrate-recognizing component of SCF-E3 ligase complex[203]. E3 ligases are often found in complexes together with DUBs, a minimalistic view for this observation, is that E3 ligases form these complexes to maintain cellular levels of E3 ligases that have a tendency to auto-ubiquitylate. Preliminary experiments though, suggest that USP46 is not regulating the stability of FBXO11 in a significant way. Another possibility that we have not explored is that USP46 works in partnership with FBXO11 to dynamically regulate the ubiquitylation status of proteins.

There have been several substrates identified for FBXO11 and through them FBXO11 regulates apoptosis[203] and exit from cell cycle[232]. It would be worth investigating if USP46 could influence the ubiquitylation status of known substrates of FBXO11 and what if any role it plays in apoptosis[203] and cell

cycle[232]. Because our cell lines expressed comparable levels of the wild type and catalytically inactive mutant of GFP-USP46, we were able to directly compare IPs from each cell line using SILAC. There was a bias in our dataset with interactors preferentially binding to the catalytically inactive mutant of USP46 over the wild type form, suggesting that it may act as a substrate trap. It has been technically difficult to identify substrates for DUBs using IP experiments coupled with mass spectrometry analysis, due to the transient nature of DUB substrate interactions. Therefore if the catalytically inactive mutant does acts a substrate trap it would be worth pursing this strategy further and expand it for other DUBs.

USP46 has been identified as a drug target to overcome depression. This is thought to be through the regulation of GluR1, but our interaction dataset has raised another possibility that USP46 inhibition could overcome depression through an interaction with MAOB. MAOB is an enzyme involved in the generation of dopamine, which plays a central role in pathogenesis of depression and inhibitors targeting MAOB and another isoform MAOA can be used to treat clinical depression[233]. We were unable to confirm this interaction as we could not source a reliable antibody but these results may explain another way in which USP46 could overcome depression.

The final section of the thesis has dealt with the role of established endocytic DUBs play in the regulation of retrograde transport. From this work, we identified USP8 as necessary for retrograde transport. When USP8 is depleted, it causes a missorting of newly synthesized lysosomal hydrolases into the secretory pathway and a decrease in the mature form of these enzymes. As both Furin and CI-M6PR trafficking are inhibited by USP8 depletion, one would not expect this mechanism of action to be dependent on the retromer. Rather one possible explanation is that a “traffic jam” on the sorting endosome occurs when USP8 is depleted, as there is an increase in ubiquitylated proteins on the sorting endosome, preventing efficient ubiquitylation dependent sorting. The question that still needs addressing is if there is a decrease in lysosomal function. To test this we would need to use a model substrate for lysosomal degradation, however it is difficult to dissect out

USP8 dependent defects in lysosomal function from the sorting defects of USP8.

USP8 has been identified as a drug target for over coming Gefitinib resistance in lung cancer and compounds have been developed to inhibit USP8[138]. Studying the early effects of USP8 inhibition may shed some light on the mechanism of action, as one would not expect a “traffic jam” of proteins to occur on the sorting endosome with acute inhibition. Long-term questions about USP8, should address whether the anti-cancer potential of USP8 inhibition is due to effects on the trafficking of RTKs or if it is due to a more general disruption of endocytic trafficking. Questions about the targets of USP8 also remain, it is clear that depletion causes an increase in the cellular levels of ubiquitylated species[230], largely on the endosome[133]. Exploring the binding partners of USP8 maybe a fruitful strategy to identifying substrates, using the same method presented in this thesis to identify interactors of USP46. An alternative strategy would be to isolate endosomes from cells, either depleted with USP8 or not, in SILAC configuration.

Bibliography

1. Levi-Montalcini, R. & Hamburger, V. Selective growth stimulating effects of mouse sarcoma on the sensory and sympathetic nervous system of the chick embryo. *The Journal of experimental zoology* **116**, 321-361 (1951).
2. Cohen, S., Levi-Montalcini, R. & Hamburger, V. A Nerve Growth-Stimulating Factor Isolated from Sarcom as 37 and 180. *Proc Natl Acad Sci U S A* **40**, 1014-1018 (1954).
3. Cohen, S. Purification of a Nerve-Growth Promoting Protein from the Mouse Salivary Gland and Its Neuro-Cytotoxic Antiserum. *Proc Natl Acad Sci U S A* **46**, 302-311 (1960).
4. Cohen, S. Isolation of a mouse submaxillary gland protein accelerating incisor eruption and eyelid opening in the new-born animal. *J Biol Chem* **237**, 1555-1562 (1962).
5. Cohen, S. Nobel lecture. Epidermal growth factor. *Biosci Rep* **6**, 1017-1028 (1986).
6. Cohen, S. The stimulation of epidermal proliferation by a specific protein (EGF). *Dev Biol* **12**, 394-407 (1965).
7. Cohen, S., Carpenter, G. & Lembach, K.J. Interaction of epidermal growth factor (EGF) with cultured fibroblasts. *Advances in metabolic disorders* **8**, 265-284 (1975).
8. Starkey, R.H., Cohen, S. & Orth, D.N. Epidermal growth factor: identification of a new hormone in human urine. *Science* **189**, 800-802 (1975).
9. Cohen, S. & Carpenter, G. Human epidermal growth factor: isolation and chemical and biological properties. *Proc Natl Acad Sci U S A* **72**, 1317-1321 (1975).
10. Savage, C.R., Jr. & Cohen, S. Epidermal growth factor and a new derivative. Rapid isolation procedures and biological and chemical characterization. *J Biol Chem* **247**, 7609-7611 (1972).
11. Gregory, H. Isolation and structure of urogastrone and its relationship to epidermal growth factor. *Nature* **257**, 325-327 (1975).

12. Carpenter, G. & Cohen, S. 125I-labeled human epidermal growth factor. Binding, internalization, and degradation in human fibroblasts. *J Cell Biol* **71**, 159-171 (1976).
13. Haigler, H., Ash, J.F., Singer, S.J. & Cohen, S. Visualization by fluorescence of the binding and internalization of epidermal growth factor in human carcinoma cells A-431. *Proc Natl Acad Sci U S A* **75**, 3317-3321 (1978).
14. McKanna, J.A., Haigler, H.T. & Cohen, S. Hormone receptor topology and dynamics: morphological analysis using ferritin-labeled epidermal growth factor. *Proc Natl Acad Sci U S A* **76**, 5689-5693 (1979).
15. Armelin, H.A. Pituitary extracts and steroid hormones in the control of 3T3 cell growth. *Proc Natl Acad Sci U S A* **70**, 2702-2706 (1973).
16. Hollenberg, M.D. & Cuatrecasas, P. Epidermal growth factor: receptors in human fibroblasts and modulation of action by cholera toxin. *Proc Natl Acad Sci U S A* **70**, 2964-2968 (1973).
17. Nimmo, H.G. & Cohen, P. Hormonal control of protein phosphorylation. *Advances in cyclic nucleotide research* **8**, 145-266 (1977).
18. Carpenter, G. & Cohen, S. Epidermal growth factor. *Annu Rev Biochem* **48**, 193-216 (1979).
19. Carpenter, G., King, L., Jr. & Cohen, S. Epidermal growth factor stimulates phosphorylation in membrane preparations in vitro. *Nature* **276**, 409-410 (1978).
20. Wrann, M.M. & Fox, C.F. Identification of epidermal growth factor receptors in a hyperproducing human epidermoid carcinoma cell line. *J Biol Chem* **254**, 8083-8086 (1979).
21. Das, M. *et al.* Specific radiolabeling of a cell surface receptor for epidermal growth factor. *Proc Natl Acad Sci U S A* **74**, 2790-2794 (1977).
22. Hunter, T. & Sefton, B.M. Transforming gene product of Rous sarcoma virus phosphorylates tyrosine. *Proc Natl Acad Sci U S A* **77**, 1311-1315 (1980).
23. Chinkers, M. & Cohen, S. Purified EGF receptor-kinase interacts specifically with antibodies to Rous sarcoma virus transforming protein. *Nature* **290**, 516-519 (1981).

24. Carpenter, G., King, L., Jr. & Cohen, S. Rapid enhancement of protein phosphorylation in A-431 cell membrane preparations by epidermal growth factor. *J Biol Chem* **254**, 4884-4891 (1979).
25. Ushiro, H. & Cohen, S. Identification of phosphotyrosine as a product of epidermal growth factor-activated protein kinase in A-431 cell membranes. *J Biol Chem* **255**, 8363-8365 (1980).
26. Ullrich, A. *et al.* Human epidermal growth factor receptor cDNA sequence and aberrant expression of the amplified gene in A431 epidermoid carcinoma cells. *Nature* **309**, 418-425 (1984).
27. Downward, J. *et al.* Close similarity of epidermal growth factor receptor and v-erb-B oncogene protein sequences. *Nature* **307**, 521-527 (1984).
28. Yarden, Y. & Schlessinger, J. Self-phosphorylation of epidermal growth factor receptor: evidence for a model of intermolecular allosteric activation. *Biochemistry* **26**, 1434-1442 (1987).
29. Citri, A. & Yarden, Y. EGF-ERBB signalling: towards the systems level. *Nat Rev Mol Cell Biol* **7**, 505-516 (2006).
30. Schulze, W.X., Deng, L. & Mann, M. Phosphotyrosine interactome of the ErbB-receptor kinase family. *Mol Syst Biol* **1**, 2005 0008 (2005).
31. Galisteo, M.L., Dikic, I., Batzer, A.G., Langdon, W.Y. & Schlessinger, J. Tyrosine phosphorylation of the c-cbl proto-oncogene protein product and association with epidermal growth factor (EGF) receptor upon EGF stimulation. *J Biol Chem* **270**, 20242-20245 (1995).
32. Tzahar, E. *et al.* A hierarchical network of interreceptor interactions determines signal transduction by Neu differentiation factor/neuregulin and epidermal growth factor. *Mol Cell Biol* **16**, 5276-5287 (1996).
33. Baulida, J., Kraus, M.H., Alimandi, M., Di Fiore, P.P. & Carpenter, G. All ErbB receptors other than the epidermal growth factor receptor are endocytosis impaired. *J Biol Chem* **271**, 5251-5257 (1996).
34. Waterman, H., Alroy, I., Strano, S., Seger, R. & Yarden, Y. The C-terminus of the kinase-defective neuregulin receptor ErbB-3 confers mitogenic superiority and dictates endocytic routing. *Embo J* **18**, 3348-3358 (1999).
35. Lemmon, M.A. & Schlessinger, J. Cell signaling by receptor tyrosine kinases. *Cell* **141**, 1117-1134 (2010).

36. Burgess, A.W. *et al.* An open-and-shut case? Recent insights into the activation of EGF/ErbB receptors. *Mol Cell* **12**, 541-552 (2003).
37. Zhang, X., Gureasko, J., Shen, K., Cole, P.A. & Kuriyan, J. An allosteric mechanism for activation of the kinase domain of epidermal growth factor receptor. *Cell* **125**, 1137-1149 (2006).
38. Sharma, S.V., Bell, D.W., Settleman, J. & Haber, D.A. Epidermal growth factor receptor mutations in lung cancer. *Nat Rev Cancer* **7**, 169-181 (2007).
39. Mendelsohn, J. Anti-epidermal growth factor receptor monoclonal antibodies as potential anti-cancer agents. *The Journal of steroid biochemistry and molecular biology* **37**, 889-892 (1990).
40. Gill, G.N. *et al.* Monoclonal anti-epidermal growth factor receptor antibodies which are inhibitors of epidermal growth factor binding and antagonists of epidermal growth factor binding and antagonists of epidermal growth factor-stimulated tyrosine protein kinase activity. *J Biol Chem* **259**, 7755-7760 (1984).
41. Masui, H. *et al.* Growth inhibition of human tumor cells in athymic mice by anti-epidermal growth factor receptor monoclonal antibodies. *Cancer Res* **44**, 1002-1007 (1984).
42. Goldberg, R.M. Cetuximab. *Nat Rev Drug Discov* **Suppl**, S10-11 (2005).
43. Cetuximab approved by FDA for treatment of head and neck squamous cell cancer. *Cancer Biol Ther* **5**, 340-342 (2006).
44. Saltz, L., Easley, C. & Kirkpatrick, P. Panitumumab. *Nat Rev Drug Discov* **5**, 987-988 (2006).
45. Varmus, H.E. Form and function of retroviral proviruses. *Science* **216**, 812-820 (1982).
46. Meisenhelder, J., Suh, P.G., Rhee, S.G. & Hunter, T. Phospholipase C-gamma is a substrate for the PDGF and EGF receptor protein-tyrosine kinases in vivo and in vitro. *Cell* **57**, 1109-1122 (1989).
47. Margolis, B. *et al.* The tyrosine phosphorylated carboxyterminus of the EGF receptor is a binding site for GAP and PLC-gamma. *Embo J* **9**, 4375-4380 (1990).

48. Morrison, D.K. *et al.* Direct activation of the serine/threonine kinase activity of Raf-1 through tyrosine phosphorylation by the PDGF beta-receptor. *Cell* **58**, 649-657 (1989).
49. Satoh, T. *et al.* Accumulation of p21ras.GTP in response to stimulation with epidermal growth factor and oncogene products with tyrosine kinase activity. *Proc Natl Acad Sci U S A* **87**, 7926-7929 (1990).
50. Ahmadian, M.R. *et al.* Guanosine triphosphatase stimulation of oncogenic Ras mutants. *Proc Natl Acad Sci U S A* **96**, 7065-7070 (1999).
51. Scheffzek, K. *et al.* The Ras-RasGAP complex: structural basis for GTPase activation and its loss in oncogenic Ras mutants. *Science* **277**, 333-338 (1997).
52. Kolch, W. Coordinating ERK/MAPK signalling through scaffolds and inhibitors. *Nat Rev Mol Cell Biol* **6**, 827-837 (2005).
53. Sadowski, I., Stone, J.C. & Pawson, T. A noncatalytic domain conserved among cytoplasmic protein-tyrosine kinases modifies the kinase function and transforming activity of Fujinami sarcoma virus P130gag-fps. *Mol Cell Biol* **6**, 4396-4408 (1986).
54. Pawson, T. Non-catalytic domains of cytoplasmic protein-tyrosine kinases: regulatory elements in signal transduction. *Oncogene* **3**, 491-495 (1988).
55. Moran, M.F. *et al.* Src homology region 2 domains direct protein-protein interactions in signal transduction. *Proc Natl Acad Sci U S A* **87**, 8622-8626 (1990).
56. Anderson, D. *et al.* Binding of SH2 domains of phospholipase C gamma 1, GAP, and Src to activated growth factor receptors. *Science* **250**, 979-982 (1990).
57. Kholodenko, B.N., Hancock, J.F. & Kolch, W. Signalling ballet in space and time. *Nat Rev Mol Cell Biol* **11**, 414-426 (2010).
58. Gao, T., Furnari, F. & Newton, A.C. PHLPP: a phosphatase that directly dephosphorylates Akt, promotes apoptosis, and suppresses tumor growth. *Mol Cell* **18**, 13-24 (2005).

59. Rodgers, J.T., Vogel, R.O. & Puigserver, P. Clk2 and B56beta mediate insulin-regulated assembly of the PP2A phosphatase holoenzyme complex on Akt. *Mol Cell* **41**, 471-479 (2011).
60. Tanoue, T., Adachi, M., Moriguchi, T. & Nishida, E. A conserved docking motif in MAP kinases common to substrates, activators and regulators. *Nat Cell Biol* **2**, 110-116 (2000).
61. Kholodenko, B.N. Negative feedback and ultrasensitivity can bring about oscillations in the mitogen-activated protein kinase cascades. *Eur J Biochem* **267**, 1583-1588 (2000).
62. Omerovic, J., Clague, M.J. & Prior, I.A. Phosphatome profiling reveals PTPN2, PTPRJ and PTEN as potent negative regulators of PKB/Akt activation in Ras-mutated cancer cells. *Biochem J* **426**, 65-72 (2010).
63. Eden, E.R., White, I.J., Tsapara, A. & Futter, C.E. Membrane contacts between endosomes and ER provide sites for PTP1B-epidermal growth factor receptor interaction. *Nat Cell Biol* **12**, 267-272 (2010).
64. Yeung, K. *et al.* Suppression of Raf-1 kinase activity and MAP kinase signalling by RKIP. *Nature* **401**, 173-177 (1999).
65. Kramer, S., Okabe, M., Hacohen, N., Krasnow, M.A. & Hiromi, Y. Sprouty: a common antagonist of FGF and EGF signaling pathways in Drosophila. *Development* **126**, 2515-2525 (1999).
66. Hacohen, N., Kramer, S., Sutherland, D., Hiromi, Y. & Krasnow, M.A. sprouty encodes a novel antagonist of FGF signaling that patterns apical branching of the Drosophila airways. *Cell* **92**, 253-263 (1998).
67. Hanafusa, H., Torii, S., Yasunaga, T. & Nishida, E. Sprouty1 and Sprouty2 provide a control mechanism for the Ras/MAPK signalling pathway. *Nat Cell Biol* **4**, 850-858 (2002).
68. Hoshino, R. *et al.* Constitutive activation of the 41-/43-kDa mitogen-activated protein kinase signaling pathway in human tumors. *Oncogene* **18**, 813-822 (1999).
69. Davies, H. *et al.* Mutations of the BRAF gene in human cancer. *Nature* **417**, 949-954 (2002).
70. Garnett, M.J. & Marais, R. Guilty as charged: B-RAF is a human oncogene. *Cancer Cell* **6**, 313-319 (2004).

71. Wan, P.T. *et al.* Mechanism of activation of the RAF-ERK signaling pathway by oncogenic mutations of B-RAF. *Cell* **116**, 855-867 (2004).
72. Ikenoue, T. *et al.* Different effects of point mutations within the B-Raf glycine-rich loop in colorectal tumors on mitogen-activated protein/extracellular signal-regulated kinase kinase/extracellular signal-regulated kinase and nuclear factor kappaB pathway and cellular transformation. *Cancer Res* **64**, 3428-3435 (2004).
73. Dhomen, N. *et al.* Oncogenic Braf induces melanocyte senescence and melanoma in mice. *Cancer Cell* **15**, 294-303 (2009).
74. Bollag, G. *et al.* Vemurafenib: the first drug approved for BRAF-mutant cancer. *Nat Rev Drug Discov* **11**, 873-886 (2012).
75. Cohen, P. & Tcherpakov, M. Will the ubiquitin system furnish as many drug targets as protein kinases? *Cell* **143**, 686-693 (2010).
76. Yaish, P., Gazit, A., Gilon, C. & Levitzki, A. Blocking of EGF-dependent cell proliferation by EGF receptor kinase inhibitors. *Science* **242**, 933-935 (1988).
77. Ward, W.H. *et al.* Epidermal growth factor receptor tyrosine kinase. Investigation of catalytic mechanism, structure-based searching and discovery of a potent inhibitor. *Biochemical pharmacology* **48**, 659-666 (1994).
78. Azam, M., Seeliger, M.A., Gray, N.S., Kuriyan, J. & Daley, G.Q. Activation of tyrosine kinases by mutation of the gatekeeper threonine. *Nat Struct Mol Biol* **15**, 1109-1118 (2008).
79. Girotti, M.R. & Marais, R. Deja Vu: EGF receptors drive resistance to BRAF inhibitors. *Cancer discovery* **3**, 487-490 (2013).
80. Prahallad, A. *et al.* Unresponsiveness of colon cancer to BRAF(V600E) inhibition through feedback activation of EGFR. *Nature* **483**, 100-103 (2012).
81. Rajakulendran, T., Sahmi, M., Lefrancois, M., Sicheri, F. & Therrien, M. A dimerization-dependent mechanism drives RAF catalytic activation. *Nature* **461**, 542-545 (2009).
82. Hatzivassiliou, G. *et al.* RAF inhibitors prime wild-type RAF to activate the MAPK pathway and enhance growth. *Nature* **464**, 431-435 (2010).

83. Poulikakos, P.I., Zhang, C., Bollag, G., Shokat, K.M. & Rosen, N. RAF inhibitors transactivate RAF dimers and ERK signalling in cells with wild-type BRAF. *Nature* **464**, 427-430 (2010).
84. Heidorn, S.J. *et al.* Kinase-dead BRAF and oncogenic RAS cooperate to drive tumor progression through CRAF. *Cell* **140**, 209-221 (2010).
85. Budhidarmo, R., Nakatani, Y. & Day, C.L. RINGs hold the key to ubiquitin transfer. *Trends Biochem Sci* **37**, 58-65 (2012).
86. Plechanovova, A., Jaffray, E.G., Tatham, M.H., Naismith, J.H. & Hay, R.T. Structure of a RING E3 ligase and ubiquitin-loaded E2 primed for catalysis. *Nature* **489**, 115-120 (2012).
87. Pickart, C.M. Mechanisms underlying ubiquitination. *Annu Rev Biochem* **70**, 503-533 (2001).
88. Komander, D. & Rape, M. The ubiquitin code. *Annu Rev Biochem* **81**, 203-229 (2012).
89. Clague, M.J., Liu, H. & Urbe, S. Governance of endocytic trafficking and signaling by reversible ubiquitylation. *Dev Cell* **23**, 457-467 (2012).
90. Dammer, E.B. *et al.* Polyubiquitin linkage profiles in three models of proteolytic stress suggest the etiology of Alzheimer disease. *J Biol Chem* **286**, 10457-10465 (2011).
91. Keusekotten, K. *et al.* OTULIN antagonizes LUBAC signaling by specifically hydrolyzing Met1-linked polyubiquitin. *Cell* **153**, 1312-1326 (2013).
92. Tokunaga, F. *et al.* Involvement of linear polyubiquitylation of NEMO in NF-kappaB activation. *Nat Cell Biol* **11**, 123-132 (2009).
93. Clague, M.J. & Urbe, S. Ubiquitin: same molecule, different degradation pathways. *Cell* **143**, 682-685 (2010).
94. Lee, M.J., Lee, B.H., Hanna, J., King, R.W. & Finley, D. Trimming of ubiquitin chains by proteasome-associated deubiquitinating enzymes. *Mol Cell Proteomics* **10**, R110 003871 (2011).
95. Hanna, J., Leggett, D.S. & Finley, D. Ubiquitin depletion as a key mediator of toxicity by translational inhibitors. *Mol Cell Biol* **23**, 9251-9261 (2003).
96. Verma, R. *et al.* Role of Rpn11 metalloprotease in deubiquitination and degradation by the 26S proteasome. *Science* **298**, 611-615 (2002).

97. Lee, M.J., Lee, B.H., Hanna, J., King, R.W. & Finley, D. Trimming of ubiquitin chains by proteasome-associated deubiquitinating enzymes. *Mol Cell Proteomics* **10**, R110.003871 (2011).
98. Koulich, E., Li, X. & DeMartino, G.N. Relative structural and functional roles of multiple deubiquitylating proteins associated with mammalian 26S proteasome. *Mol Biol Cell* **19**, 1072-1082 (2008).
99. Lee, B.H. *et al.* Enhancement of proteasome activity by a small-molecule inhibitor of USP14. *Nature* **467**, 179-184 (2010).
100. Hanna, J. *et al.* Deubiquitinating enzyme Ubp6 functions noncatalytically to delay proteasomal degradation. *Cell* **127**, 99-111 (2006).
101. Peth, A., Besche, H.C. & Goldberg, A.L. Ubiquitinated proteins activate the proteasome by binding to Usp14/Ubp6, which causes 20S gate opening. *Mol Cell* **36**, 794-804 (2009).
102. Peth, A., Kukushkin, N., Bosse, M. & Goldberg, A.L. Ubiquitinated proteins activate the proteasomal ATPases by binding to Usp14 or Uch37 homologs. *J Biol Chem* **288**, 7781-7790 (2013).
103. Sigismund, S. *et al.* Clathrin-independent endocytosis of ubiquitinated cargos. *Proc Natl Acad Sci U S A* **102**, 2760-2765 (2005).
104. Huang, F. *et al.* Lysine 63-linked polyubiquitination is required for EGF receptor degradation. *Proc Natl Acad Sci U S A* (2013).
105. Clague, M.J. & Urbe, S. Endocytosis: the DUB version. *Trends Cell Biol* **16**, 551-559 (2006).
106. Lauwers, E., Jacob, C. & Andre, B. K63-linked ubiquitin chains as a specific signal for protein sorting into the multivesicular body pathway. *J Cell Biol* **185**, 493-502 (2009).
107. Palade, G.E. Studies on the endoplasmic reticulum. II. Simple dispositions in cells in situ. *The Journal of biophysical and biochemical cytology* **1**, 567-582 (1955).
108. Sotelo, J.R. & Porter, K.R. An electron microscope study of the rat ovum. *The Journal of biophysical and biochemical cytology* **5**, 327-342 (1959).
109. Katzmann, D.J., Babst, M. & Emr, S.D. Ubiquitin-dependent sorting into the multivesicular body pathway requires the function of a conserved

endosomal protein sorting complex, ESCRT-1. *Cell* **106**, 145-155 (2001).

110. Babst, M., Katzmann, D.J., Estepa-Sabal, E.J., Meerloo, T. & Emr, S.D. Escrt-III: an endosome-associated heterooligomeric protein complex required for mvb sorting. *Dev Cell* **3**, 271-282 (2002).
111. Babst, M., Katzmann, D.J., Snyder, W.B., Wendland, B. & Emr, S.D. Endosome-associated complex, ESCRT-II, recruits transport machinery for protein sorting at the multivesicular body. *Dev Cell* **3**, 283-289 (2002).
112. Henne, W.M., Buchkovich, N.J. & Emr, S.D. The ESCRT Pathway. *Dev Cell* **21**, 77-91 (2011).
113. Williams, R.L. & Urbe, S. The emerging shape of the ESCRT machinery. *Nat Rev Mol Cell Biol* **8**, 355-368 (2007).
114. Bilodeau, P.S., Winistorfer, S.C., Kearney, W.R., Robertson, A.D. & Piper, R.C. Vps27-Hse1 and ESCRT-I complexes cooperate to increase efficiency of sorting ubiquitinated proteins at the endosome. *J Cell Biol* **163**, 237-243 (2003).
115. Teo, H., Veprintsev, D.B. & Williams, R.L. Structural insights into endosomal sorting complex required for transport (ESCRT-I) recognition of ubiquitinated proteins. *J Biol Chem* **279**, 28689-28696 (2004).
116. Alam, S.L. *et al.* Structural basis for ubiquitin recognition by the human ESCRT-II EAP45 GLUE domain. *Nat Struct Mol Biol* **13**, 1029-1030 (2006).
117. Dikic, I., Wakatsuki, S. & Walters, K.J. Ubiquitin-binding domains - from structures to functions. *Nat Rev Mol Cell Biol* **10**, 659-671 (2009).
118. Ye, Y. *et al.* Ubiquitin chain conformation regulates recognition and activity of interacting proteins. *Nature* **492**, 266-270 (2012).
119. Urbé, S. *et al.* The UIM domain of Hrs couples receptor sorting to vesicle formation. *J. Cell Sci.* **116**, 4169-4179 (2003).
120. Sorkin, A. & von Zastrow, M. Endocytosis and signalling: intertwining molecular networks. *Nat Rev Mol Cell Biol* **10**, 609-622 (2009).

121. Goh, L.K., Huang, F., Kim, W., Gygi, S. & Sorkin, A. Multiple mechanisms collectively regulate clathrin-mediated endocytosis of the epidermal growth factor receptor. *J Cell Biol* **189**, 871-883 (2010).
122. Teis, D., Wunderlich, W. & Huber, L.A. Localization of the MP1-MAPK scaffold complex to endosomes is mediated by p14 and required for signal transduction. *Dev Cell* **3**, 803-814 (2002).
123. Taub, N., Teis, D., Ebner, H.L., Hess, M.W. & Huber, L.A. Late endosomal traffic of the epidermal growth factor receptor ensures spatial and temporal fidelity of mitogen-activated protein kinase signaling. *Mol Biol Cell* **18**, 4698-4710 (2007).
124. Brankatschk, B. *et al.* Regulation of the EGF transcriptional response by endocytic sorting. *Sci Signal* **5**, ra21 (2012).
125. Omerovic, J., Hammond, D.E., Prior, I.A. & Clague, M.J. A global snap-shot of the influence of endocytosis upon EGF receptor signaling output. *J. Proteome Res.* **in press.** (2012).
126. Omerovic, J., Hammond, D.E., Prior, I.A. & Clague, M.J. Global snapshot of the influence of endocytosis upon EGF receptor signaling output. *J Proteome Res* **11**, 5157-5166 (2012).
127. Komander, D., Clague, M.J. & Urbe, S. Breaking the chains: structure and function of the deubiquitinases. *Nat Rev Mol Cell Biol* **10**, 550-563 (2009).
128. Clague, M.J. *et al.* Deubiquitylases from genes to organism. *Physiol Rev* **93**, 1289-1315 (2013).
129. McCullough, J., Clague, M.J. & Urbe, S. AMSH is an endosome-associated ubiquitin isopeptidase. *J Cell Biol* **166**, 487-492 (2004).
130. Ishii, N. *et al.* Loss of neurons in the hippocampus and cerebral cortex of AMSH-deficient mice. *Mol Cell Biol* **21**, 8626-8637 (2001).
131. Kikuchi, K., Ishii, N., Asao, H. & Sugamura, K. Identification of AMSH-LP containing a Jab1/MPN domain metalloenzyme motif. *Biochem Biophys Res Commun* **306**, 637-643 (2003).
132. Row, P.E., Prior, I.A., McCullough, J., Clague, M.J. & Urbe, S. The ubiquitin isopeptidase UBPY regulates endosomal ubiquitin dynamics and is essential for receptor down-regulation. *J Biol Chem* **281**, 12618-12624 (2006).

133. Mizuno, E., Kobayashi, K., Yamamoto, A., Kitamura, N. & Komada, M. A Deubiquitinating Enzyme UBPY Regulates the Level of Protein Ubiquitination on Endosomes. *Traffic* **7**, 1017-10131 (2006).
134. Mizuno, E. *et al.* Regulation of Epidermal Growth Factor Receptor Down-Regulation by UBPY-mediated Deubiquitination at Endosomes. *Mol Biol Cell* **16**, 5163-5174 (2005).
135. Row, P.E. *et al.* The MIT domain of UBPY constitutes a CHMP binding and endosomal localization signal required for efficient epidermal growth factor receptor degradation. *J Biol Chem* **282**, 30929-30937 (2007).
136. Bowers, K. *et al.* Degradation of endocytosed epidermal growth factor and virally ubiquitinated major histocompatibility complex class I is independent of mammalian ESCRTII. *J Biol Chem* **281**, 5094-5105 (2006).
137. Ali, N. *et al.* Recruitment of UBPY and ESCRT exchange drive HD-PTP-dependent sorting of EGFR to the MVB. *Curr Biol* **23**, 453-461 (2013).
138. Byun, S. *et al.* USP8 Is a Novel Target for Overcoming Gefitinib Resistance in Lung Cancer. *Clin Cancer Res* **19**, 3894-3904 (2013).
139. Liu, Z. *et al.* The ubiquitin-specific protease USP2a prevents endocytosis-mediated EGFR degradation. *Oncogene* **32**, 1660-1669 (2013).
140. Pareja, F. *et al.* Deubiquitination of EGFR by Cezanne-1 contributes to cancer progression. *Oncogene* **31**, 4599-4608 (2012).
141. Moretti, J. *et al.* The ubiquitin-specific protease 12 (USP12) is a negative regulator of notch signaling acting on notch receptor trafficking toward degradation. *J Biol Chem* **287**, 29429-29441 (2012).
142. Kowalski, J.R., Dahlberg, C.L. & Juo, P. The deubiquitinating enzyme USP-46 negatively regulates the degradation of glutamate receptors to control their abundance in the ventral nerve cord of Caenorhabditis elegans. *J Neurosci* **31**, 1341-1354 (2011).
143. Seaman, M.N. Recycle your receptors with retromer. *Trends Cell Biol* **15**, 68-75 (2005).

144. Johannes, L. & Popoff, V. Tracing the retrograde route in protein trafficking. *Cell* **135**, 1175-1187 (2008).
145. Kooner, J.S. *et al.* Genome-wide association study in individuals of South Asian ancestry identifies six new type 2 diabetes susceptibility loci. *Nat Genet* **43**, 984-989 (2011).
146. MacLeod, D.A. *et al.* RAB7L1 interacts with LRRK2 to modify intraneuronal protein sorting and Parkinson's disease risk. *Neuron* **77**, 425-439 (2013).
147. Bonifacino, J.S. & Rojas, R. Retrograde transport from endosomes to the trans-Golgi network. *Nat Rev Mol Cell Biol* **7**, 568-579 (2006).
148. Cullen, P.J. & Korswagen, H.C. Sorting nexins provide diversity for retromer-dependent trafficking events. *Nat Cell Biol* **14**, 29-37 (2012).
149. Seaman, M.N., Marcusson, E.G., Cereghino, J.L. & Emr, S.D. Endosome to Golgi retrieval of the vacuolar protein sorting receptor, Vps10p, requires the function of the VPS29, VPS30, and VPS35 gene products. *J Cell Biol* **137**, 79-92 (1997).
150. Seaman, M.N., McCaffery, J.M. & Emr, S.D. A membrane coat complex essential for endosome-to-Golgi retrograde transport in yeast. *J Cell Biol* **142**, 665-681 (1998).
151. Seaman, M.N. & Williams, H.P. Identification of the functional domains of yeast sorting nexins Vps5p and Vps17p. *Mol Biol Cell* **13**, 2826-2840 (2002).
152. van Weering, J.R., Verkade, P. & Cullen, P.J. SNX-BAR proteins in phosphoinositide-mediated, tubular-based endosomal sorting. *Semin Cell Dev Biol* **21**, 371-380 (2010).
153. Gomez, T.S. & Billadeau, D.D. A FAM21-containing WASH complex regulates retromer-dependent sorting. *Dev Cell* **17**, 699-711 (2009).
154. Jia, D. *et al.* WASH and WAVE actin regulators of the Wiskott-Aldrich syndrome protein (WASP) family are controlled by analogous structurally related complexes. *Proc Natl Acad Sci U S A* **107**, 10442-10447 (2010).
155. Derivery, E. *et al.* The Arp2/3 activator WASH controls the fission of endosomes through a large multiprotein complex. *Dev Cell* **17**, 712-723 (2009).

156. Padrick, S.B. & Rosen, M.K. Physical mechanisms of signal integration by WASP family proteins. *Annu Rev Biochem* **79**, 707-735 (2010).
157. Hao, Y.H. *et al.* Regulation of WASH-dependent actin polymerization and protein trafficking by ubiquitination. *Cell* **152**, 1051-1064 (2013).
158. Seaman, M.N. Cargo-selective endosomal sorting for retrieval to the Golgi requires retromer. *J Cell Biol* **165**, 111-122 (2004).
159. Rothbauer, U. *et al.* A versatile nanotrap for biochemical and functional studies with fluorescent fusion proteins. *Mol Cell Proteomics* **7**, 282-289 (2008).
160. Cox, J. & Mann, M. MaxQuant enables high peptide identification rates, individualized p.p.b.-range mass accuracies and proteome-wide protein quantification. *Nat Biotechnol* **26**, 1367-1372 (2008).
161. Chiu, Y.H., Zhao, M. & Chen, Z.J. Ubiquitin in NF-kappaB signaling. *Chem Rev* **109**, 1549-1560 (2009).
162. Xu, L., Lubkov, V., Taylor, L.J. & Bar-Sagi, D. Feedback regulation of Ras signaling by Rabex-5-mediated ubiquitination. *Curr Biol* **20**, 1372-1377 (2010).
163. Sasaki, A.T. *et al.* Ubiquitination of K-Ras enhances activation and facilitates binding to select downstream effectors. *Sci Signal* **4**, ra13 (2011).
164. Kim, S.E. *et al.* H-Ras is degraded by Wnt/beta-catenin signaling via beta-TrCP-mediated polyubiquitylation. *J Cell Sci* **122**, 842-848 (2009).
165. Burrows, J.F. *et al.* USP17 regulates Ras activation and cell proliferation by blocking RCE1 activity. *J Biol Chem* **284**, 9587-9595 (2009).
166. Yang, W.L. *et al.* Cycles of ubiquitination and deubiquitination critically regulate growth factor-mediated activation of Akt signaling. *Sci Signal* **6**, ra3 (2013).
167. Hayes, S.D. *et al.* Direct and indirect control of mitogen-activated protein kinase pathway-associated components, BRAP/IMP E3 ubiquitin ligase and CRAF/RAF1 kinase, by the deubiquitylating enzyme USP15. *J Biol Chem* **287**, 43007-43018 (2012).

168. Matheny, S.A. & White, M.A. Ras-sensitive IMP modulation of the Raf/MEK/ERK cascade through KSR1. *Methods Enzymol* **407**, 237-247 (2006).
169. Matheny, S.A. *et al.* Ras regulates assembly of mitogenic signalling complexes through the effector protein IMP. *Nature* **427**, 256-260 (2004).
170. Therrien, M., Michaud, N.R., Rubin, G.M. & Morrison, D.K. KSR modulates signal propagation within the MAPK cascade. *Genes Dev* **10**, 2684-2695 (1996).
171. McKay, M.M., Ritt, D.A. & Morrison, D.K. Signaling dynamics of the KSR1 scaffold complex. *Proc Natl Acad Sci U S A* **106**, 11022-11027 (2009).
172. Kortum, R.L. & Lewis, R.E. The molecular scaffold KSR1 regulates the proliferative and oncogenic potential of cells. *Mol Cell Biol* **24**, 4407-4416 (2004).
173. Matheny, S.A. & White, M.A. Signaling threshold regulation by the Ras effector IMP. *J Biol Chem* **284**, 11007-11011 (2009).
174. Sigismund, S. *et al.* Clathrin-mediated internalization is essential for sustained EGFR signaling but dispensable for degradation. *Dev Cell* **15**, 209-219 (2008).
175. Ciaccio, M.F., Wagner, J.P., Chuu, C.P., Lauffenburger, D.A. & Jones, R.B. Systems analysis of EGF receptor signaling dynamics with microwestern arrays. *Nat Methods* **7**, 148-155 (2010).
176. Cano, F. *et al.* The RNA-binding E3 ubiquitin ligase MEX-3C links ubiquitination with MHC-I mRNA degradation. *EMBO J* **31**, 3596-3606 (2012).
177. Faronato, M. *et al.* The deubiquitylase USP15 stabilizes newly synthesized REST and rescues its expression at mitotic exit. *Cell Cycle* **12**, 1964-1977 (2013).
178. Sowa, M.E., Bennett, E.J., Gygi, S.P. & Harper, J.W. Defining the human deubiquitinating enzyme interaction landscape. *Cell* **138**, 389-403 (2009).

179. Isumi, Y. *et al.* Transgenic overexpression of USP15 in the heart induces cardiac remodeling in mice. *Biochem Biophys Res Commun* **405**, 216-221 (2011).
180. Inui, M. *et al.* USP15 is a deubiquitylating enzyme for receptor-activated SMADs. *Nat Cell Biol* **13**, 1368-1375 (2011).
181. Eichhorn, P.J. *et al.* USP15 stabilizes TGF-beta receptor I and promotes oncogenesis through the activation of TGF-beta signaling in glioblastoma. *Nat Med* **18**, 429-435 (2012).
182. Haigler, H.T., McKanna, J.A. & Cohen, S. Direct visualisation of the binding and internalisation of a ferritin conjugate of epidermal growth factor in human carcinoma cells A-431. *J. Cell Biol.* **81**, 382-395 (1979).
183. Argenzio, E. *et al.* Proteomic snapshot of the EGF-induced ubiquitin network. *Mol Syst Biol* **7**, 462 (2011).
184. Urbe, S. *et al.* Systematic survey of deubiquitinase localisation identifies USP21 as a regulator of centrosome and microtubule associated functions. *Mol Biol Cell* **23**, 1095-1103 (2012).
185. Olsen, J.V. *et al.* Global, in vivo, and site-specific phosphorylation dynamics in signaling networks. *Cell* **127**, 635-648 (2006).
186. Hammond, D.E. *et al.* Quantitative analysis of HGF and EGF-dependent phosphotyrosine signaling networks. *J Proteome Res* **9**, 2734-2742 (2010).
187. Blagoev, B., Ong, S.E., Kratchmarova, I. & Mann, M. Temporal analysis of phosphotyrosine-dependent signaling networks by quantitative proteomics. *Nat Biotechnol* **22**, 1139-1145 (2004).
188. Muhsin, M., Graham, J. & Kirkpatrick, P. Gefitinib. *Nat Rev Drug Discov* **2**, 515-516 (2003).
189. Knight, Z.A. *et al.* Isoform-specific phosphoinositide 3-kinase inhibitors from an arylmorpholine scaffold. *Bioorg Med Chem* **12**, 4749-4759 (2004).
190. Huynh, H., Soo, K.C., Chow, P.K. & Tran, E. Targeted inhibition of the extracellular signal-regulated kinase kinase pathway with AZD6244 (ARRY-142886) in the treatment of hepatocellular carcinoma. *Mol Cancer Ther* **6**, 138-146 (2007).

191. Lloyd, T.E. *et al.* Hrs regulates endosome membrane invagination and tyrosine kinase receptor signaling in Drosophila. *Cell* **108**, 261-269 (2002).
192. Li, X. *et al.* The deubiquitination enzyme USP46 functions as a tumor suppressor by controlling PHLPP-dependent attenuation of Akt signaling in colon cancer. *Oncogene* **32**, 471-478 (2013).
193. Liu, Z. *et al.* The ubiquitin-specific protease USP2a prevents endocytosis-mediated EGFR degradation. *Oncogene* (2012).
194. Bomberger, J.M., Barnaby, R.L. & Stanton, B.A. The deubiquitinating enzyme USP10 regulates the endocytic recycling of CFTR in airway epithelial cells. *Channels (Austin)* **4**, 150-154 (2010).
195. McCullough, J. *et al.* Activation of the endosome-associated ubiquitin isopeptidase AMSH by STAM, a component of the multivesicular body-sorting machinery. *Curr Biol* **16**, 160-165 (2006).
196. Tomida, S. *et al.* Usp46 is a quantitative trait gene regulating mouse immobile behavior in the tail suspension and forced swimming tests. *Nat Genet* **41**, 688-695 (2009).
197. Imai, S. *et al.* Ubiquitin-specific peptidase 46 (Usp46) regulates mouse immobile behavior in the tail suspension test through the GABAergic system. *PLoS ONE* **7**, e39084 (2012).
198. Pareja, F. *et al.* Deubiquitination of EGFR by Cezanne-1 contributes to cancer progression. *Oncogene* (2012).
199. Lobert, V.H. *et al.* Antibody crossreactivity between the tumour suppressor PHLPP1 and the proto-oncogene beta-catenin. *EMBO Rep* **14**, 10-11 (2013).
200. Kee, Y. *et al.* WDR20 regulates activity of the USP12 x UAF1 deubiquitinating enzyme complex. *J Biol Chem* **285**, 11252-11257 (2010).
201. Joo, H.Y. *et al.* Regulation of histone H2A and H2B deubiquitination and Xenopus development by USP12 and USP46. *J Biol Chem* **286**, 7190-7201 (2011).
202. Trinkle-Mulcahy, L. *et al.* Identifying specific protein interaction partners using quantitative mass spectrometry and bead proteomes. *J Cell Biol* **183**, 223-239 (2008).

203. Duan, S. *et al.* FBXO11 targets BCL6 for degradation and is inactivated in diffuse large B-cell lymphomas. *Nature* **481**, 90-93 (2012).
204. Shevchenko, A., Tomas, H., Havlis, J., Olsen, J.V. & Mann, M. In-gel digestion for mass spectrometric characterization of proteins and proteomes. *Nat Protoc* **1**, 2856-2860 (2006).
205. Cohn, M.A., Kee, Y., Haas, W., Gygi, S.P. & D'Andrea, A.D. UAF1 is a subunit of multiple deubiquitinating enzyme complexes. *J Biol Chem* (2008).
206. Zhang, P., Hu, X., Xu, X., Chen, Y. & Bache, R.J. Dimethylarginine dimethylaminohydrolase 1 modulates endothelial cell growth through nitric oxide and Akt. *Arteriosclerosis, thrombosis, and vascular biology* **31**, 890-897 (2011).
207. Skaar, J.R., Pagan, J.K. & Pagano, M. Mechanisms and function of substrate recruitment by F-box proteins. *Nat Rev Mol Cell Biol* **14**, 369-381 (2013).
208. Abbas, T. *et al.* CRL1-FBXO11 promotes Cdt2 ubiquitylation and degradation and regulates Pr-Set7/Set8-mediated cellular migration. *Mol Cell* **49**, 1147-1158 (2013).
209. Rossi, M. *et al.* Regulation of the CRL4(Cdt2) ubiquitin ligase and cell-cycle exit by the SCF(Fbxo11) ubiquitin ligase. *Mol Cell* **49**, 1159-1166 (2013).
210. Hardisty-Hughes, R.E. *et al.* A mutation in the F-box gene, Fbxo11, causes otitis media in the Jeff mouse. *Hum Mol Genet* **15**, 3273-3279 (2006).
211. Kim, W. *et al.* Systematic and Quantitative Assessment of the Ubiquitin-Modified Proteome. *Mol Cell* **44**, 325-340 (2011).
212. Gieselmann, V., Pohlmann, R., Hasilik, A. & Von Figura, K. Biosynthesis and transport of cathepsin D in cultured human fibroblasts. *J Cell Biol* **97**, 1-5 (1983).
213. de Lartigue, J. *et al.* PIKfyve regulation of endosome-linked pathways. *Traffic* **10**, 883-893 (2009).
214. Zaidi, N., Maurer, A., Nieke, S. & Kalbacher, H. Cathepsin D: a cellular roadmap. *Biochem Biophys Res Commun* **376**, 5-9 (2008).

215. Hierro, A. *et al.* Functional architecture of the retromer cargo-recognition complex. *Nature* **449**, 1063-1067 (2007).
216. Chia, P.Z., Gasnereau, I., Lieu, Z.Z. & Gleeson, P.A. Rab9-dependent retrograde transport and endosomal sorting of the endopeptidase furin. *J Cell Sci* **124**, 2401-2413 (2011).
217. Chojnowska-Monga, M., Vol. Doctor of Philosophy 289 (University of Liverpool 2011).
218. Choy, R.W., Cheng, Z. & Schekman, R. Amyloid precursor protein (APP) traffics from the cell surface via endosomes for amyloid beta (Abeta) production in the trans-Golgi network. *Proc Natl Acad Sci U S A* **109**, E2077-2082 (2012).
219. Popoff, V. *et al.* Analysis of articulation between clathrin and retromer in retrograde sorting on early endosomes. *Traffic* **10**, 1868-1880 (2009).
220. Chin, L.S., Raynor, M.C., Wei, X., Chen, H.Q. & Li, L. Hrs interacts with sorting nexin 1 and regulates degradation of epidermal growth factor receptor. *J Biol Chem* **276**, 7069-7078 (2001).
221. Razi, M. & Futter, C.E. Distinct roles for Tsg101 and Hrs in multivesicular body formation and inward vesiculation. *Mol Biol Cell* **17**, 3469-3483 (2006).
222. Balut, C.M., Loch, C.M. & Devor, D.C. Role of ubiquitylation and USP8-dependent deubiquitylation in the endocytosis and lysosomal targeting of plasma membrane KCa3.1. *Faseb J* **25**, 3938-3948 (2011).
223. Zhou, R. *et al.* Ubiquitin-specific peptidase 8 (USP8) regulates endosomal trafficking of the epithelial Na+ channel. *J Biol Chem* **288**, 5389-5397 (2013).
224. Mukai, A. *et al.* Balanced ubiquitylation and deubiquitylation of Frizzled regulate cellular responsiveness to Wg/Wnt. *Embo J* **29**, 2114-2125 (2010).
225. Belenkaya, T.Y. *et al.* The retromer complex influences Wnt secretion by recycling wntless from endosomes to the trans-Golgi network. *Dev Cell* **14**, 120-131 (2008).

226. Yang, P.T. *et al.* Wnt signaling requires retromer-dependent recycling of MIG-14/Wntless in Wnt-producing cells. *Dev Cell* **14**, 140-147 (2008).
227. Port, F. *et al.* Wingless secretion promotes and requires retromer-dependent cycling of Wntless. *Nat Cell Biol* **10**, 178-185 (2008).
228. Franch-Marro, X. *et al.* Wingless secretion requires endosome-to-Golgi retrieval of Wntless/Evi/Sprinter by the retromer complex. *Nat Cell Biol* **10**, 170-177 (2008).
229. Tiedemann, R.E. *et al.* Identification of molecular vulnerabilities in human multiple myeloma cells by RNA interference lethality screening of the druggable genome. *Cancer Res* **72**, 757-768 (2012).
230. Naviglio, S. *et al.* UBPY: a growth-regulated human ubiquitin isopeptidase. *Embo J* **17**, 3241-3250 (1998).
231. Mahindra, A. *et al.* Latest advances and current challenges in the treatment of multiple myeloma. *Nature reviews. Clinical oncology* **9**, 135-143 (2012).
232. Abbas, T., Keaton, M. & Dutta, A. Regulation of TGF-beta signaling, exit from the cell cycle, and cellular migration through cullin cross-regulation: SCF-FBXO11 turns off CRL4-Cdt2. *Cell Cycle* **12**, 2175-2182 (2013).
233. Shulman, K.I., Herrmann, N. & Walker, S.E. Current place of monoamine oxidase inhibitors in the treatment of depression. *CNS drugs* **27**, 789-797 (2013).
234. Kyuuma, M. *et al.* AMSH, an ESCRT-III Associated Enzyme, Deubiquitinates Cargo on MVB/Late Endosomes. *Cell Struct Funct* (2006).
235. Zhang, L. *et al.* USP4 is regulated by AKT phosphorylation and directly deubiquitylates TGF-beta type I receptor. *Nat Cell Biol* **14**, 717-726 (2012).
236. Hassink, G.C. *et al.* The ER-resident ubiquitin-specific protease 19 participates in the UPR and rescues ERAD substrates. *EMBO Rep* **10**, 755-761 (2009).

237. Nakamura, N. & Hirose, S. Regulation of Mitochondrial Morphology by USP30, a Deubiquitinating Enzyme Present in the Mitochondrial Outer Membrane. *Mol Biol Cell* **19**, 1903-1911 (2008).
238. Akhavantabasi, S. *et al.* USP32 is an active, membrane-bound ubiquitin protease overexpressed in breast cancers. *Mammalian genome : official journal of the International Mammalian Genome Society* **21**, 388-397 (2010).
239. Thorne, C., Eccles, R.L., Coulson, J.M., Urbe, S. & Clague, M.J. Isoform-specific localization of the deubiquitinase USP33 to the Golgi apparatus. *Traffic* **12**, 1563-1574 (2011).
240. Endo, A. *et al.* Nucleolar structure and function are regulated by the deubiquitylating enzyme USP36. *J Cell Sci* **122**, 678-686 (2009).

Supplementary Figures

DUB Family	Gene Name	Subcellular localization	Response	Notes	Ref
Jamm/MPN+	AMSH	Endosomal/ Nuclear/ Cytosolic	No	There is an apparent decrease in punctae but this is not a consistent effect.	195, 234
	AMSH-lp	Endosomal/ Nuclear/ Cytosolic	No	-	
	BRCC3	Predominantly nuclear/ Cytosolic	No	Peri-nucleclolar structures observed	
	COPs5	Cytosolic/ nuclear	No	Dual localization observed not dependent of EGF.	
	COPs6	Predominantly nuclear/ Cytosolic	Yes	Cells exhibit change in morphology, look stressed with EGF.	
	EIF3s3	Predominantly nuclear/ Cytosolic/ PM	No	Aggregates	
	EIF3s5	Punctate aggregates	No	Aggregates	
	FLJ4981	Cytosolic	No	-	
	MYSM	Nuclear	No	Low expression levels some background fluorescence in pictures.	
	PSMD7	Cytosolic/ PM	No	-	

Otubain	A20	Cytosolic aggregates	No	Aggregates	
	Cezanne	Nuclear/ Cytosolic/ PM	No	Regulates EGFR degradation	
	OTUB1	Nuclear/ Cytosolic/ PM	No	Dual localization not dependent on EGF	
	OTUB2	Nuclear/ Cytosolic	No	-	
	OTUD3	Cytosolic	No	Excluded from vacuolar type structures	
	OTUD4	Cytosolic	No	Excluded from vacuolar type structures	
	OTUD6a	Cytosolic	No	Excluded from vacuolar type structures. Bright spot in cytoplasm.	
	OTUD6b	Cytosolic	No	Excluded from vacuolar type structures	
	YOD1	Predominately Nuclear/ Cytosolic	No	Fine punctae observed in cytoplasm	
	TRABID	Predominately Nuclear/ Cytosolic/ PM	No	-	
Ubiquitin carboxyl-terminal hydrolase	BAP1	Predominately Nuclear/ Nucleoli/ Cytoplasm	No	Dual localization not dependent of EGF	
	UCHL1	Nuclear/ Cytoplasmic	No	-	
	UCHL3	Nuclear/ Cytoplasmic	No	-	
	UCHL5	Nuclear	Yes	Punctae structures occur at a higher frequency in serum starved conditions	
Josephin	JOSD1	PM/ Cytosolic/ Nuclear	No	Partial co-localization with Actin	
	JOSD2	Cytoplasmic	No	-	
	ATXN3	Predominantly Nuclear/ Cytoplasmic	No	-	
	ATXN3l	Cytoplasmic	No	-	
Ubiquitin Specific Protease	USP2a	Cytoplasmic Punctae	No	Reported as endosomal but we couldn't repeat co-localization	[139]
	USP4	PM/ Cytosolic/ Nuclear	Yes	Less PM becoming enriched in nucleus	[235]
	USP5	Nuclear	No	Found in EGF-Ubome	[183]
	USP6	PM	No	Found in pTyr IP	
	USP7	Nuclear	No	No	
	USP8	Cytoplasmic/ Endosomal	Yes		
	USP9x	Predominantly Nuclear/	No	No	

		Cytoplasmic			
	USP10	Cytoplasmic/	No	Excluded from vacuolar type structures	
	USP11	Nuclear	No	Found in EGF-Ub-ome	[183]
	USP12	Cytoplasmic/ Peri-nuclear	No	-	
	USP13	Predominantly Nuclear/ Cytoplasmic	No	-	
	USP14	Cytoplasmic	No	-	
	USP15	Cytoplasmic	No	Found in EGF-Ub-ome	
	USP16	Cytoplasmic	No	-	
	USP18	Cytoplasmic	No	-	
	USP19	Endoplasmic Reticulum	No	-	[236]
	USP20	Cytoplasmic Peri-nuclear	No	-	
	USP21	Cytoplasmic/Microtubules	No	-	[184]
	USP26	Nuclear	No	-	
	USP29	Nuclear	No	-	
	USP30	Mitochondria	No	-	[237]
	USP32	Perinuclear/Golgi	No	-	[238]
	USP33	Perinuclear/Golgi	No	-	[239]
	USP36	Nucleolar	No	-	[240]
	USP38	Nuclear	No	-	
	USP39	Nuclear	No	Large structures present in nucleus	
	USP42	Nuclear	No	Large speckles present in nucleus	
	USP44	Nuclear	No	-	
	USP45	Cytoplasmic/ Peri-nuclear	No	-	
	USP46	Cytoplasmic/ Endosomal	Yes	Becoming more endosomal with EGF application	
	USP49	Nuclear	No	-	
	USP50	Cytoplasmic	No	-	
	USP52	Cytoplasmic/ Peri-nuclear	No	-	
	USP53	Cell-Cell Junctions	No	-	
	CYLD	Cytoplasmic/ Peri-nuclear	No	Found in 2 independent pTyr IP	

Table S1. Summery of DUB screen

Table 4.2 is a summary of GFP-DUB screen indicating the localization and changes or notes from the screen. Where a definitive localization is given the reference is indicated in final column.

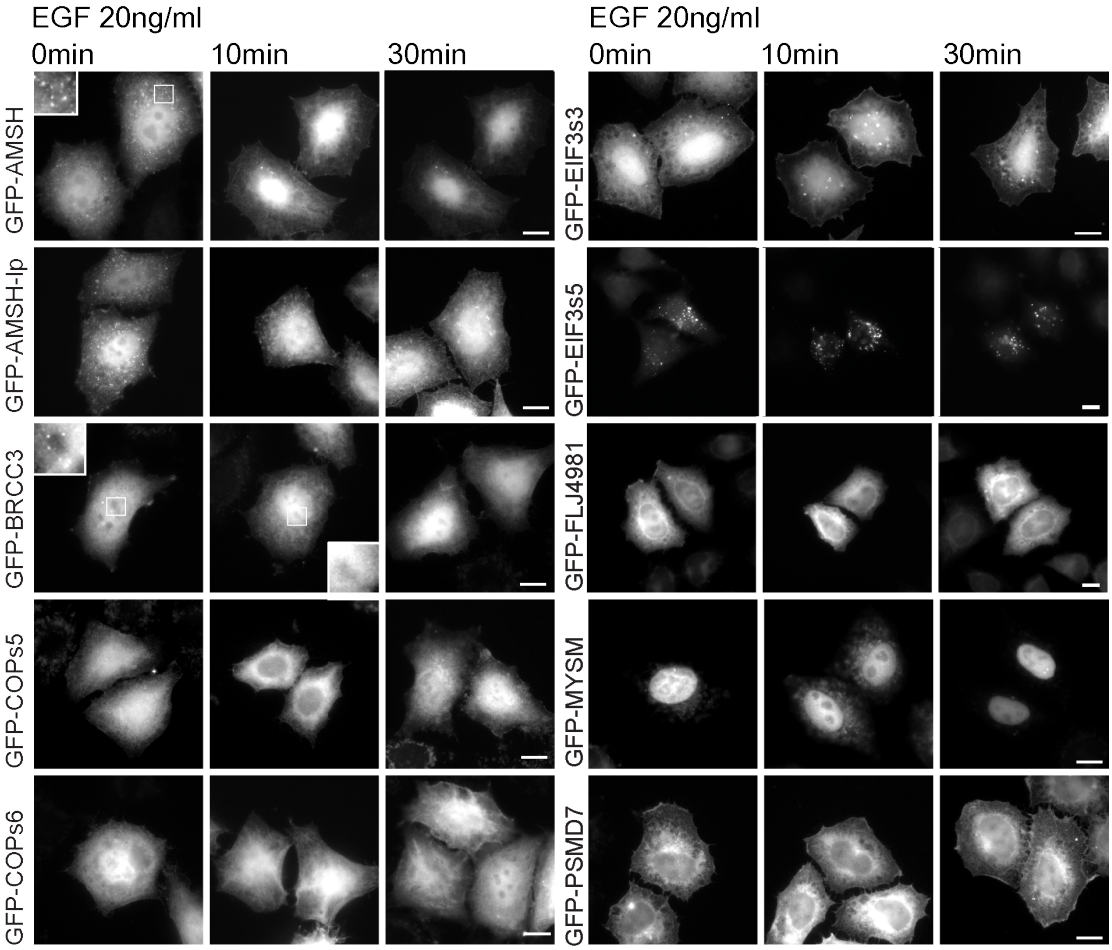

Figure S1. JAMM/MPN+ family DUB-EGF screen.

Representative images from JAMM/MPN+ family in the DUB EGF screen. HeLa cells were transfected with 1µg of GFP-DUB constructs for 24hours, serum starved for 16hours then subsequently stimulated with 20ng/ml of EGF for the time indicated before fixation in 4% PFA. Cells were then imaged using fluorescence microscopy to judge changes in subcellular localization. Representative images shown in panels. Scale bar = 10µm.

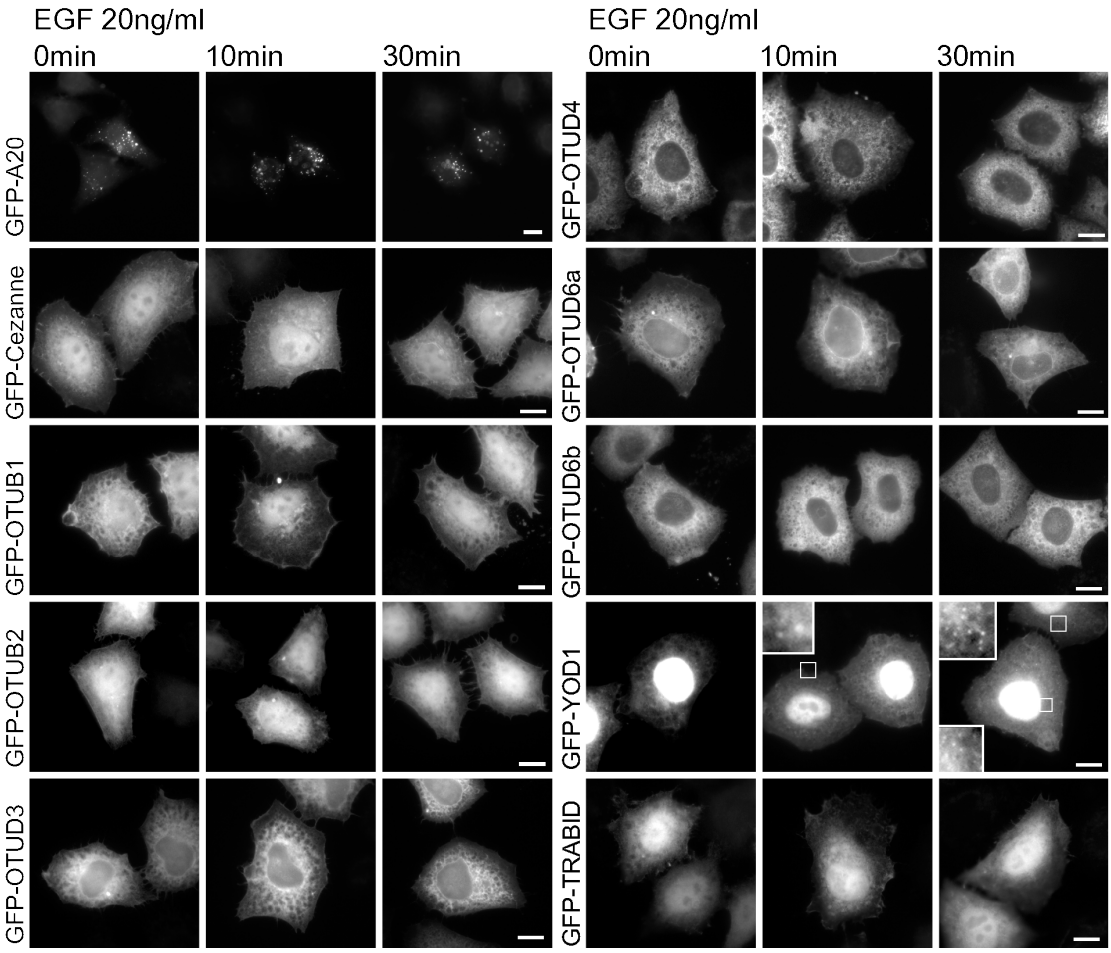

Figure S2. Otubain family DUB-EGF screen.

Representative images from OTU family in the DUB EGF screen. HeLa cells were transfected with 1µg of GFP-DUB constructs for 24hours, serum starved for 16hours then subsequently stimulated with 20ng/ml of EGF for the time indicated before fixation in 4% PFA. Cells were then imaged using fluorescence microscopy to judge changes in subcellular localization. Representative images shown in panels. Scale bar =10µm.

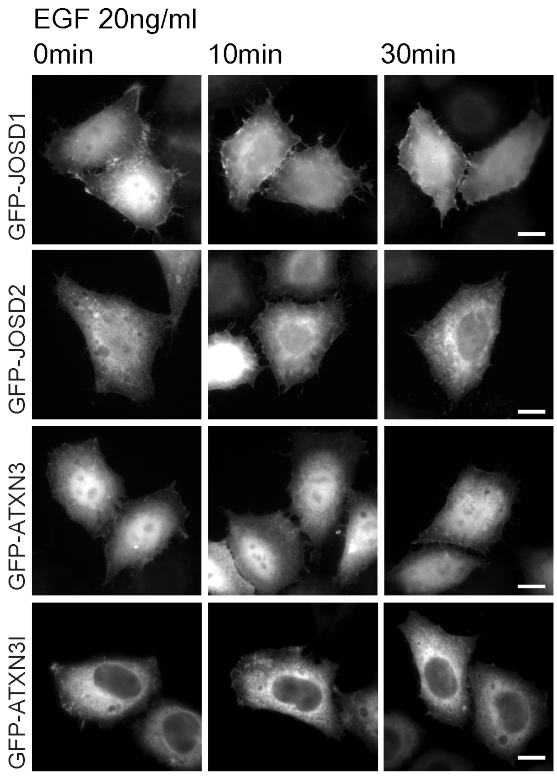

Figure S3. Josephin family of enzymes, DUB-EGF screen.

Representative images from Josephin family in the DUB EGF screen. HeLa cells were transfected with 1µg of GFP-DUB constructs for 24hours, serum starved for 16hours then subsequently stimulated with 20ng/ml of EGF for the time indicated before fixation in 4% PFA. Cells were then imaged using fluorescence microscopy to judge changes in subcellular localization. Representative images shown in panels. Scale bar =10µm.

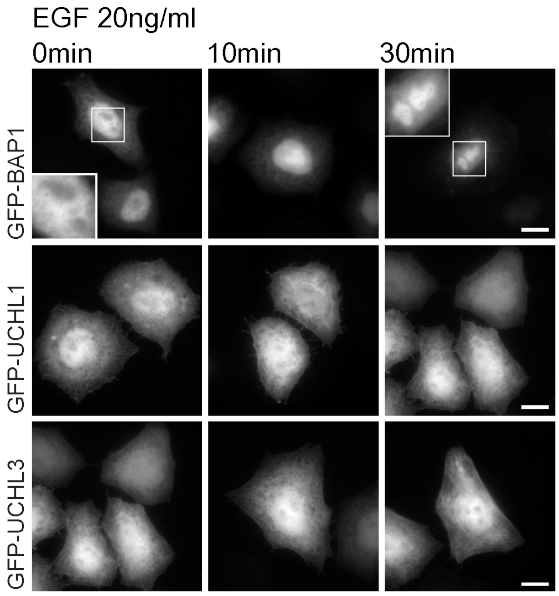

Figure S4. UCH family of enzymes, DUB-EGF screen.

Representative images from UCH family in the DUB EGF screen. HeLa cells were transfected with 1µg of GFP-DUB constructs for 24hours, serum starved for 16hours then subsequently stimulated with 20ng/ml of EGF for the time indicated before fixation in 4% PFA. Cells were then imaged using fluorescence microscopy to judge changes in subcellular localization. Representative images shown in panels. Scale bar =10µm.

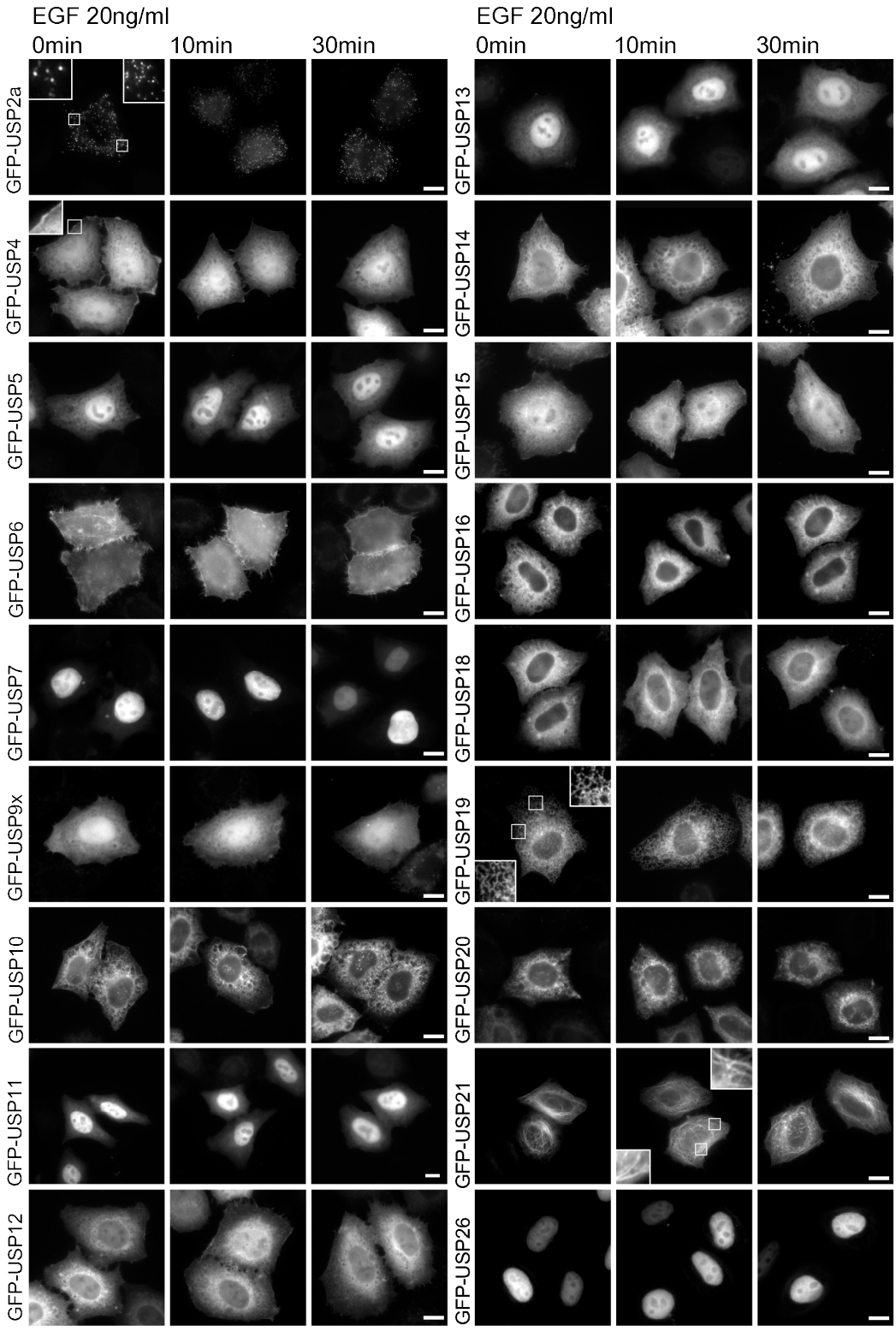

Figure S5. USP family part 1, DUB-EGF screen.

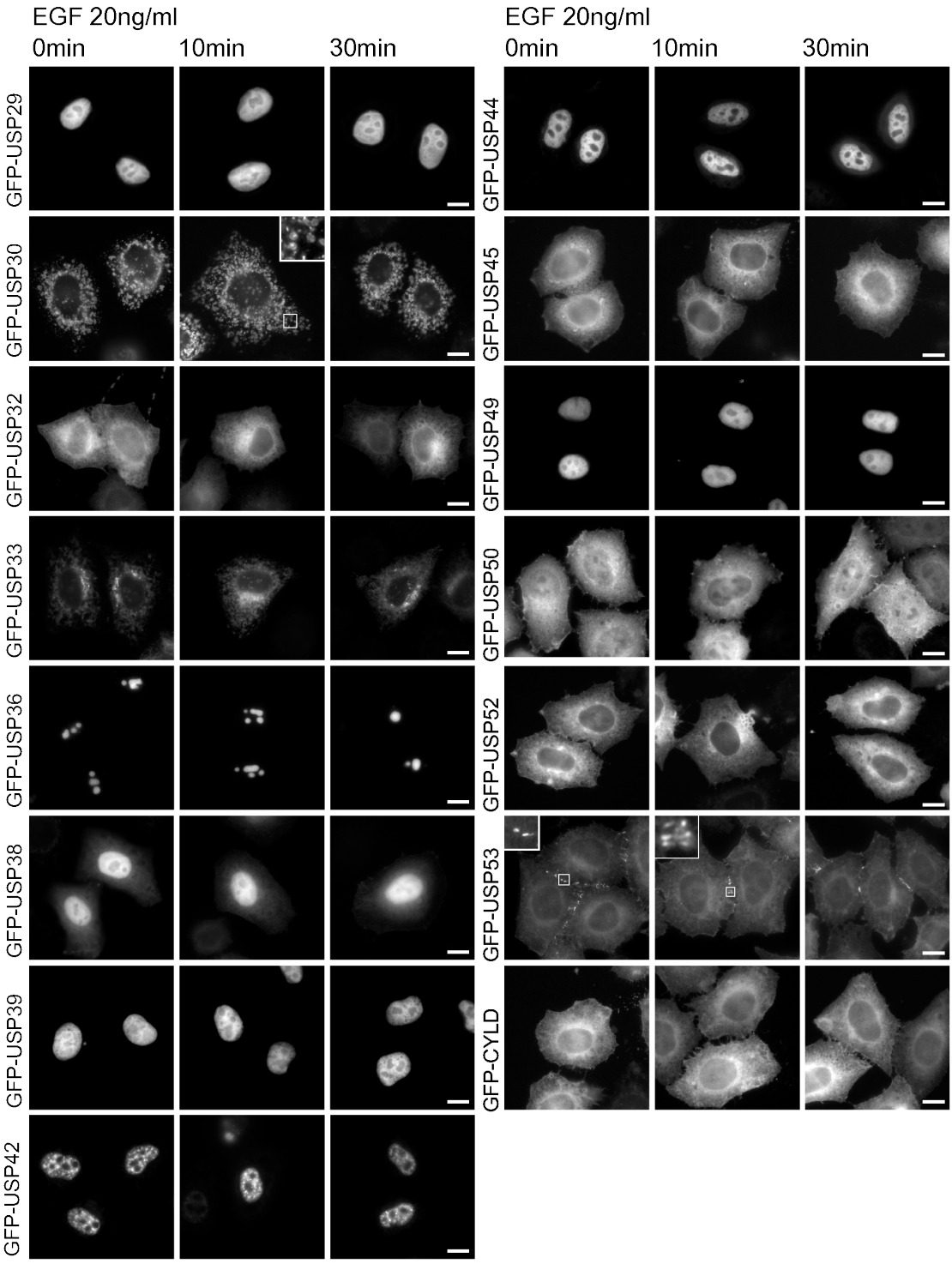

Figure S6. USP family part 2, DUB-EGF screen.

Representative images from USP family in the DUB EGF screen. HeLa cells were transfected with 1µg of GFP-DUB constructs for 24hours, serum starved for 16hours then subsequently stimulated with 20ng/ml of EGF for the time indicated before fixation in 4% PFA. Cells were then imaged using fluorescence microscopy to judge changes in subcellular localization. Representative images shown in panels.

Gene Name	Peptides identified	PEP	Ratio M/L	Ratio H/L	Ratio H/M	Intensity	Intensity L	Intensity M	Intensity H	LOG_{10} Intensity	Trinkle-Mulcahy et al. Blacklist	Lab Blacklist	LOG_2 M/L	LOG_2 H/L	LOG_2 H/M
HSP90AB1	2	1.67E-12	4.3	0.5	0.1	730250	116840	552360	61052	5.9	+	+	2.1	-1.0	-3.1
PPIB	1	0.0080389	3.8	0.6	0.2	184320	46276	120340	17703	5.3		+	1.9	-0.8	-2.7
EPRS	1	0.043386	1.5	0.6	0.4	50748	15724	24111	10913	4.7		+	0.6	-0.8	-1.3
EEF2	4	7.80E-07	1.8	0.6	0.3	489890	147260	252900	89726	5.7		+	0.8	-0.8	-1.6
RANP1	1	0.0093934	2.7	0.6	0.2	63190	11180	42913	9096.5	4.8		+	1.4	-0.7	-2.2
RPL8	1	0.018819	1.9	0.6	0.3	52246	15653	27948	8644.8	4.7		+	0.9	-0.6	-1.6
KRT18	3	9.33E-06	5.7	0.6	0.1	317690	31403	271670	14617	5.5		+	2.5	-0.6	-3.1
RPL38	1	0.045945	2.5	0.7	0.3	143440	38551	77983	26904	5.2		+	1.3	-0.5	-1.8
HNRNPH1	1	0.012469	3.3	0.8	0.2	156690	27558	106040	23093	5.2		+	1.7	-0.4	-2.1
BASP1	2	6.54E-05	5.1	0.8	0.2	292550	41473	218990	32085	5.5		+	2.3	-0.3	-2.7
HSPA9	2	0.00016069	3.1	0.8	0.2	315590	63064	198100	54433	5.5		+	1.6	-0.3	-2.0
NONO	1	0.0041526	3.7	1.0	0.3	96725	19442	55837	21447	5.0	+	+	1.9	0.0	-1.9
XRCC6	2	5.48E-06	5.0	1.1	0.2	354360	55663	246150	52544	5.5		+	2.3	0.2	-2.1
HNRNPC	2	0.00054434	10.7	3.3	0.2	172940	7087.3	153820	12036	5.2		+	3.4	1.7	-2.6
BANF1	1	0.0025215	8.6	0.7	0.1	196410	21228	161960	13218	5.3		+	3.1	-0.6	-3.7
SCHIP1	1	0.043109	0.0	0.1	1.4	243210	206860	13529	22821	5.4	+		-4.6	-4.1	0.5
GAPDH	2	0.00010579	1.8	0.3	0.2	371110	117920	215330	37861	5.6	+		0.8	-1.7	-2.6
SLC25A5	2	0.00013144	2.3	0.4	0.2	164480	51068	96672	16737	5.2	+		1.2	-1.2	-2.2
PPIA	3	2.15E-09	2.0	0.5	0.2	467510	134040	265920	67553	5.7	+		1.0	-1.0	-2.2
PRDX1	7	4.63E-19	1.3	0.5	0.4	3925300	1414500	1792800	717980	6.6	+		0.4	-1.0	-1.3
RPS7	1	0.0060346	2.2	0.5	0.3	87995	27266	47071	13658	4.9	+		1.1	-0.9	-2.0

TMPO	2	0.0004823	2.6	0.6	0.2	424190	104030	262950	57214	5.6	+		1.4	-0.8	-2.2
RPS12	1	0.016268	2.1	0.6	0.3	186120	63761	99400	22961	5.3	+		1.0	-0.8	-1.7
RPS5	1	0.039788	2.1	0.6	0.3	144960	42443	76112	26408	5.2	+		1.1	-0.8	-1.8
RPS24	1	0.062951	2.3	0.6	0.3	73425	19780	40960	12685	4.9	+		1.2	-0.8	-2.0
RPS19	1	0.010769	1.3	0.6	0.5	165490	50800	73754	40933	5.2	+		0.3	-0.7	-1.1
SERBP1	1	7.62E-15	1.5	0.6	0.4	347150	114920	161530	70695	5.5	+		0.6	-0.6	-1.2
RPS23	1	0.027323	2.5	0.7	0.3	91781	21366	57127	13289	5.0	+		1.3	-0.6	-1.9
PHGDH	3	8.82E-06	2.2	0.7	0.3	1012200	276870	552030	183290	6.0	+		1.2	-0.6	-1.8
RPL11	2	3.84E-05	2.7	0.7	0.3	546640	134360	319700	92584	5.7	+		1.4	-0.6	-2.0
EEF1E1	1	0.027264	1.5	0.7	0.5	55763	21343	22115	12305	4.7	+		0.6	-0.5	-1.1
HSP90AA1	2	3.85E-11	3.2	0.7	0.2	60816	18461	32327	10027	4.8	+		1.7	-0.5	-2.2
EIF4A3	1	0.010326	4.2	0.7	0.2	65087	11657	44346	9084.2	4.8	+		2.1	-0.5	-2.5
RPS14	2	0.00036884	3.3	0.8	0.2	255860	51486	163270	41099	5.4	+		1.7	-0.4	-2.1
HSPA8	12	3.21E-53	2.0	0.8	0.4	8188100	2212700	4347500	1627900	6.9	+		1.0	-0.3	-1.4
MIF	3	2.83E-16	1.1	0.8	0.7	41736000	13754000	14419000	13562000	7.6	+		0.1	-0.3	-0.4
HSPA5	2	0.00018146	2.4	0.8	0.3	616590	179930	319290	117370	5.8	+		1.3	-0.3	-1.6
PARP1	2	0.0022195	3.0	0.8	0.3	33872	6877.7	23767	3227.5	4.5	+		1.6	-0.3	-1.9
HIST1H4A	8	4.58E-26	24.6	0.8	0.0	6985300	250150	6566900	168330	6.8	+		4.6	-0.3	-4.9
RPLP1	1	1.30E-06	2.2	0.8	0.4	153340	39859	79576	33903	5.2	+		1.1	-0.3	-1.4
LMNA	19	7.22E-61	4.6	0.8	0.2	5557000	936900	3813400	806660	6.7	+		2.2	-0.3	-2.5
HSPA6	5	7.66E-20	2.1	0.8	0.4	823590	217060	447870	158660	5.9	+		1.1	-0.3	-1.4
CPS1	5	8.75E-07	4.3	0.8	0.3	312460	53554	209910	49001	5.5	+		2.1	-0.3	-1.9
PDIA6	3	4.57E-11	1.3	0.8	0.7	830400	266670	334540	229190	5.9	+		0.4	-0.3	-0.5
TUBB	11	6.27E-44	2.4	0.9	0.4	8858700	2211800	4711200	1935600	6.9	+		1.2	-0.2	-1.4
HSPD1	1	0.010423	3.0	0.9	0.3	201220	45496	119730	36001	5.3	+		1.6	-0.2	-1.8
NPM1	1	0.015871	7.2	0.9	0.1	270720	35767	202440	32512	5.4	+		2.8	-0.1	-3.0

PKM2	13	2.58E-50	1.2	0.9	0.8	9519900	3007200	3609000	2903600	7.0	+		0.2	-0.1	-0.4
VIM	8	3.43E-16	9.7	1.0	0.1	1725000	189680	1407500	127800	6.2	+		3.3	0.1	-3.2
TXN	1	0.0020187	1.6	1.1	0.7	403640	125200	152080	126360	5.6	+		0.7	0.1	-0.6
HIST1H1B	2	0.00014319	6.3	1.1	0.2	213700	3972.1	188710	21015	5.3	+		2.6	0.1	-2.6
PCBP1	2	3.59E-07	1.8	1.1	0.6	559430	144080	268050	147310	5.7	+		0.8	0.1	-0.7
HSPA1B	9	4.09E-25	2.6	1.1	0.5	2170200	484620	1123500	562020	6.3	+		1.4	0.2	-1.1
HIST1H2AB	1	0.0026064	23.7	1.5	0.1	445430	9188.6	419890	16361	5.6	+		4.6	0.6	-4.0
HIST2H2BE	4	5.54E-64	18.0	1.8	0.1	9155800	264500	8463900	427390	7.0	+		4.2	0.8	-3.8
POTEA	1	0.014786	63.6	2.0	0.0	732040	11048	716060	4932.8	5.9	+		6.0	1.0	-5.0
HDAC6	1	0.019708	NaN	NaN	NaN	0	0	0	0	NaN	+		NaN	NaN	NaN
ASH1L	1	0.050074	NaN	NaN	NaN	0	0	0	0	NaN	+		NaN	NaN	NaN
EIF4A2	1	0.015196	3.5	NaN	NaN	87473	20117	60368	6987.8	4.9	+		1.8	NaN	NaN
YBX1	1	0.0089051	NaN	NaN	NaN	0	0	0	0	NaN	+		NaN	NaN	NaN
SERPINH1	1	0.024439	NaN	NaN	NaN	0	0	0	0	NaN	+		NaN	NaN	NaN
HIST1H1C	1	0.0019972	4.3	NaN	NaN	73654	9816	59295	4543.1	4.9	+		2.1	NaN	NaN
HIST1H1E	1	0.011273	5.5	NaN	NaN	160010	25408	130080	4526.6	5.2	+		2.5	NaN	NaN
RPL27	1	0.029382	NaN	NaN	NaN	0	0	0	0	NaN	+		NaN	NaN	NaN
CCT3	2	1.17E-05	NaN	NaN	NaN	0	0	0	0	NaN	+		NaN	NaN	NaN
HSP90AB2P	2	5.42E-12	NaN	NaN	NaN	0	0	0	0	NaN	+		NaN	NaN	NaN
RPL27A	1	0.0097477	NaN	NaN	NaN	0	0	0	0	NaN	+		NaN	NaN	NaN
GFP	10	5.29E-24	0.1	0.1	0.7	5016000	3639100	816840	560050	6.7			-3.0	-4.1	-0.4
LOC100290710	1	0.022291	0.1	0.1	0.9	184280	163890	10160	10225	5.3			-3.2	-3.3	-0.2
PGAP2	1	0.058921	12.6	0.2	0.0	132090	6823.9	123360	1907.1	5.1			3.7	-2.1	-5.8
KIAA0748	1	0.021891	3.9	0.4	0.1	105280	22137	75423	7716.2	5.0			2.0	-1.4	-3.4
FBXO11	1	0.034421	3.7	0.4	0.1	176380	38321	116370	21690	5.2			1.9	-1.2	-3.1
PRSS35	1	0.022805	2.1	0.5	0.2	331720	96594	185470	49655	5.5			1.1	-1.0	-2.1

ACO2	1	0.029561	2.0	0.5	0.2	352040	102180	205100	44757	5.5			1.0	-1.0	-2.0
DYTN	1	0.010947	2.0	0.5	0.2	352040	102180	205100	44757	5.5			1.0	-1.0	-2.0
NUAK1	1	0.031235	1.8	0.5	0.3	182440	63251	88579	30606	5.3			0.8	-1.0	-1.8
FTH1	1	0.044182	2.5	0.5	0.2	46205	11553	29979	4673.5	4.7			1.3	-1.0	-2.3
HNRNPU	1	0.019612	3.9	0.6	0.2	107050	21660	72228	13166	5.0			2.0	-0.7	-2.7
RPSAP15	1	0.001868	1.8	0.6	0.4	230200	68722	117680	43796	5.4			0.9	-0.7	-1.4
BRD4	1	0.020145	1.9	0.7	0.3	509030	155970	258430	94630	5.7			1.0	-0.6	-1.6
IQGAP1	1	9.61E-07	1.8	0.7	0.4	82695	24878	43503	14314	4.9			0.8	-0.6	-1.3
ISOC2	1	0.0081068	1.1	0.7	0.6	357810	132620	135660	89521	5.6			0.1	-0.5	-0.6
ANKRD30B	1	0.023804	2.1	0.7	0.3	203710	51920	111110	40674	5.3			1.0	-0.5	-1.6
EEF1A1	10	1.19E-31	1.9	0.7	0.4	7179000	2004100	3788100	1386900	6.9			1.0	-0.5	-1.4
HNRNPM	2	0.00015895	4.2	0.7	0.2	226060	41524	154940	29591	5.4			2.1	-0.4	-2.5
RPS18	1	0.011713	1.9	0.7	0.4	186510	35452	69126	81936	5.3			0.9	-0.4	-1.4
PKP3	1	0.025178	1.0	0.7	0.7	355020	131940	132030	91054	5.6			0.0	-0.4	-0.4
MAPK1	1	0.0020731	1.3	0.8	0.7	258770	84880	97039	76849	5.4			0.4	-0.3	-0.6
DNL1	1	0.032992	1.3	0.9	0.7	137150	45149	52075	39926	5.1			0.4	-0.2	-0.6
C17orf44	1	0.037931	1.3	0.9	0.8	217360	76571	75933	64858	5.3			0.3	-0.1	-0.3
FAM73B	1	0.020564	1.3	0.9	0.8	217360	76571	75933	64858	5.3			0.3	-0.1	-0.3
S100A4	1	0.07239	3.0	0.9	0.3	106120	22934	62611	20579	5.0			1.6	-0.1	-1.7
CSTB	1	0.031406	1.7	1.0	0.6	318500	108270	121590	88639	5.5			0.8	-0.1	-0.8
KCP	1	0.15055	0.3	1.0	3.8	191860	46275	19539	126050	5.3			-1.9	0.1	1.9
LGALS1	1	0.016295	2.2	1.1	0.5	214480	47659	116660	50153	5.3			1.1	0.1	-1.0
KLK8	1	0.025982	2.3	1.1	0.5	194290	43377	94640	56273	5.3			1.2	0.1	-1.1
UBB	2	4.80E-05	6.3	1.1	0.2	561810	68669	384710	108440	5.7			2.7	0.1	-2.5
FOXK1	1	0.050752	3.7	1.1	0.3	97391	5213.6	72156	20022	5.0			1.9	0.1	-1.7
HAGH	1	0.034776	1.1	1.2	1.1	114330	33202	39531	41600	5.1			0.2	0.3	0.1

BAZ1A	1	0.024496	10.6	1.6	0.2	179400	16619	136260	26520	5.3			3.4	0.7	-2.7
CMBL	3	1.34E-07	1.4	1.7	1.2	870500	206080	319530	344900	5.9			0.5	0.8	0.3
C14orf43	1	0.038563	41.1	2.3	0.1	4286000	100980	4001600	183400	6.6			5.4	1.2	-4.2
WDR20	1	0.016108	4.8	3.1	0.6	137030	6091.5	78799	52137	5.1			2.3	1.6	-0.6
USP46	5	1.36E-10	5.3	3.2	0.6	1790700	135970	977980	676720	6.3			2.4	1.7	-0.6
MAOB	1	0.047068	0.8	4.2	5.2	124510	11042	14988	98482	5.1			-0.3	2.1	2.4
WDR48	4	3.68E-07	6.7	4.2	0.6	500080	28716	329380	141990	5.7			2.7	2.1	-0.7
DDAH1	1	0.039914	25.4	4.9	0.2	1888700	62749	1653800	172170	6.3			4.7	2.3	-2.4
ABCG1	1	0.024701	20.4	5.8	0.3	979170	32623	752520	194020	6.0			4.3	2.5	-1.8
CPEB1	1	0.11573	0.4	6.3	14.4	141430	10695	9905.5	120820	5.2			-1.2	2.7	3.8
DAGLA	1	0.025678	7.4	NaN	NaN	34240	2343.5	31896	0	4.5			2.9	NaN	NaN
FAM54A	1	0.024428	NaN	NaN	NaN	0	0	0	0	NaN			NaN	NaN	NaN
C1orf96	1	0.011069	NaN	NaN	NaN	0	0	0	0	NaN			NaN	NaN	NaN
ZNF280C	1	0.023778	NaN	NaN	NaN	0	0	0	0	NaN			NaN	NaN	NaN
CRYGD	1	0.04099	NaN	NaN	NaN	0	0	0	0	NaN			NaN	NaN	NaN
HNRNPA1	1	0.0080084	NaN	NaN	NaN	48787	0	48787	0	4.7			NaN	NaN	NaN
FAM186A	1	0.13183	NaN	NaN	NaN	35420	35420	0	0	4.5			NaN	NaN	NaN
STK35	1	0.0455	NaN	NaN	NaN	103400	103400	0	0	5.0			NaN	NaN	NaN
IMPDH2	1	0.022409	NaN	NaN	NaN	0	0	0	0	NaN			NaN	NaN	NaN
CBLB	1	0.038884	NaN	NaN	NaN	0	0	0	0	NaN			NaN	NaN	NaN
RABEP1	1	0.070771	NaN	NaN	NaN	102830	0	102830	0	5.0			NaN	NaN	NaN
ABCE	1	0.019596	NaN	NaN	NaN	0	0	0	0	NaN			NaN	NaN	NaN
CEBPZ	1	0.02083	NaN	NaN	NaN	0	0	0	0	NaN			NaN	NaN	NaN
ARL13B	1	0.026317	NaN	NaN	NaN	0	0	0	0	NaN			NaN	NaN	NaN
LRCH3	1	0.046699	NaN	NaN	NaN	226350	0	0	226350	5.4			NaN	NaN	NaN
BCL2L11	1	0.018075	NaN	NaN	NaN	30397	0	0	30397	4.5			NaN	NaN	NaN

CYP2D6	1	0.015545	NaN	NaN	NaN	0	0	0	0	NaN			NaN	NaN	NaN
DES	2	0.00086055	NaN	NaN	NaN	0	0	0	0	NaN			NaN	NaN	NaN
TAOK2	1	0.056441	NaN	NaN	NaN	0	0	0	0	NaN			NaN	NaN	NaN
FCRLB	1	0.083132	3.4	NaN	NaN	24429	2620.6	20038	1771.1	4.4			1.8	NaN	NaN
IPI00748203.3	1	0.041971	NaN	NaN	NaN	1351100	0	1351100	0	6.1			NaN	NaN	NaN
IPI00748203.3	1	0.026147	NaN	NaN	NaN	43214	43214	0	0	4.6			NaN	NaN	NaN
FAM59B	1	0.0066949	NaN	NaN	NaN	453420	0	453420	0	5.7			NaN	NaN	NaN
IPI00936336.1	1	0.081038	NaN	NaN	NaN	0	0	0	0	NaN			NaN	NaN	NaN
IPI00937073.1	1	0.055539	NaN	NaN	NaN	0	0	0	0	NaN			NaN	NaN	NaN
IPI00937519.1	1	0.052502	NaN	NaN	NaN	0	0	0	0	NaN			NaN	NaN	NaN
IPI00937553.1	1	0.081038	NaN	NaN	NaN	0	0	0	0	NaN			NaN	NaN	NaN

Supplementary Table 1. Full list of proteins from GFP-USP46/GFP-USP46-C44S IP experiments.

Annotated MaxQuant output file for GFP/GFP-USP46-C44S/GFP-USP46 SILAC experiment. Proteins are annotated with their respective gene names. The peptides identified column, indicates the number of peptides seen for each protein. Proteins were black listed either because they were identified in the Trinkle-Mulcahy et al. (2008) dataset as an IP contaminant or they were blacklist from commonly seen proteins in IP mass experiment experiments in the lab. PEP (Posterior Error Probability) score essentially acts a p value, the lower the number the higher the confidence of correct identification.